A HIGH ARCTIC MICROCLIMATIC HOTSPOT ASSESSMENT, CAPE BOUNTY, NUNAVUT

MADELEINE C. GARIBALDI
Bachelor of Science, University of California Irvine, 2016

A Thesis
Submitted to the School of Graduate Studies
of the University of Lethbridge
in Partial Fulfilment of the
Requirements of the Degree

MASTER OF SCIENCE

Department of Geography
University of Lethbridge
LETHBRIDGE, ALBERTA, CANADA

A HIGH ARCTIC MICROCLIMATIC HOTSPOT ASSESSMENT, CAPE BOUNTY, NUNAVUT

MADELEINE GARIBALDI

Date of Defence: July 9, 2018

Dr. P. Bonnaventure Supervisor	Assistant Professor	Ph.D.
Dr. R. Barendregt Thesis Examination Committee Member	Professor	Ph.D.
Dr. L. Flanagan Thesis Examination Committee Member	Professor	Ph.D.
Dr. S. Kienzle Thesis Examination Committee Member	Professor	Ph.D.
Dr. T. Johnston Chair, Thesis Examination Committee	Associate Professor	Ph.D.

Abstract

Ground surface and permafrost temperatures in the High Arctic have been considered homogeneous. However, due to differential snow cover, there is a substantial degree of heterogeneity present. The objectives of this thesis were to model the ground thermal regime at Cape Bounty, Nunavut, using the TTOP model, for current conditions and climate change scenarios. While air temperature was mostly uniform, ground surface temperatures ranged from about -3.8 °C to about -13.8 °C. The spatial models showed warmer ground surface temperatures in topographic hollows, where snow accumulates, and colder temperatures in areas of topographic prominence, where snow is scoured. Under climate change, the models predicted areas with the coldest permafrost to have the largest magnitude of warming, while areas of relatively warm permafrost became closer to 0 °C. This thermal heterogeneity may have implications for ground stability, hydrological connectivity, and microbial activity, all of which influence solute movement and mercury release.

Acknowledgements

This thesis would not have been possible without the help and support of so many people. I would like to thank everyone at the Cape Bounty Arctic Watershed Observatory (CBAWO) for their field assistance, trekking around looking for loggers, digging a snow pit, and probing the active layer when I was too short. I would especially like to thank Scott Lamoureux for his help in all aspects of this project. Additionally, I would like to thank my committee for all their guidance.

My time during my Master's would have been much less enjoyable without my fellow graduate students. Thank you to the other members of the Bonnaventure Lab, Rory Gibson and Kyle Bexte for the laughs, I would not be Muddy G. without you guys. I would like to thank my Graduate Research Methods classmates, Josh Read, Rafaela Marasco, Martha Astorquiza, and Trevor Deering, for all their support in and outside of class. A very special thank you to Trevor for the random office conversations, cookies, and for just being a great friend during this whole process. It would not have been the same experience without you. I owe a special thanks to my supervisor, Dr. Philip Bonnaventure, for all his guidance, support and for giving me opportunities to expand my research skills outside of my thesis. Thank you for taking a chance on a girl from Southern California who had only ever been to the snow. Finally, I would like to give a special thanks to my family for all their love and support. I cannot express my gratitude to them enough, their phone calls and texts help me push through the tough times.

This project was generously supported by grants held by Dr. Scott Lamoureux from NSERC, ArcticNet, and PCSP and Dr. Philip Bonnaventure from NSERC.

Table of Contents

List of Figures

List of Tables

List of Equations

List of Abbreviations

AMAT	Annual mean air temperature
AMGST	Annual mean ground surface temperature
BTS	Basal temperature of snow
CBAWO	Cape Bounty Arctic Watershed Observatory
DD	Degree days
DEM	Digital elevation model
FDD	Freezing degree days (a or g represents air or ground)
GIS	Geographic information system
LAI	Leaf area index
MAAT	Mean annual air temperature
MAGT	Mean annual ground temperature
MAGST	Mean annual ground surface temperature
NEST	Northern ecosystem soil temperature
n_f	Freezing n-factor
n_t	Thawing n-factor
PISR	Potential incoming solar radiation
RCP	Representative concentration pathways
r_k	Ratio of thawed to frozen thermal conductivity
RMSE	Root mean squared error
SLR	Surface lapse rate
TTD	Thawing degree days (a or g represent air or ground)
TONE	Thermal 1D model
TPI	Topographic position index
TSP	Thermal state of permafrost
TTOP	Temperature at top of permafrost

Chapter 1

Thesis Introduction

1.1 Introduction

The average global air temperature is predicted to rise by 2.6 - 4.8 °C by 2100. Temperatures in the High Arctic however, are expected to respond to the effects of climate change in a more pronounced manner, increasing yearly air temperatures by 9-11 °C by 2100 as a result of arctic amplification through positive feedback mechanisms (Serreze & Barry, 2011; IPCC, 2014). The impact of this warming on the underlying permafrost has implications for terrain stability (Harris et al., 2001; Lantz & Kokelj, 2008), hydrology (Woo, 1986; Woo et al., 2008), carbon storage (Schuur et al., 2008; Tarnocai et al., 2009), and the storage of other contaminants including mercury (Obrist et al., 2017; Schuster et al., 2018). It is therefore, important to understand current ground and permafrost temperatures and estimate the impact warming air temperatures will have on the ground thermal regime.

One of the most common ways of spatially modelling permafrost temperatures is the temperature at top of permafrost (TTOP) model (Smith & Riseborough, 1996; Henry & Smith, 2001; Smith & Riseborough, 2002; Bonnaventure et al., 2016). However, most modelling studies of High Arctic permafrost temperatures are generally completed at regional or national scales. Since these studies are conducted at such a course resolution, they generally predict High Arctic permafrost temperatures to be relatively homogeneous (e.g. Henry and Smith, Figure 7). However, due to differential snow cover, ground surface and permafrost temperatures are actually quite heterogeneous (Bonnaventure et al., 2016). The resulting heterogeneity, specifically the locations of warmer ground surface and permafrost, may have implications for subsurface hydrologic connections

(e.g. Quinton et al., 2004; Nicole et al., 2009), which influences solute transportation (e.g. Lamhonwah et al., 2016) and may act as biological refugia, areas in which organisms can survive through periods of unfavorable conditions (e.g. Rivkina et al., 2000; Price & Sowers, 2004; Bakermans & Skidmore, 2011). Additionally, under climate warming, the existing heterogeneity makes it unlikely that the permafrost will respond uniformly to the warming in air temperature. As a result, areas of colder permafrost may experience a larger magnitude of warming, while areas of warmer permafrost may become closer to 0 ° C.

The purpose of this thesis is to outline the heterogeneity that exists in temperature surfaces including the current and future air, ground surface, and permafrost temperatures over two paired watersheds at Cape Bounty, Melville Island, Nunavut, through spatial modelling. These models were constructed using the TTOP model and may be used to assess areas of importance for future studies on microbiological activity, hydrological flow, and ground stability.

1.2 Objectives

The overall goal of this research is to understand and model the spatial extent of the thermal heterogeneity, generated by differential snow cover, for present conditions as well as under predicted climate warming across two paired watersheds in the Cape Bounty Arctic Watershed Observatory (CBAWO), Melville Island, Nunavut. The research objectives underlying this goal are to:

1. Describe the spatial variability of current air, ground surface, and TTOP temperatures through the creation of modeled high-resolution, continuous surfaces for each temperature field.

2. Predict permafrost temperature response to climate warming under equilibrium conditions.
3. Identify areas of permafrost within the landscape which are most susceptible to the effects of climate change, to be of use for modelling hydrological and ecological changes.

1.3 Thesis Structure

This thesis consists of six chapters. This first provides introductory background on the purpose of the thesis and gives the thesis objectives. The second chapter is a literature review, introducing the different types of permafrost models and highlighting the gaps and uncertainties in High Arctic permafrost modelling specifically. The third chapter expands upon the methods and rational behind the field methods and logger placement as well as those used to construct the models. Results for the current and future models are given in chapter four. Chapter five reviews discussion topics, including error calculations for the models, comparison of results to previous studies, and implications for the existing heterogeneity and future warming. Lastly, chapter six consists of conclusions.

Chapter 2

Literature Review

2.1 Introduction

The spatial distribution of High Arctic ground surface and permafrost temperature is often viewed and subsequently modelled as homogeneous, when in reality, evidence shows there can be considerable variability over short distances generated by differential snow cover (Bonnaventure et al., 2016). The assumption of homogeneity is problematic for many reasons. Perhaps most impactful is that this can lead to predictions of uniform permafrost warming across the High Arctic regardless of the applied climate change scenario (Henry & Smith, 2001; Koven et al., 2013). The current thermal heterogeneity is likely to have a profound effect on the evolution of the landscape, impacting the magnitude and distribution of permafrost warming along with associated changes to landforms, water quality and ecological structure as new thermal equilibriums are established (Lewkowicz & Harris 2005; Lantz & Kokelj, 2008; Berteaux et al., 2016; Roberts et al., 2017). It is, therefore, essential to understand the nature of current High Arctic thermal heterogeneity over multiple fields, identifying and quantifying the spatial distribution of microclimates. This task will provide orders of magnitude more data than currently exists, aiding predictions of permafrost response to projected climate change, and will help to better characterize the evolution of the High Arctic system as a whole.

2.2 Relations between Permafrost, Climate, and Environmental Features

Permafrost is defined as earth materials which remain at or below 0 °C for at least two consecutive years (French, 2007). Permafrost is the only element of the cryosphere that people live on year-round and is important at both local and global scales as it

impacts hydrology (Woo, 1986; Woo et al., 2008), terrain stability (Harris et al., 2001; Lantz & Kokelj, 2008), carbon storage (Schuur et al., 2008) and the storage of other contaminants including mercury (Obrist et al., 2017; Schuster et al., 2018). Permafrost can be described by extent as continuous (90-100%), discontinuous (50-90%), sporadic (10-50%), and isolated (0-10%) with the classification based on the percentage of land underlain by permafrost (Heginbottom, 1995; French, 2007) (Figure 1).

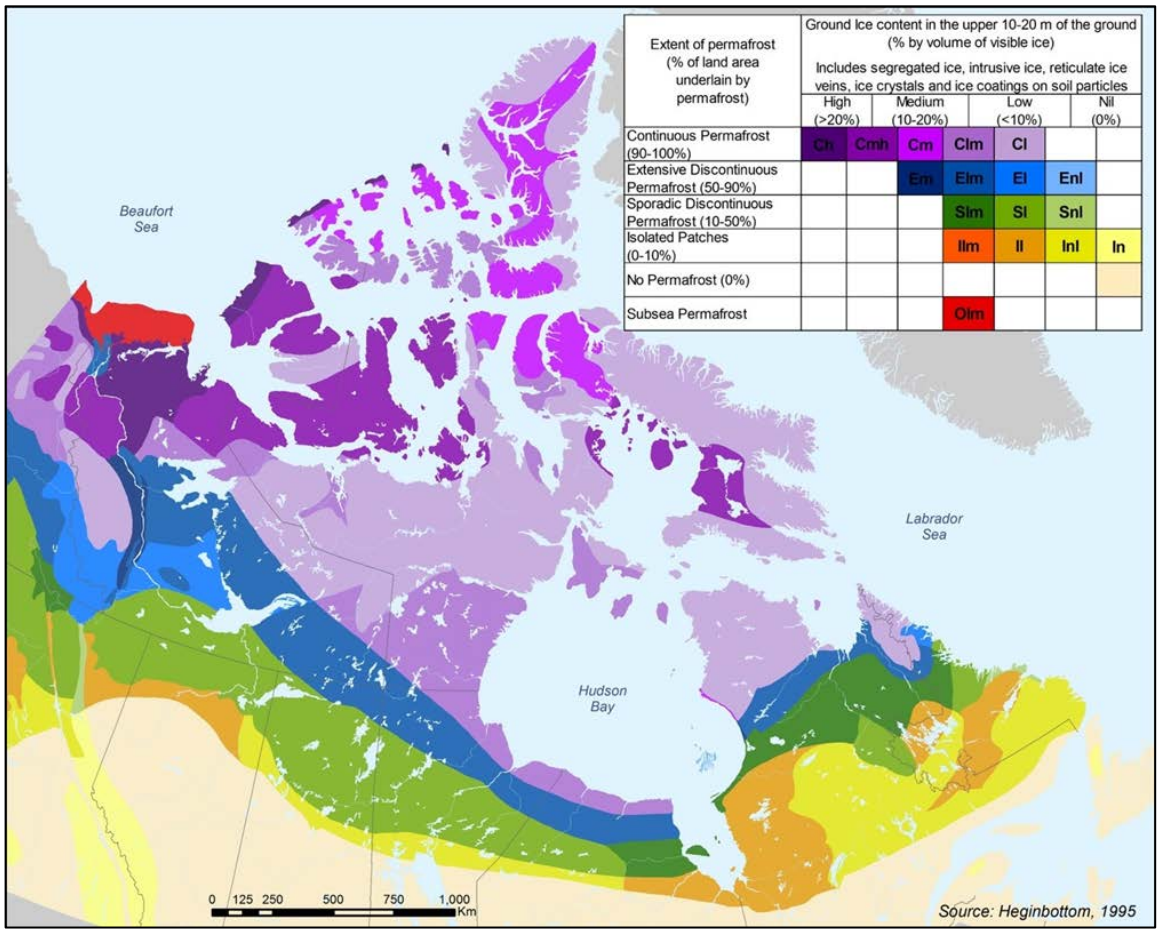

Figure 1. Permafrost map of Canada with zonation and ground ice content (Heginbottom et al., 1995). From National Atlas of Canada, 5th edition, Plate 2.1 (MCR 4177), scale 1: 7,500,000.

The primary control on permafrost distribution is climate, with mean annual air temperature (MAAT) being the most significant contributing factor influencing ground and permafrost temperatures on a regional scale (Etzelmüller et al., 1998; Juliussen &

Humlum, 2007; Shur & Jorgenson, 2007). On local to micro scales, however, other environmental factors such as snow cover, vegetation, and sediment thermal conductivity, can also substantially impact both the distribution and thermal state of permafrost (TSP) as these factors moderate the transfer of heat in and out of the ground (Williams & Smith, 1989; Smith & Riseborough, 1996; French, 2007; Juliussen & Humlum, 2007). In areas of continuous permafrost, seasonal snow cover influenced by wind, microrelief, and vegetation has been shown to be one of the most important factors influencing permafrost and ground temperatures, especially during winter (Zhang et al., 1997). Based on the study by Lachenbruch et al. (1988), permafrost temperature can be related to historical patterns of air temperature. The permafrost-climate relation is often conceptualized using three distinct fields including air temperature, ground surface temperature, and temperature at the top of permafrost (TTOP) (Smith & Riseborough, 1996; Henry & Smith, 2001), allowing for a conceptualization of the vertical temperature profile across the fields (Figure 2).

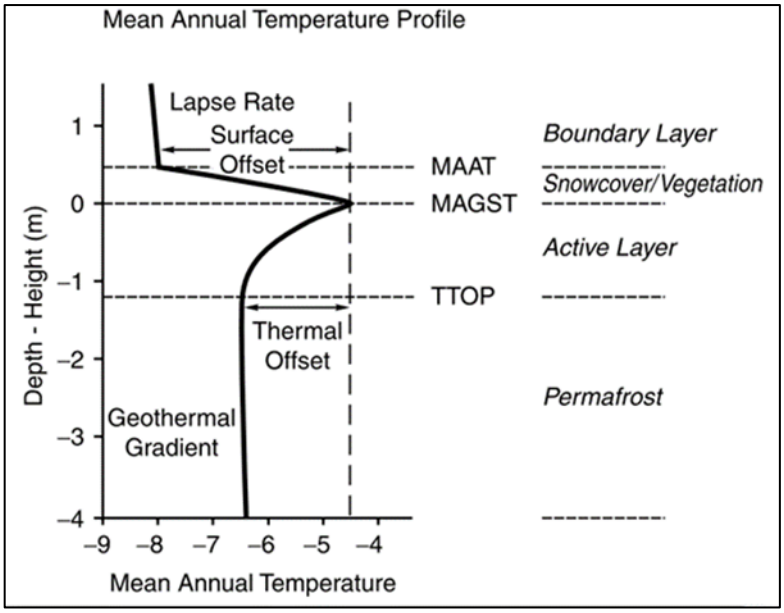

Figure 2. Mean annual temperature profiles through the lower atmosphere and into the subsurface for permafrost underlain terrain (Henry and Smith, 2001).

The temperature difference between the MAAT and the mean annual ground surface temperature (MAGST) is referred to as the surface offset (Henry & Smith, 2001; Smith & Riseborough, 2002). The magnitude of the surface offset is dependent on surface cover, namely vegetation and snow cover. The accumulation of snow cover in autumn and early winter is shown to have a strong influence on MAGST by insulating the ground from the coldest winter temperatures, resulting in warmer MAGSTs than at uncovered locations (Gold, 1963; Goodrich, 1982; Zhang, 2005). Vegetation influences ground surface temperatures both directly, through the cooling effects of evapotranspiration and changes in soil moisture, and indirectly, through changes in snow accumulation and shielding from solar radiation (Brown, 1966; Storck et al., 2002; Yi et al., 2007). In windy areas of shrub cover, snow, is trapped by the vegetation, accumulating more under this cover than in open terrain, while trees often intercept snow preventing it from collecting on the ground (Brown, 1966; Péwé & Brown, 1973; Tyrtikov, 1976; Sturm et al., 2001). This results in a greater surface offset in areas with shrub cover and a smaller

surface offset under trees. In the High Arctic, since there is little vegetation, its influence on ground temperatures and wind-driven snow accumulation are minimal compared to the effects of topography (Brown, 1972; Woo et al., 1983; Woo & Young, 1997). Additionally, although the total amount of precipitation in High Arctic polar deserts is minimal, large variations in snow depth occur due to wind-blown snow accumulation in sheltered areas such as gullies and valleys, and on leeward slopes (Yang & Woo, 1999; Bonnaventure et al., 2016). Therefore, variability exists in ground surface temperatures due to the insulating effect of differential snow cover with warmer ground surface temperatures in areas of high snow compared to locations with wind-blown snow loss (Bonnaventure et al., 2016).

The thermal offset, or the temperature difference between the MAGST and TTOP, is largely influenced by the thermal conductivity of the sediment, specifically the difference in thermal conductivity between frozen and thawed materials as well the sediment water content (Goodrich, 1982; Smith & Riseborough, 1996, 2002; Westermann et al., 2015; Way & Lewkowicz, 2016). Therefore, dry sediments have small seasonal variation in thermal conductivity compared to wet sediments leading to a thermal conductivity ratio (thawed thermal conductivity: frozen thermal conductivity) close to one (Burn & Smith, 1988; Bonnaventure & Lamoureux, 2013).

2.3 Permafrost Modelling

A model is an idealized representation of reality described in either conceptual, physical, or mathematical terms which expresses the essential elements of a system (Inkpen, 2005). Modelling is one of the most commonly used methods to study permafrost distribution and thermal characteristics as neither of these can be directly observed by remote sensing like other elements of the cryosphere (e.g. glaciers and sea

ice) (Kääb, 2008). Since permafrost distribution is the result of complex environmental interactions, two generalized techniques for modelling permafrost-climate relations have recently emerged in the literature (Riseborough et al., 2008; Bonnaventure & Lewkowicz, 2013). The first technique is a numerical approach which models the energy balance directly to identify ground temperature conditions, while the second, empirical models, associate topographic and/or climate variables to permafrost distribution or attributes (Riseborough et al., 2008; Bonnaventure & Lamoureux, 2013; Etzelmüller, 2013)

2.3.1 Numerical Models

Numerical models directly estimate the ground-atmosphere energy exchange using theories of heat transfer and flow to create an energy balance equation (Sazonova & Romanovsky, 2003; Zhang et al., 2003; Bonnaventure & Lamoureux, 2013; Kurylyk & Hayashi, 2016; Yin et al., 2016). One benefit to using this type of modelling is that it is flexible enough to handle variations in environmental features such as surface material and boundary conditions (Riseborough et al., 2008). However, since numerical models directly calculate the energy balance of a location, they require a large amount of input data and are computationally intensive which limits their use in modelling studies, especially in remote locations (Riseborough et al., 2008; Bonnaventure & Lamoureux, 2013). As a result, these studies are primarily used as point source models and are rarely, if ever, used for spatial studies (Sazonova & Romanovsky, 2003; Riseborough et al., 2008; Bonnaventure & Lamoureux, 2013; Kurylyk et al., 2014). Numerical models perform best in areas with known boundary conditions and forcing parameters as they require large amounts of site specific data (Oelke et al., 2003; Riseborough et al., 2008).

Examples of numerical models include the Stefan model, the Kudryavtsev model the Northern Ecosystem Soil Temperature (NEST) model, and the Thermal One-Dimensional (TONE) model (Kudryavstev et al., 1974; Zhang et al., 1996; Oelke et al., 2003; Zhang et al., 2003; Riseborough et al., 2008).

2.3.1.1 Stefan Model

In permafrost terrain, the Stefan model is widely used to determine active layer thickness, through calculations of the seasonal thaw depth (Riseborough et al., 2008; Bonnaventure & Lamoureux, 2013; Yin et al., 2016). The Stefan model is computationally simplistic, requiring few data inputs, and the required inputs, air temperature and sediment thermal conductivity, are easy to obtain (Equation 1)(Bonnaventure & Lamoureux, 2013).

$$X = \sqrt{\frac{2\lambda I}{L}} \qquad (1)$$

In the equation X is the depth of thaw (m), λ is the thermal conductivity of the sediment in the thawed state ($W \cdot m^{-1}K^{-1}$), I is the index of freezing or thawing ($°C \cdot day^{-1}$), and L is the volumetric latent heat of fusion ($J \cdot m^{-3}$).

However, the Stefan model assumes frozen ground maintains a temperature of 0 ° C, which may not hold true, especially in the cold permafrost of the continuous zone (Bonnaventure & Lamoureux, 2013; Kurylyk & Hayashi, 2016; Yin et al., 2016). Additionally, heat exchange is only calculated in the vertical direction, ignoring advective or horizontal heat transport. This omission often leads to imprecise predictions of thaw depth, particularly in areas in which groundwater or other mechanisms transport heat horizontally (Kurylyk et al., 2014). To account for these inaccuracies, correction factors

may be applied to the Stefan model to improve the active layer depth predictions, however, none provide accurate results if the initial temperature is different than 0° C (Kurylyk & Hayashi, 2016). To remedy this, Kurylyk and Hayashi (2016) proposed four different equations and correction factors for varying initial temperatures and phase changes, increasing the usability and accuracy of the Stefan equation over a wider range of conditions. The correction factors were shown to increase the accuracy of the Stefan equation results under several hypothetical scenarios by accounting for non-zero initial temperatures and the heat capacity of the soil. However, the addition of correction factors increased the computational complexity of the model and the amount of environmental input data required. Therefore, it is possible that additional errors may be introduced through estimations in environmental conditions. As a result, the use of Stefan equation correction factors is dependent on the purpose of the model, whether the goal is to maximize accuracy or to maximize temporal and computational efficiency, and whether the necessity for accuracy in the modelled active layer depths exceeds the impact of increased complexity and additional data collection.

2.3.1.2 Kudryavtsev Model

Similar to the Stefan model, the Kudryavtsev model is used to predict active layer depth, but is also can be modified to calculate permafrost temperature (Riseborough et al., 2008; Bonnaventure & Lamoureux, 2013). The Kudryavtsev model performs better in areas of cold permafrost than the Stefan model and also accounts for the impact of thermal properties, vegetation, snow cover, and regional climate variations on active layer thickness (Sazonova & Romanovsky, 2003). However, the inclusion of this additional information increases the complexity of the equation and the amount of site specific data

required, making it impractical over large areas (Equations 2-3) (Bonnaventure & Lamoureux, 2013; Yin et al., 2016).

$$X(2\bar{A}C_T + \rho L) = 2A_{gs} - |TTOP|\sqrt{\frac{\lambda_T C_T P}{\pi}} + \frac{(2\bar{A}C_T X_{2C} + \rho LX)\rho L\sqrt{\frac{\lambda_T P}{\pi C_T}}}{2\bar{A}C_T X_{2C} + \rho LX + (2AC_T X_{2C} + \rho LX)\sqrt{\frac{\lambda_T P}{\pi C_T}}} \quad (2)$$

Where:

$$\bar{A} = \frac{A_{gs} - TTOP}{\ln\left(\frac{A_{gs} + \frac{\rho L}{2C_T}}{|TTOP| - \frac{\rho L}{2C_T}}\right)} - \frac{\rho L}{2C_t} \quad (3)$$

$$X_{2C} = \frac{2(A_{gs} - |TTOP|)\sqrt{\frac{\lambda_T C_T P}{\pi}}}{2\bar{A}C_T + \rho L}$$

In these equations C_T is the volumetric heat capacity of unfrozen ground ($J \cdot m^{-3}$), A_{gs} is the temperature amplitude at the ground surface (°C), λ is the thermal conductivity of the sediment in the thawed state ($W \cdot m^{-1} \cdot K^{-1}$), L is the volumetric latent heat of water ($J \cdot m^{-3}$), ρ is the density of the sediment ($kg \cdot m^{-3}$), and TTOP is the annual average top of permafrost temperature (°C).

As a result of the Kudryavtsev model's complexity and data requirements, it is frequently utilized in one dimensional studies at single points to obtain the most accurate active layer depth estimations and representation of energy balances (Riseborough et al., 2008; Bonnaventure & Lamoureux, 2013). The Kudryavtsev model is also best used in areas where validation data exists, such as an instrumented borehole.

2.3.1.3 Northern Ecosystem Soil Temperature (NEST) Model

The Northern Ecosystem Soil Temperature (NEST) model was developed to assess the impact of climate warming, and the subsequent increase in summer thaw depth and permafrost degradation on northern ecosystem functions and dynamics (Zhang et al., 2003). Using a combination of soil-vegetation-atmosphere systems and strengths from existing permafrost models, NEST treats soil, vegetation and the atmosphere as an integrated system. Since it is a numerical model, NEST uses one dimensional heat conduction and energy balance equations to determine thermal dynamics of the ground and snow layers in the model (Figure 3).

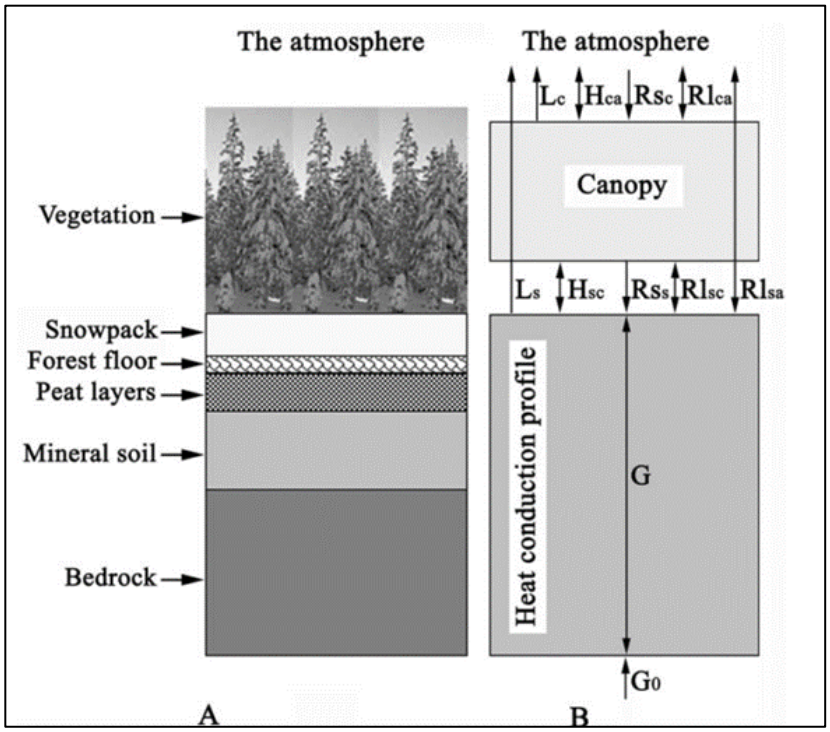

Figure 3. A) The environmental components used in the NEST model. B) Exchange of energy between soil, vegetation, and atmosphere accounted for in the NEST model. The energy balance equation created for the model includes the sensible heat (H), the latent heat (L), solar radiation (Rs), long-wave radiation (Rl), and the convective hear flux (G) exchange between the ground surface (s), the vegetation canopy (c), and the atmosphere (a). Zhang et al. (2003)

One important potential use for this model is to simulate the transient impacts of climate change on northern ecosystems by modelling the consequences of altered soil thermal regimes and permafrost degradation on ecosystems and biogeochemical cycles across different vegetation and ground conditions (Zhang et al., 2003). One of the main drawbacks to the NEST model is that as a numerical model, it requires a large quantity of site specific data related to vegetation, ground conditions, and atmospheric climate to calculate the energy balance of a site (Zhang et al., 2003; Riseborough et al., 2008). The required data may also vary from site to site over small distances as surface properties and environmental conditions change. Therefore, it is possible that when used spatially, the NEST model may miss variation at sub resolution scales. Additionally, as a numerical model, NEST does not perform well in areas of complex topography, which causes large climate heterogeneities. As a result, the NEST model is generally only used in circumpolar studies.

2.3.1.4 TONE Model

The TONE model is a finite element one-dimensional heat conduction model with phase change (Zhang et al., 1996; Oelke et al., 2003). In this model the spatial component is depth, and the model is generally used to predict ground temperature profiles (Riseborough, 2004). The TONE model is also used to estimate changes in depth or temperature over time (Riseborough, 2004; Riseborough, 2008). Since the TONE model accounts for the latent heat of soil water freezing and thawing, it provides superior results in soils with a substantial freezing characteristic (the relation between temperature and unfrozen water content) (Riseborough, 2002; Smith & Riseborough, 2010). As a numerical model, TONE also produces accurate active layer depths and soil temperatures

at point locations with well-known boundary conditions and forcing parameters (Zhang et al., 1996; Zhang & Stamnes, 1998; Oelke et al., 2003). The TONE model has been used to estimate the thickness of the active layer and the depth of taliks (Riseborough, 2008).

2.3.2 Empirical Models

Empirical models, unlike numerical models, use easily computed or measured topographic and climatic variables as proxies for the energy transfer between the ground surface and the atmosphere, rather than explicitly calculating the energy balance (Hoelzle et al., 2001; Riseborough et al., 2008; Bonnaventure & Lamoureux, 2013). These variables are chosen depending on the influence of each on the energy balance equation and, therefore, may vary between locations, limiting the number of required input parameters, and allowing the model to be run without direct climate data (Hoelzle et al., 2001; Bonnaventure & Lamoureux, 2013). For these reasons, empirical models are more frequently used to model permafrost spatially than numerical models (Henry & Smith, 2001; Riseborough et al., 2008; Westermann et al., 2015; Way & Lewkowicz, 2016). Additionally, empirical models are best suited for modelling in remote locations compared to numerical models, since there is often sparse or temporally limited or disjointed data in these areas (Etzelmüller et al., 2006; Riseborough et al., 2008). Finally, empirical models are well suited for examining impacts of climate change on permafrost as their inputs are easy to manipulate in platforms such as GIS (Etzelmüller et al., 1998; Wright et al., 2003; Juliussen & Humlum, 2007; Gisnås et al., 2013).

2.3.2.1 TTOP Model

The TTOP model is an empirical model which is most often used to predict the presence of permafrost by calculating the average permafrost temperature at the base of

the active layer (the layer above permafrost which freezes and thaws on a seasonal basis) (Smith & Riseborough, 1996; Henry & Smith, 2001; Smith & Riseborough, 2002; Riseborough et al., 2008; Bonnaventure & Lamoureux, 2013; Bonnaventure et al., 2016). Additionally, TTOP is also used to predict permafrost temperature changes due to climate warming, and is an input for other types of models (e.g. the Kudryavtsev model) (Smith & Riseborough, 1996, 2002; Juliussen & Humlum, 2007; Bonnaventure & Lamoureux, 2013). This model uses climate data in the form of seasonal n-factors combined with lower atmosphere freezing and thawing indices to produce a numerical value for TTOP using Equation 4, where n_t and n_f are the thawing and freezing n-factors, λ_T and λ_F are the thawing and freezing thermal conductivities of the sediment, FDD_a and TDD_a are the freezing and thawing degree days of the air, and P is the annual period (365 days).

$$TTOP = \frac{(n_t * \lambda_T * TDD_a) - (n_f * \lambda_F * FDD_a)}{\lambda_F * P} \quad (4)$$

This equation can be simplified to

$$TTOP = \frac{(n_t * TDD_a * r_K) - (n_f * FDD_a)}{P} \quad (5)$$

Where r_k is the ratio of thawed to frozen thermal conductivity of the sediment.

The main advantages of the TTOP model are its simplicity and that it uses data such as snow depth and air temperature, which are commonly measured by meteorological stations (Juliussen & Humlum, 2007). Another advantage of the TTOP model is that it may also be used under semi-transient conditions, since it functions at a shallow depth (Smith & Riseborough, 2002). Alternatively, the main challenge is determining the values of the scaling factors, the n-factors for both freezing and thawing,

and the ratio of thermal conductivity between the frozen and thawed ground (Juliussen & Humlum, 2007). The TTOP model assumes a single value for the thermal conductivity of frozen sediment (mineral and organic sediment), which, due to its dependence on the sediment's unfrozen water content, may not hold true for all sediments (Riseborough, 2002).

2.3.2.2 n-factors

n-factors are transfer functions or ratios representing the energy fluxes at a single location. They are essential components of the TTOP model and are often used in conjunction with other models to improve results (Henry & Smith, 2001; Bonnaventure & Lamoureux, 2013). n-factors are calculated using Equation 6, where *DD* represents degree-days (the absolute value of the sum of the average daily temperatures for freezing and thawing seasons) and the subscripts g and a denote ground and air.

$$n = \frac{DD_g}{DD_a} \tag{6}$$

Freezing and thawing seasons are determined by the first daily average temperature above or below 0 °C respectively.

Since the surface offset is influenced by surface properties, including vegetation and snow cover which vary seasonally, it is modelled using two n-factors n_f and n_t (Equation 7).

$$n_f = \frac{FDD_g}{FDD_a} \quad \text{and} \quad n_t = \frac{TDD_g}{TDD_a} \tag{7}$$

Where FDD_g and TDD_g are the freezing and thawing degree days in the ground and FDD_a and TDD_a are the freezing and thawing degree days in the air. The value of n_f is influenced by snow cover and the MAAT, with areas of higher snow cover producing

smaller n_f values as a result of the insulation of the ground surface from the coldest winter air temperatures (Smith & Riseborough, 2002). If the air and the ground are in perfect connection, the n_f is 1. n_t is determined by vegetation with high amounts lowering the value of n_t as a product of shading and transpiration, keeping the ground surface cooler than the air (Smith & Riseborough, 2002). In areas with little to no vegetation, n_t may exceed 1 as the ground becomes warmer than the air.

Over large areas and in High Arctic environments the freezing n-factor has been shown to have a larger impact on ground surface temperature than the thawing n-factor (Riseborough & Smith, 1998; Henry & Smith, 2001). In High Arctic environments, this is likely a result of the dominance of the winter season and the limited vegetation cover. The value of the freezing n-factor (n_f) has been shown to be a function of both MAAT and snow depth, with colder temperatures yielding larger n-factors than warmer temperatures given the same snow depths (Figure 4) (Smith & Riseborough, 2002).

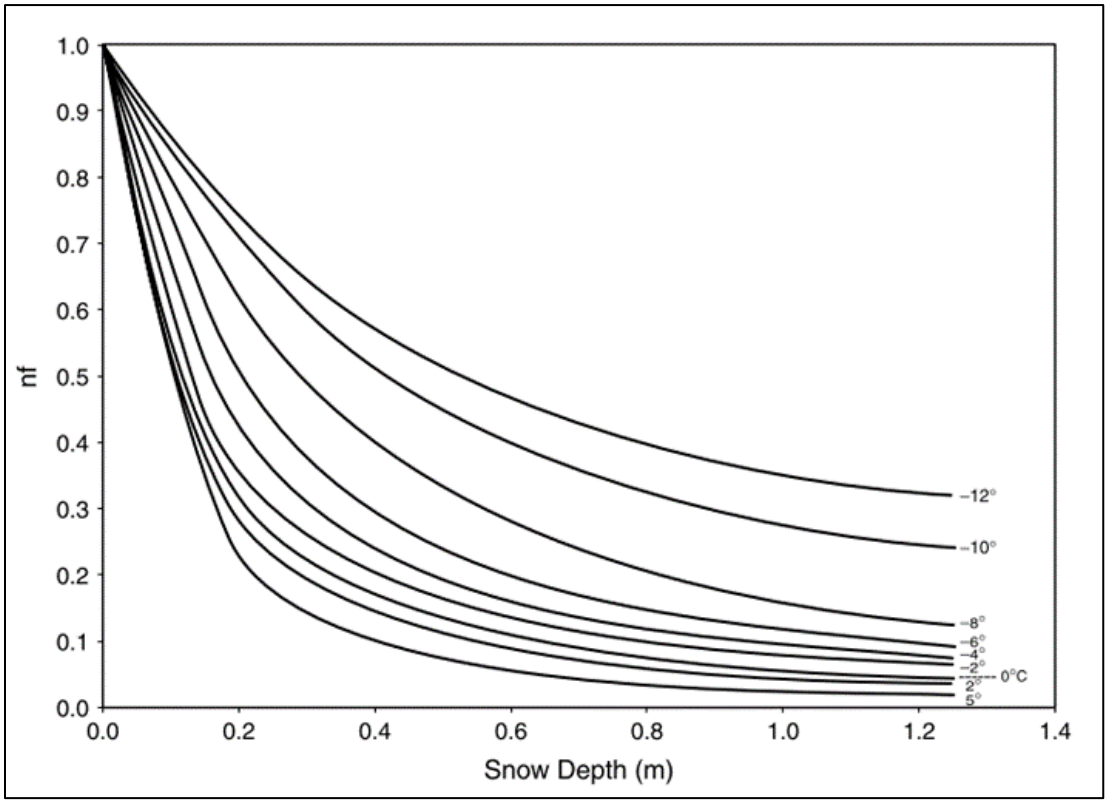

Figure 4. Theoretical curves showing n_f as a function of MAAT and snow depth (Smith & Riseborough, 2002)

The theoretical n_f curves demonstrate that there is an approximate limit to the magnitude of n_f determined only by MAAT, meaning the addition of snow past this threshold will not substantially decrease the value of n_f, as the insulating effects of snow cover reaches an approximate maximum. This is a product of the underlying permafrost. As the active layer freezes, most of the energy is used as latent heat, limiting the temperature change of the sediment, known as the zero-curtain effect (Smith & Riseborough, 2002). In permafrost terrain, there is a limit to the freezing depth and eventually the active layer freezes to the permafrost. Once this happens the latent heat pump keeping the ground surface warm stops and the ground begins to cool. The shallower the active layer the sooner this process stops, explaining why in cold permafrost environments, n_f does not become as small as in areas of warm permafrost or

areas of seasonal frost. If the MAAT of a location changes it will also change the depth of the active layer, thereby altering the possible values of n_f even if snow depth remains constant.

2.3.3 Recent Spatial Modelling Studies

The models previously discussed simulate permafrost and other aspects of periglacial environments at point locations in one dimension. To use one of the models to represent permafrost spatially, it is important to relate model outputs and estimates at one location to others with similar features, as modelling each point of an area directly is not practical or possible (Klene et al., 2001; Gisnås et al., 2013). The creation of surface layers of attributes influencing the ground thermal regime such as elevation, vegetation cover, snow depth, aspect, latitude, and slope, allow for model estimations to create a continuous surface of permafrost probability (e.g. Bonnaventure et al., 2012), ground and TTOP temperatures (e.g. Way & Lewkowicz, 2016; Way & Lewkowicz, 2018), or active layer thickness predictions (e.g. Lewkowicz & Ednie, 2004; Juliussen & Humlum, 2007; Shiklomanov et al., 2007; Bonnaventure & Lewkowicz, 2008; Hachem et al., 2009; Nguyen et al., 2009; Zhang et al., 2012; Gisnås et al., 2013; Ou et al., 2014). These layers are often constructed using digital elevation models (DEMs) to determine slope and elevation, measurements of incoming solar radiation to represent aspect, interpolation from climate station data to create average temperature and snow depth layers, and vegetation surveys or remote sensing for the construction of vegetation layers (Lewkowicz & Ednie, 2004; Juliussen & Humlum, 2007; Shiklomanov et al., 2007; Bonnaventure & Lewkowicz, 2008; Nguyen et al., 2009; Zhang et al., 2012; Gisnås et al., 2013; Ou et al., 2014).

One recent advancement in spatial modelling studies is the use of remote sensing to collect data on vegetation and ground surface temperature. Remote sensing collects information about a surface using reflected ultraviolet, visible, infrared, and microwave electromagnetic radiation, which is then analyzed using image processing techniques (Jenson, 2007; Purkis & Klemas, 2013; Santosh & Sundaresan, 2014). In spatial permafrost modeling studies, vegetation and surface temperature data layers are often produced using remote sensing. The characteristics of the spectral reflectance of vegetation, namely that it reflects near infrared radiation and green wavelengths while absorbing red and blue, are used to distinguish different types of vegetation cover and are often analyzed through vegetation indices (Jenson, 2007). Since an object's internal kinetic energy is converted into radiant energy, temperature is able to be remotely sensed through thermal infrared radiation under the assumption that there is high correlation between the true kinetic temperature and the radiant temperature of an object (Jenson, 2007). Remote sensing is an important tool in spatial mapping as it provides information about land-cover over large areas that would be impractical to fully survey on the ground and provides consistent temporal coverage (Aplin, 2004).

This section of background focuses specifically on recent spatial modelling studies conducted in the Arctic and High Arctic to illuminate possible research gaps in these areas. Therefore, recent modelling studies focused specifically in mountainous terrain or on permafrost outside the Arctic region are not discussed in this chapter. More specifically, the goal of this chapter is to determine research gaps in ground and permafrost temperature studies in Arctic regions. As such, the recent studies,

subsequently discussed, concentrate on estimating ground and permafrost temperatures, rather than predicting active layer depth.

2.3.3.1 Spatial Modelling with NEST

Due to the necessity for copious data, numerical models are not often used for detailed spatial studies of permafrost distribution. Recently, however, the NEST model has been used in several studies in both the Northwest Territories and the Hudson Bay lowlands regions of Canada. The NEST model was used to predict and map permafrost and active layer thickness in Wapusk National Park in the northwest Hudson Bay lowlands (Zhang et al., 2012). To obtain the required data inputs for each 30 m x 30 m map pixel, field measurements and LANDSAT (remotely sensed) data were used to identify 14 land-cover types. Leaf area index (LAI), elevation and land-cover type were then used to estimate peat thickness, and climate data was interpolated from climate stations in and around the park. Due to computational time constraints, rather than running the model for each pixel, elevation and LAI were divided into discrete classes and only pixels with unique combinations of input data were modelled. The modelled summer thaw depths were validated against observed summer thaw depths at 100 sites within the park. The modelled results were similar in magnitude to the observed depths in most locations, however, the summer thaw depth at five locations was largely underestimated, likely due to an overestimation of the peat thickness and an underestimation of snow cover accumulation at these locations (Zhang et al., 2012). It is also possible there are additional discrepancies over small distances which were not accounted for in the modelled results. Additionally, since there was already a computational time constraint at this resolution, it may be difficult to use this model for

finer resolution studies, or even studies at the same resolution over larger areas or more complex terrain.

Ou et al. (2014) also used the NEST model in combination with remotely sensed data to map the probability of permafrost occurrence and to determine the evolution of permafrost under three climate warming scenarios (low, medium, and high) based on global climate model projections, for a large area in the Northwest Territories of Canada. General land conditions were determined using land cover maps from satellites, specifically high-resolution visible and infrared images from SPOT-5, yielding 13 land cover types used in the model (Ou et al., 2014). Field observations for each land-cover types were then used to estimate the probability of the organic layer thickness. LAI was estimated using LANDSAT data and climate data for each grid cell were calculated through interpolation of climate station data. Then, the progression of permafrost for each land-cover type and climate scenario was simulated using the NEST model. Solar radiation was estimated using a DEM and the thickness of the organic layer was estimated using a modified logistic function created using field sampling observations. Similar to the previous NEST study, only unique combinations of input parameters were run through the model to reduce computational time. Finally, the permafrost probability in each grid cell was determined by modelling permafrost dynamics using all ground types under each of the three warming scenarios. Two areas where the model and actual ground conditions differed were in locations with non-vegetated land-cover and modelled summer thaw depths at a few sites. The lack of permafrost modelled in areas with no vegetation, despite the observed occurrence of permafrost, may be due to disturbance and the addition of peat material. Inaccuracies in summer thaw depth calculations may stem

from heterogeneity in soil type, vegetation, and hydrologic conditions. This also indicates there may be heterogeneity in other data layers which is undetected by the collection methods since it occurs over distances smaller than the 20m by 20 m resolution of the model. Additionally, the climate change projections for this study do not include changes to other input variables such as snow cover, vegetation changes, or increasing fire frequency, all of which may alter the permafrost regime.

2.3.3.2 Spatial Modelling with TTOP

Gisnås et al. (2013) used the TTOP model, referred to in this study as CryoGRID 1.0, to determine permafrost distribution in Norway, improving previous spatial models by accounting for the spatial variation in vegetation, snow cover, and ground properties. To model the spatial distribution of permafrost in Norway the factors influencing the presence of permafrost (snow cover, vegetation, and ground surface properties) needed to be determined for each 1 km^2 grid covering the extent of Norway. To spatially map snow cover, Gisnås et al. (2013), used snow map data produced in previous studies by models using gridded snow height, air temperature, and snow water equivalence. To account for inaccuracies in the snow map models, mainly the impact of snow cover redistributed by wind, two snow height scenarios were considered, the modelled snow cover data and one with a reduction of 30 % in snow cover above the treeline. Gisnås et al. (2013) determined the land cover in each grid using natural n-factors to convert the 44 vegetation classes for Norway into 5 land cover classes. The spatial ground properties were then calculated using Geologic Survey of Norway's point measurements and maps of classes

for both bedrock and surface geology, and by using the thermal properties and conductivity assigned to these classes by other models and literature (Figure 5).

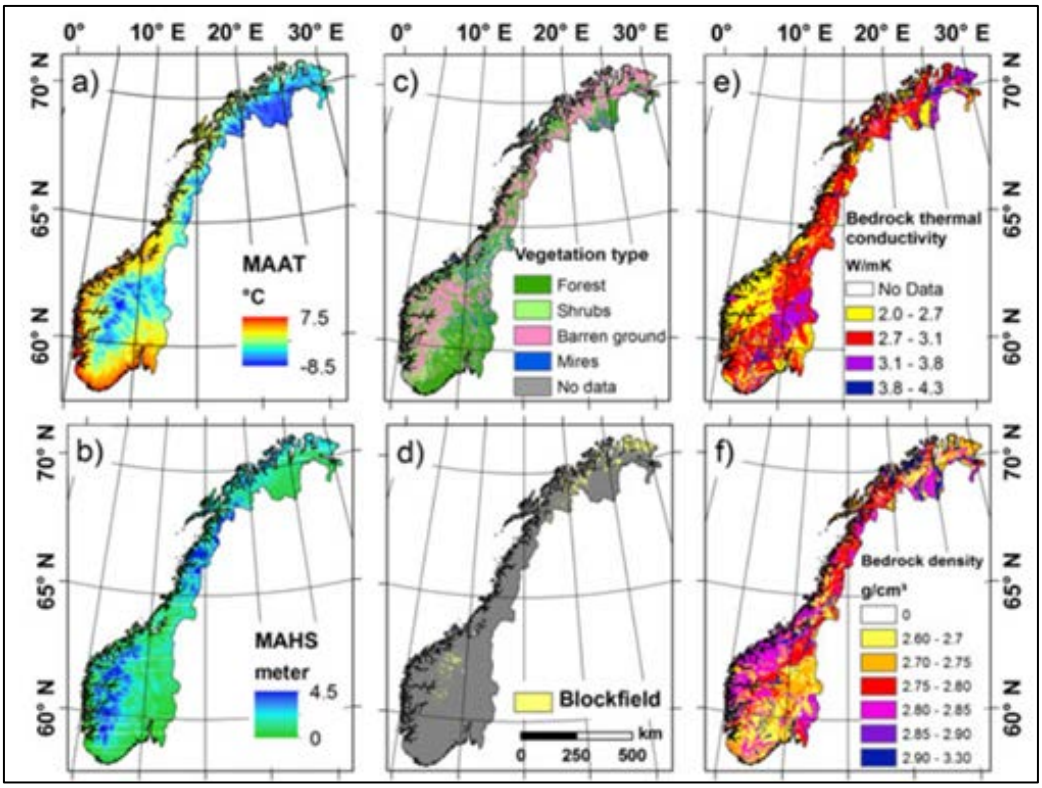

Figure 5. a) mean annual air temperature b) mean annual snow height c) reclassification of CORINE Land Cover 2000 vegetation map d) locations of blockfields determined using LANDSAT images e) thermal conductivity of bedrock f) density of bedrock determined using Geological Survey of Norway petrophysical data (Gisnås et al., 2013)

Once the environmental and geologic conditions for each grid had been identified, freezing and thawing n-factors were attributed to each land cover class, and the thermal conductivity for frozen and thawed soils were assigned to each of the different sediment classes, allowing for the estimation of TTOP and the presence of permafrost in each grid. The results of the model were then validated using borehole temperatures, permafrost landforms, and comparison to a basal temperature of snow (BTS) model of permafrost probability. The validation showed good agreement between the CryoGRID 1.0

estimations and physical measurements, although there are likely variations in ground surface temperatures on scales smaller than the grid area which the model fails to produce.

A modified TTOP equation was also used in a high resolution permafrost distribution study in Labrador-Ungava (Way & Lewkowicz, 2016). TTOP and mean annual ground temperatures (MAGT) for the 1,200,000 km^2 were modelled at a 250 m by 250 m resolution, using air temperature station data throughout the region and a unique n-factor parameterization method to account for the large regional snow cover differences in the study area. The ground surface temperatures produced in this study showed good agreement with those from previous MAGT maps. Additionally, the model was shown to correctly predict the presence of permafrost above the tree line in the mountains of eastern Labrador and the absence of permafrost in low elevation of the Torngat Mountains. However, permafrost in palsa fields (peaty permafrost mound containing segregated ice layers) along the Labrador coastline is not shown by the model, despite its known presence in these areas. The authors cite several possible explanations, including that the model uses resolution with is not fine enough to distinguish these areas from the surrounding environment, possible discrepancy in the land-cover classification leading to incorrect n-factor and thermal offset parameterizations, or that the palsas are at a disequilibrium with the current climate. Despite the differences between the model and reality in some regions, this study indicates that the TTOP model is applicable at high resolution and also highlights the variability demonstrated by high resolution models not produced through coarser resolution studies.

2.3.4 High Arctic Permafrost Modelling

2.3.4.1 CryoGRID

CryoGRID 1 was also used in conjunction with remotely sensed ground surface temperatures to predict the presence of permafrost on land bordering the North Atlantic, including Scandinavia, parts of the Canadian Archipelago, Greenland, and Siberia (Westermann et al., 2015). The resolution of the study was 1 km by 1 km, corresponding to the resolution of the MODIS sensor used to determine ground temperatures. However, due to clouds, which interfere with remote sensing technology, prolonged periods with no data existed over the study period. To combat this, ERA reanalysis (combination of observed and modelled data) was used to merge the MODIS temperature data with a gap-free time series from meteorological stations and observations. The modelled ground surface temperature values were then compared to borehole temperatures from the International Permafrost Association. Once the ground surface temperature map was complete (Figure 6), the CryoGRID 1 model was utilized to determine TTOP across the study area.

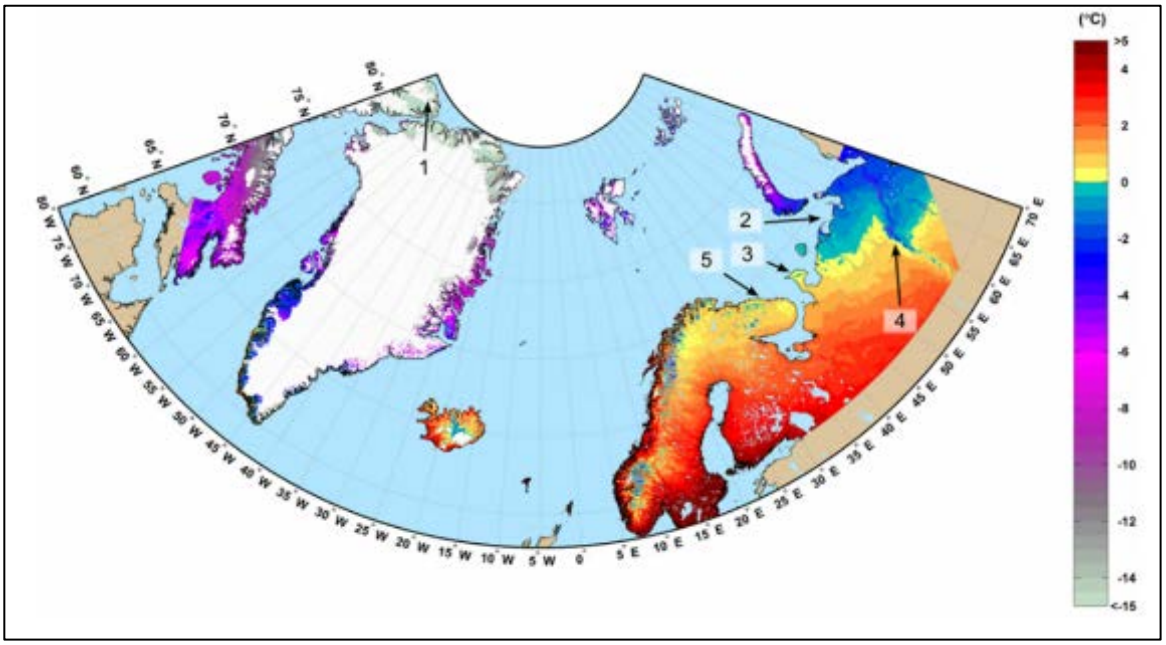

Figure 6. Average modelled MAGT for the North Atlantic study region. Numbers indicate specific geographic features within the study area (Westermann et al., 2015)

When compared with the borehole temperatures, the remotely sensed temperatures were in good agreement, however, the largest standard deviations occurred on Baffin and Ellesmere Islands in the Canadian Archipelago. This may indicate large spatial variations in temperatures in these locations, which may not be detected by the model or remote sensing data, possibly due to the model resolution or errors in the correction for windblown snow redistribution used over areas of bare ground or low vegetation as determined by MODIS land cover detection. Additionally, one drawback to using remotely sensed data, aside from gaps due to cloud cover, is that the satellite limits the resolution of the study, however, as technology improves this may become less of an issue. This study, however, does detect some variability in MAGT on Baffin and Ellesmere Island which have not been demonstrated in previous modelling studies, most likely since this model uses higher resolution. Therefore, it may also be hypothesized that studies using even higher resolution may identify further variations.

2.3.4.2 TTOP Model

Henry and Smith (2001) also used the TTOP model in permafrost regions of Canada to produce a national-scale map of near surface ground temperatures using Geographic Information Systems (GIS) software. The inputs required for the TTOP model were compiled into geographic data layers for the study area. The air freezing and thawing indices layers were created using point location, monthly air temperature data from Environment Canada's monthly climate data which was then interpolated using the inverse squared distance weighting method to produce a continuous surface. Since the surface offset is largely determined by the freezing n-factor, the thawing n-factor in this study was assigned a uniform value of one. The freezing n-factor layer was produced using snow depth data from the Meteorological Services of Canada's Canadian snow data and the Canadian monthly climate data from Environment Canada. The data for each point station were averaged over the recorded period and then interpolated to estimate snow cover depth for areas that did not have direct measurements. Lastly, the range of thermal conductivity ratios for the study area were estimated by using a surface geology map of Canada and dividing the surface material into three classes to infer about the soil properties at each map grid. Using GIS, Henry, and Smith (2001) calculated the value of TTOP for each 10 km x 10 km grid by inputting the parameters for each individual grid cell, determined from the individual layers, into the TTOP calculation equation. The results of this model show TTOP for the Canadian High Arctic as less than -15 °C (Figure 7).

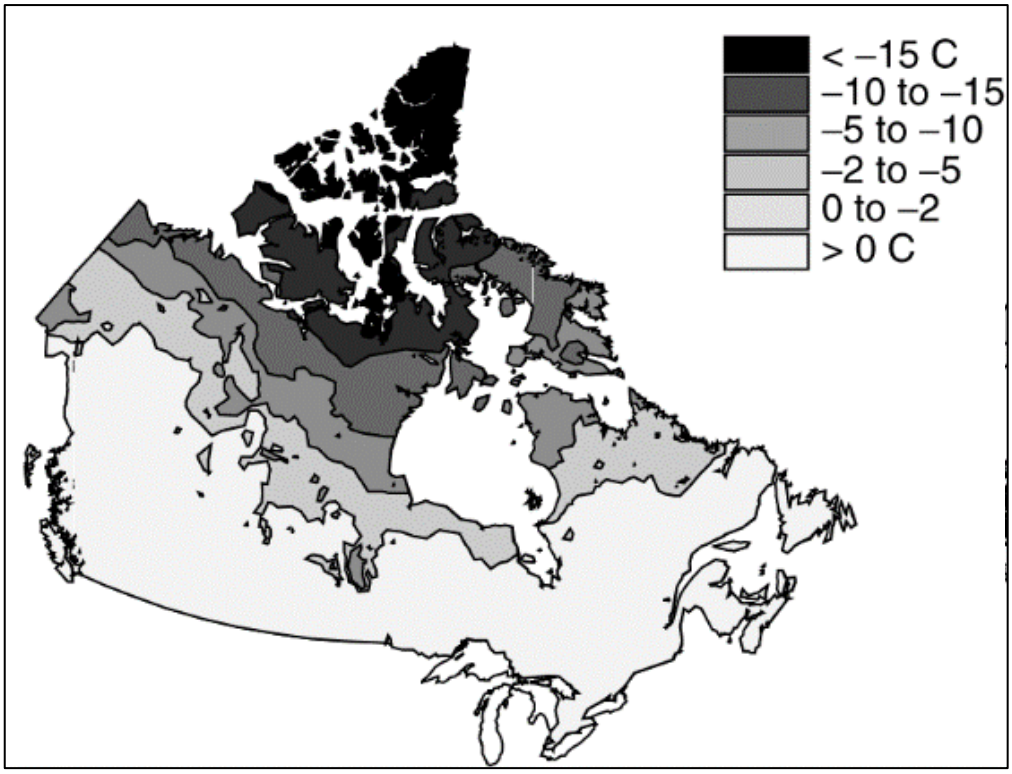

Figure 7. Map of ground temperatures calculated using the TTOP model. These temperatures were then used to predict the presence or absence of permafrost throughout Canada. (Henry & Smith, 2001)

A visual and statistical comparison between the model's output map for ground temperatures and the published ground temperature map of Canada yielded similar results, confirming that the TTOP model can be used as a method for determining permafrost distribution over large areas. However, once again local variability in TTOP is not detected by the model since it is produced at a coarse resolution. Additionally, the length of the temperature record, limited by station data, may also be a source of error since the time used may not be indicative of the normal climate, leading to uncertainty about permafrost extent, especially near the zonal boundaries.

At Cape Bounty on Melville Island in the High Arctic, the TTOP model was used to determine MAGST and TTOP for point locations across a stream channel to identify

possible areas of increased aquatic and biochemical activity due to variation in snow cover (Bonnaventure et al., 2016). Climate data from 2013 as well as generalized thermal conductivity for the frozen and unfrozen soil were used as inputs for the TTOP model. The results showed large differences in near surface ground temperature, with a smallest surface offset of 0 °C and the largest thermal offset of +30 °C. This indicates the thermal heterogeneity of the High Arctic ground surface and the need to reconsider the notion of High Arctic homogeneity in permafrost modelling studies. One source of uncertainty in TTOP modelling studies is the use of climate data for only one year to estimate ground surface and TTOP, since if the year used was different from the climate normal, it is possible that the ground surface temperatures and TTOP may be over- or underestimated.

2.4 Gaps and Areas for Future Work

Most permafrost modelling studies in the High Arctic consider the area to be homogeneous and often model at national or regional scales (Henry & Smith, 2001; Westermann et al., 2015). Therefore, these studies miss thermal variability at the sub grid cell level as demonstrated by Bonnaventure et al. (2016) (Figure 8).

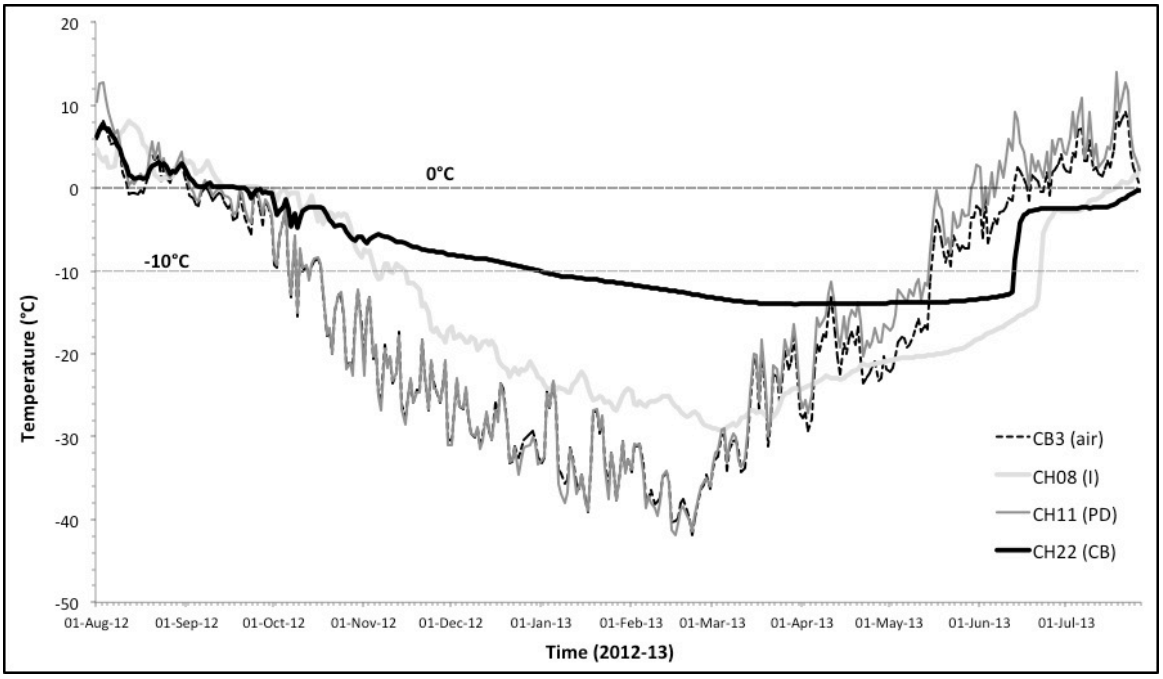

Figure 8. Comparison of ground surface temperatures and an air temperature at different vegetation classes near a channel bed at Cape Bounty. (Bonnaventure et al., 2016)

The results of this study also demonstrate the need to reconsider the notion of High Arctic homogeneity in permafrost modelling studies as the microscale temperature variations may have a significant impact on changes to High Arctic permafrost under climate change. Therefore, more studies considering the spatial, thermal heterogeneity of the High Arctic are necessary to further understanding of current thermal conditions and to improve predictions of thermal conditions under climate change.

For these studies the most logical model to use is the TTOP model, which, in conjunction with n-factors, predicts permafrost and ground temperatures, has been shown to be accurate at high resolution over local scales, and requires few input parameters and less computational time than the NEST model (Bonnaventure et al., 2016; Riseborough et al., 2008). The TTOP model has been successful previously when used over regions of the High Arctic, while studies using the NEST model have not been conducted in this region (Westermann et al., 2015; Ou et al., 2014; Zhang et al., 2012). Therefore, to ensure

accurate representation of ground and permafrost temperatures, the NEST model will first need to be validated for use in High Arctic studies. Additionally, even if the NEST model was validated, studies will be preliminary in both scale and location and currently there may not be enough climate and environmental data to accurately run the NEST model. Furthermore, the NEST model uses LAI, determined using remote sensing, which is currently not collected at resolution fine enough for microscale modelling studies. It can, therefore, be concluded that the TTOP model is currently the most applicable model for microscale ground and permafrost temperatures studies in the High Arctic.

Chapter 3

Methods

3.1 Study Area

The study area for this project is a paired watershed at the CBAWO on the south-central coast of Melville Island, Nunavut (Figure 9).

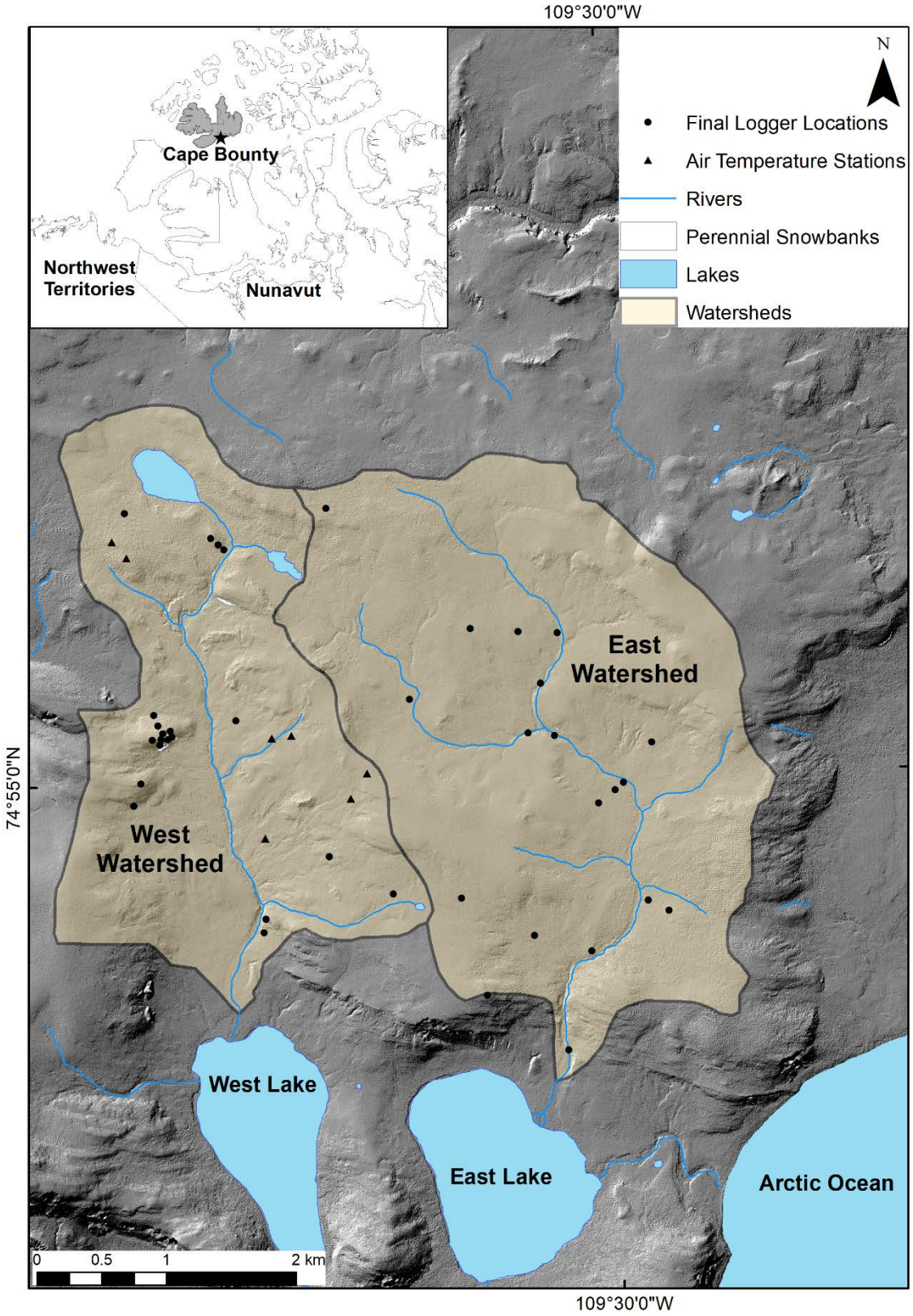

Figure 9. Map of study area. Total area is less than 25 km^2

Cape Bounty is a polar desert with an annual mean air temperature (AMAT) ranging between -10.0 and -12.8 °C (2005-12) and annual precipitation of ~125 mm, of which about 60 % falls as snow (Maxwell, 1981; Woo & Young, 1997). Winter is the dominant season, lasting from September to late May, and summers are short lasting only from June to August. The 2013- 2014 July and January temperatures averaged 6 °C and -26 °C, respectively. Cape Bounty is underlain by continuous permafrost and has a total relief of about 100 meters (Lewis et al., 2012) (Figure 1). Ground ice content in the upper 10-20 meters is considered to be medium to low, ranging from 20 % to less than 10 % (Figure 1). The vegetation is composed of sparse polar desert tundra communities including polar semi- desert, mesic tundra, and wet sedge meadows and the siltstone and sandstone bedrock is overlain by unconsolidated glacial and marine sediment (Figure 10) (Hodgson et al., 1984; Walker et al., 2002; Gregory, 2011; Lewis et al., 2012).

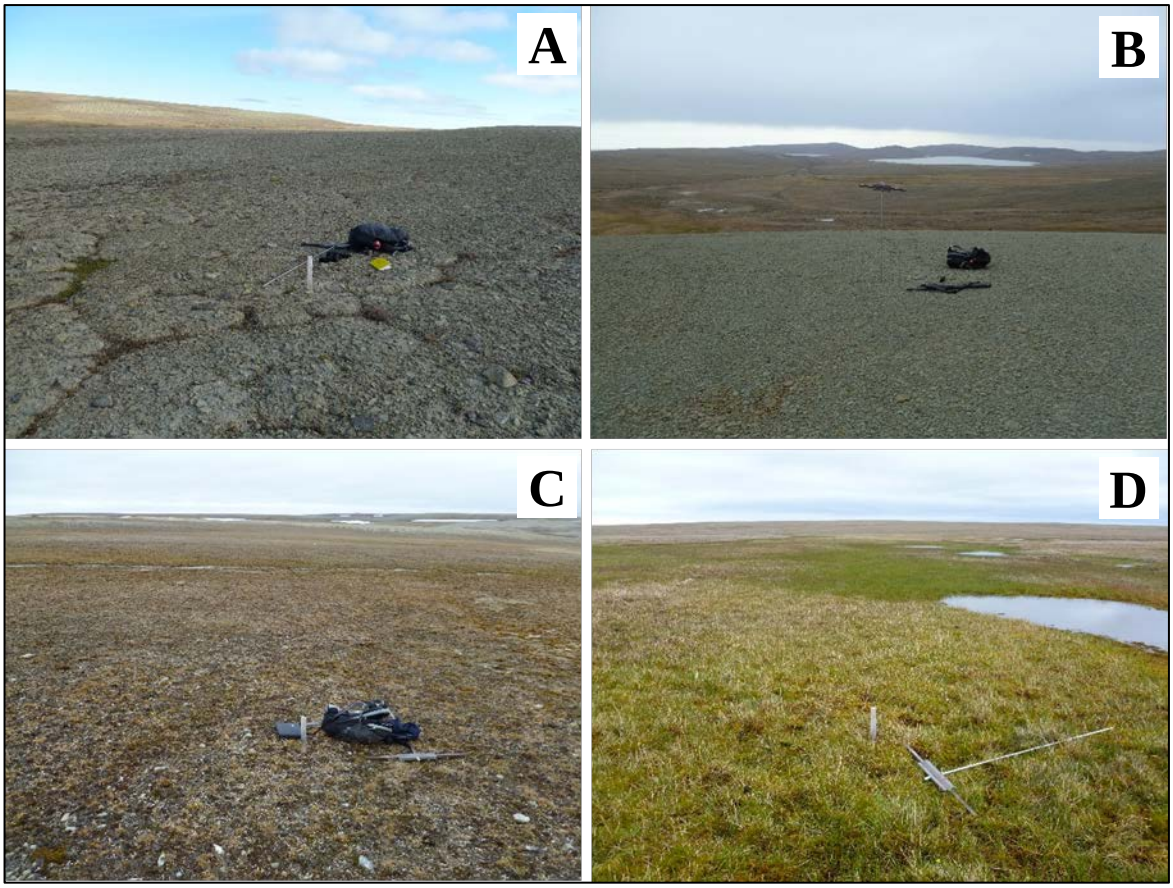

Figure 10. A Land-cover classification for Cape Bounty A) Polar desert B) Bare ground C) Mesic Tundra D) Wet Sedge

The paired watershed consists of the West and East watershed (Figure 9), which are similar in topography and vegetation. The CBAWO was chosen as it is an area of continuous permafrost with known variation in snow depth (e.g. Bonnaventure et al., 2016), both of which are necessary study area features for this project. Additionally, the study area was chosen for logistical reasons as this location is visited each year by other researchers, who helped in the deployment and maintenance of the data loggers, and the site is more accessible and easier to travel to than other more remote High Arctic locations. From a data stand point, this location was suitable for this study as there is already an existing network of loggers for air and ground temperatures and baseline climate data are available. Lastly, the natural division of the study area into the East and

West watersheds allows for a built-in validation study to test the produced models since the vegetation and topography are similar.

3.2 Data Collection and Field Methods

To gather data on ground surface temperatures, Onset Hobo™ pendant (UA-001-64) (Onset, USA) loggers, were deployed throughout the study area during mid-August 2016. This specific data logger was selected as it is inexpensive enough to allow the necessary number to be purchased while also recording temperature at a high enough accuracy (0.54 °C) and precision (0.14 °C) to capture the variability across the temporal and spatial extent of the study and area. These loggers also demonstrated an accuracy of about 0.6 °C at temperatures of -60 °C in cold chambers (Bonnaventure et al., 2016).

Possible locations for logger placement were analyzed using high-resolution surface layers for a variety of topographic variables, including elevation, aspect, topographic position index (TPI), surface roughness, wetness and moisture, wind exposure, and vegetation. A DEM of Cape Bounty, generated from a high-resolution satellite image, and spatial analyst tools in ArcGIS 10 (ERSI, USA) were utilized to create the TPI, slope, potential incoming solar radiation (PISR), and wetness index maps used to select sites. A wind exposure map was generated by inputting the prevailing winter wind direction at Cape Bounty (south) into a wind sheltering algorithm in the statistical program R (RSAGA package, Alexander Brenning). The land cover classification was created by classifying two satellite images using the three vegetation classes in Cape Bounty (polar semi- desert, mesic tundra, and wet sedge meadows) and barren, water, or permanent snow bank non-vegetated classes (Gregory, 2011). These topographic variables influence where redistributed snow is deposited and where it is

removed. TPI and slope were considered in selecting sites as snow generally accumulates in gullies and valleys and the thinnest snow cover is found on hilltops and flat, exposed areas (Woo et al., 1983; Yang & Woo, 1999). Snow depth in relation to slope orientation is dependent upon the dominant wind direction explaining why both PISR (proxy for aspect) and wind sheltering model are considered in site selection (Woo et al., 1983; Yang & Woo, 1999). PISR is a linear variable, making it easier to incorporate in a model than aspect which is circular (0 and 350° are closer than 0 and 180°). The primary variables considered during site selections were the topographic influences on snow cover including terrain, slope, concavity, channeled area versus non-channeled areas, and vegetation, since snow cover is known to be the dominant influence on ground surface temperature and TTOP. Sites were then selected to maximize the heterogeneity of snow cover by placing loggers in areas with the highest and lowest expected snow cover based on the aforementioned topographic variables (Figures 11-16 and figures in appendix). Additionally, sites were also selected to collected ground temperature data under the entire range of snow cover conditions.

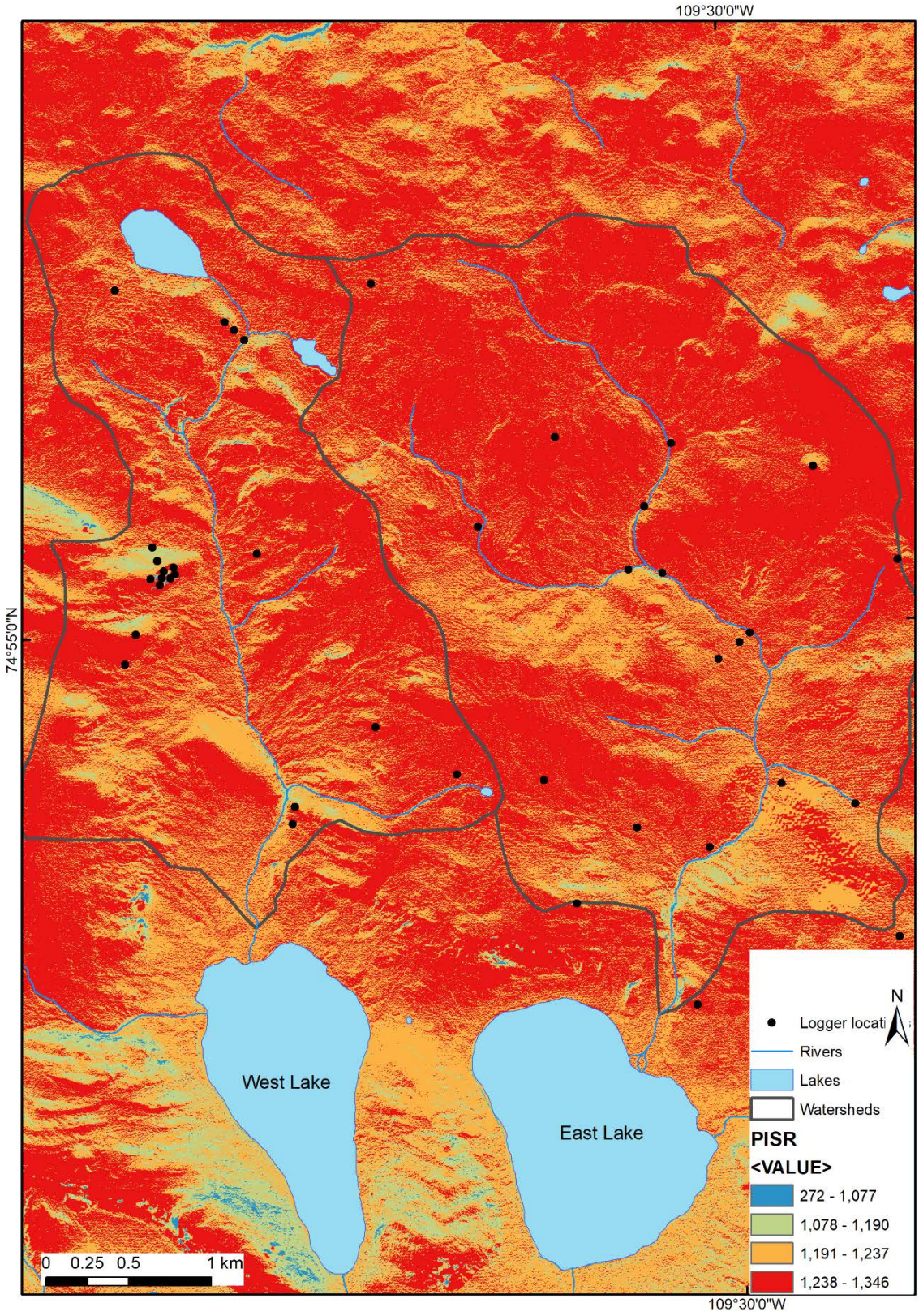

Figure 11. Potential incoming solar radiation (PISR) over the study area. PISR is used as a proxy for aspect

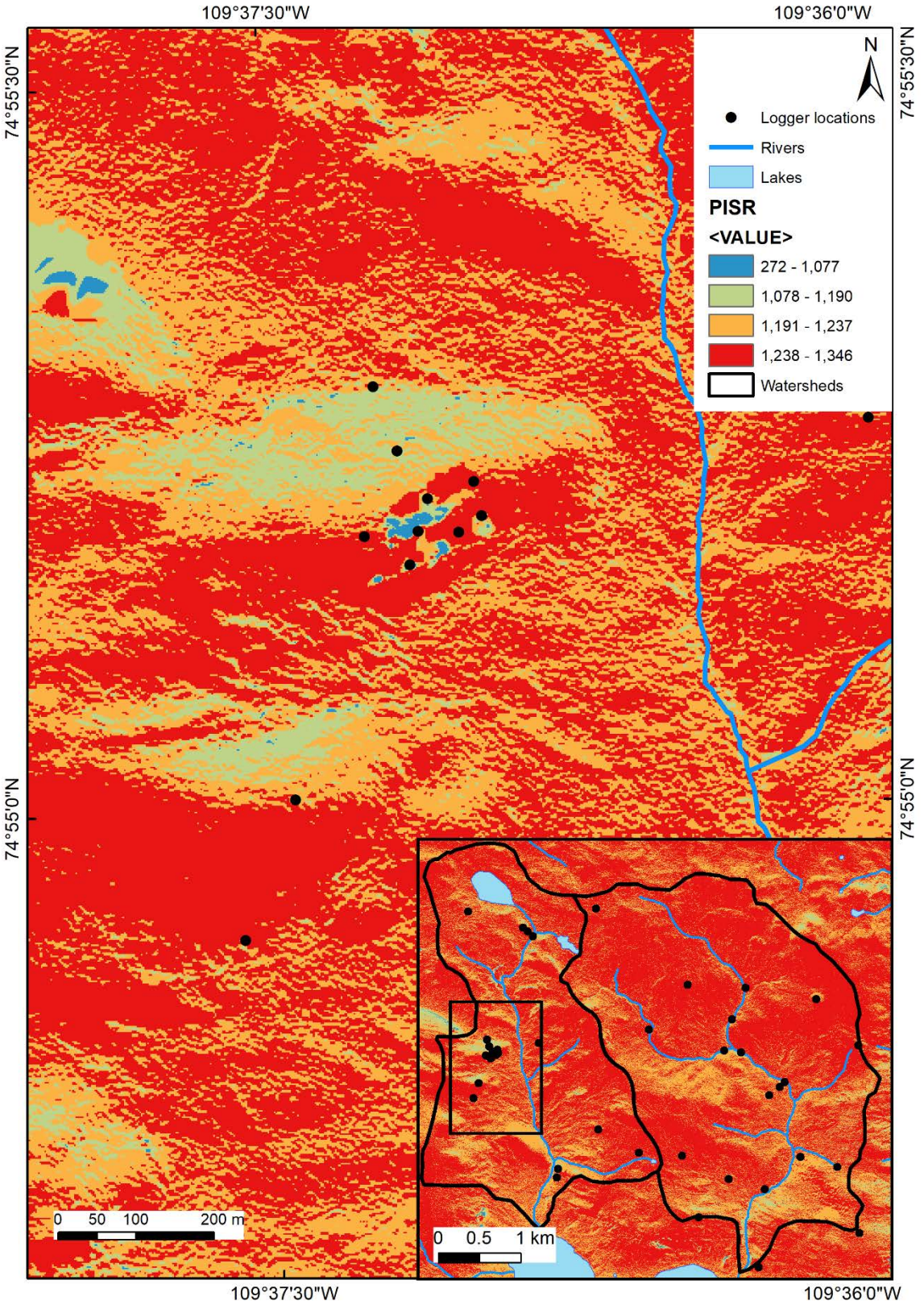

Figure 12. Closer view of PISR for cluster of loggers in the West watershed

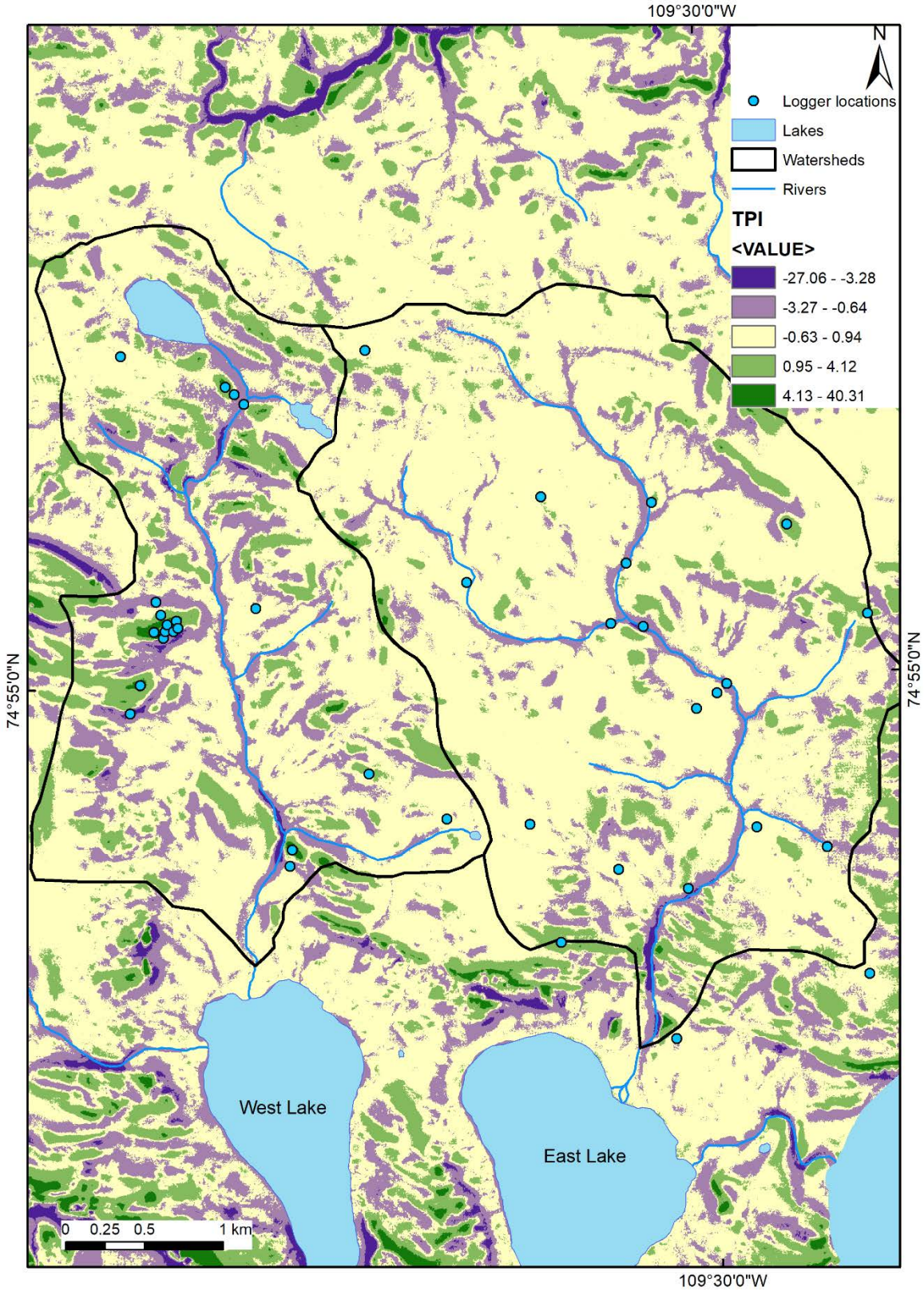

Figure 13. Topographic position index (TPI) over study area

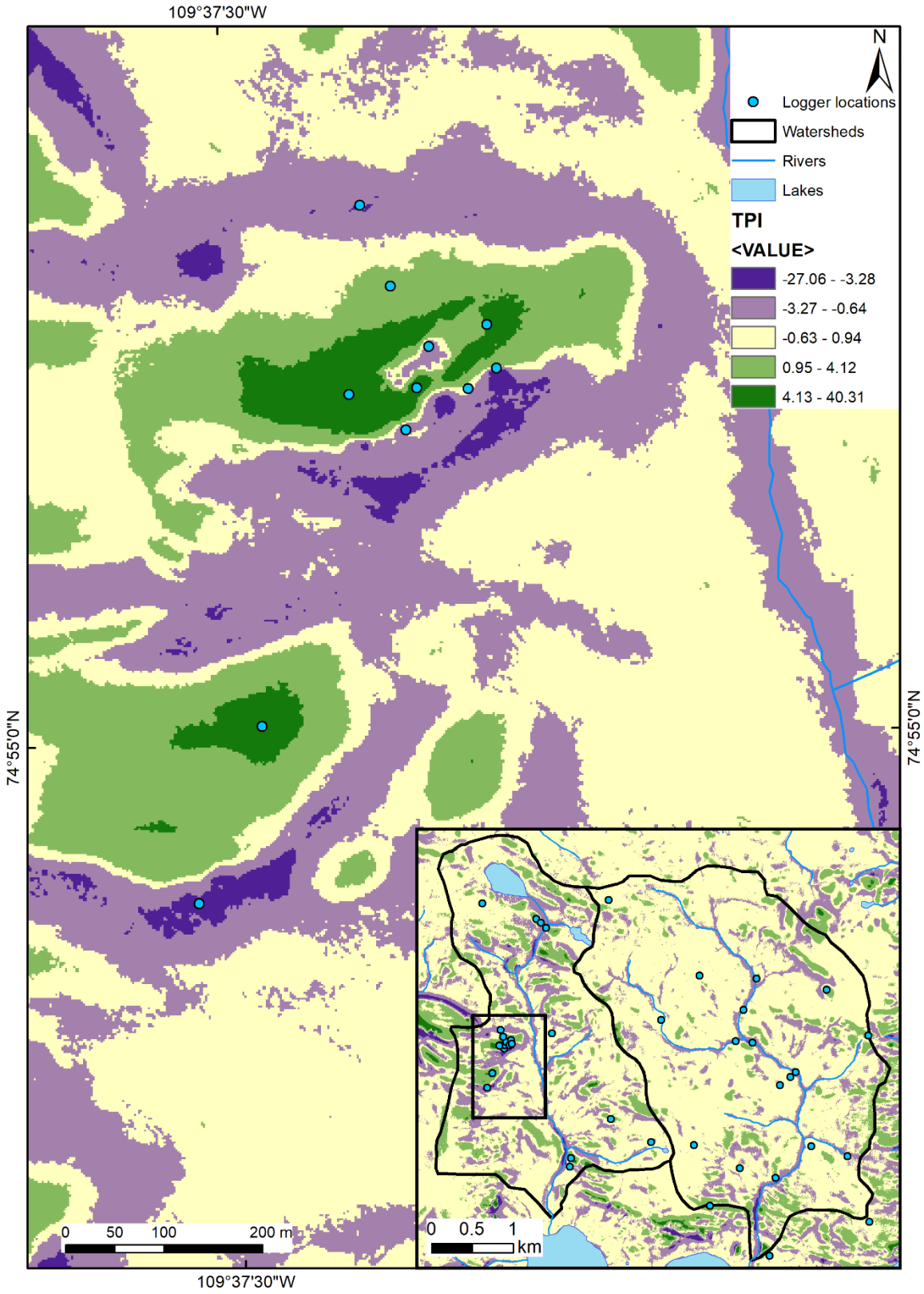

Figure 14. Closer view of TPI for cluster of loggers in the West watershed

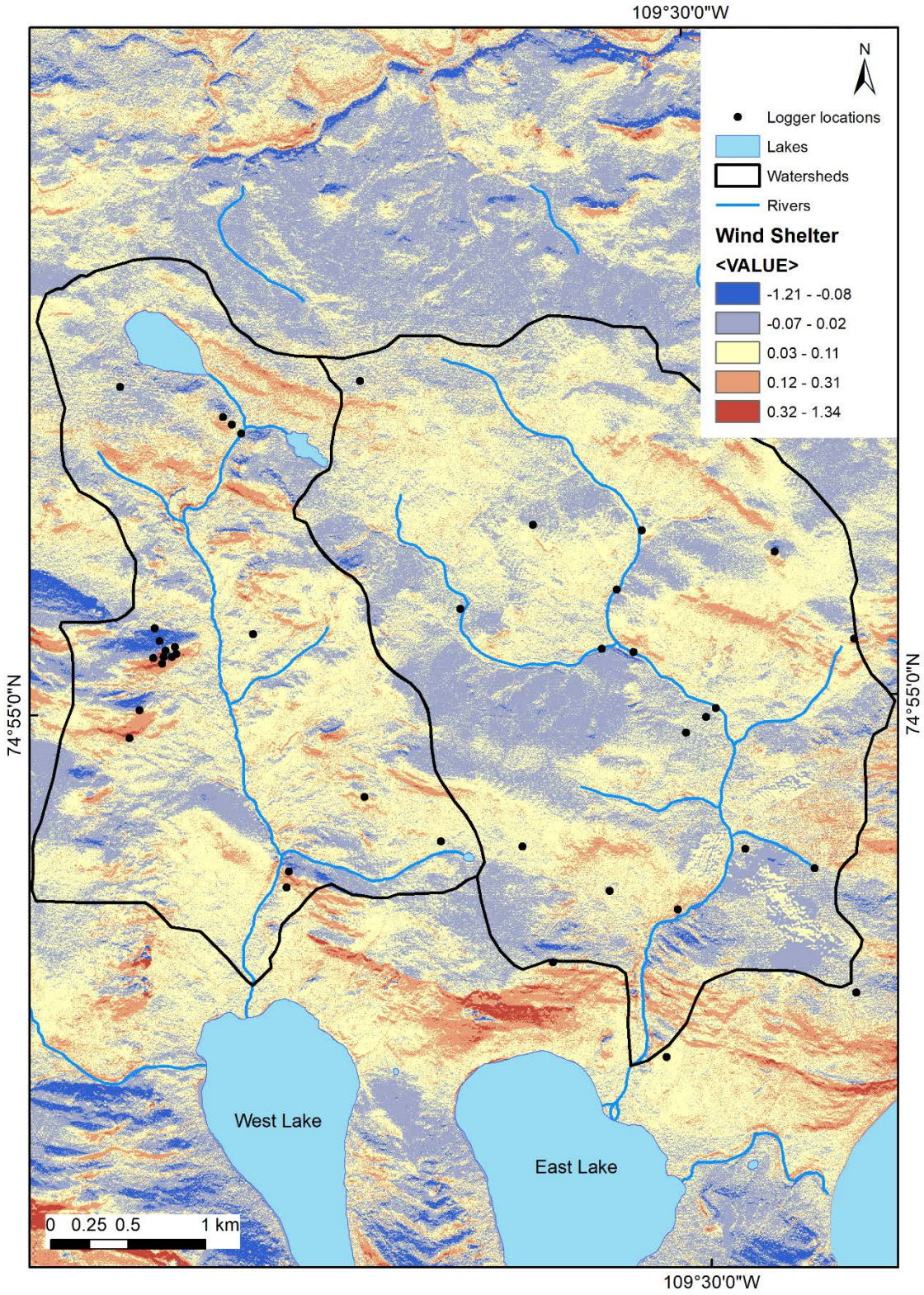

Figure 15. Wind shelter over the study area with a high wind shelter indication locations of snow deposition and areas of low wind shelter indicate locations of snow removal

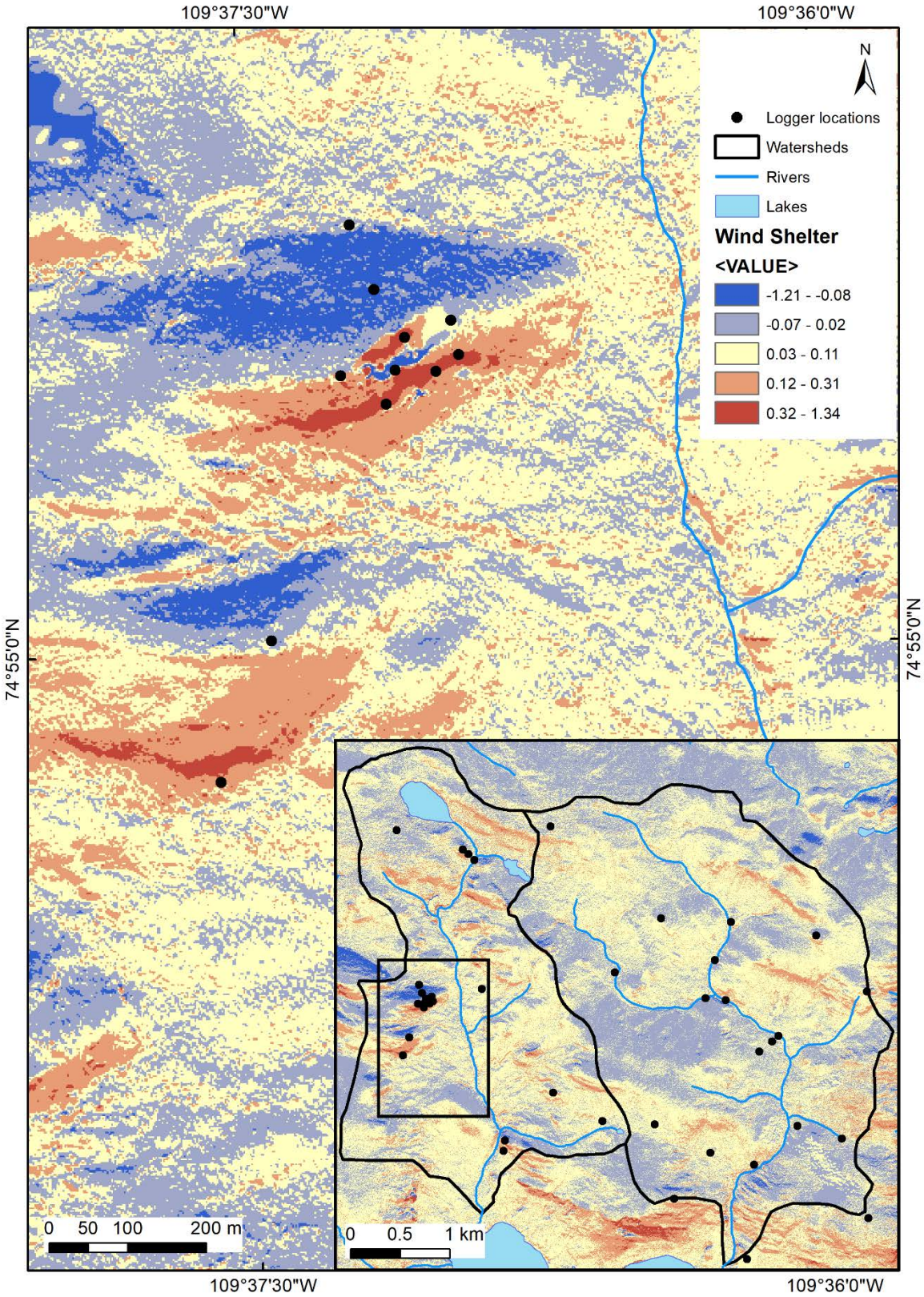

Figure 16. Closer view of wind shelter for cluster of loggers in the West watershed

The loggers were deployed during the middle of August 2016 with 19 loggers placed in the East watershed and 20 placed in the West watershed. Loggers were buried just beneath the ground surface at a depth of about 2-5 cm and recorded temperature hourly. During the 2017 field season, the loggers were collected and replaced, barring any loss or disturbance. Of the 40 loggers proposed only 39 were deployed (20 in the West watershed and 19 in the East watershed). E10 was not deployed as its location was deemed to be too close to the coast and would increase the chance of encounters with bears. Additionally, the locations of four loggers in the East watershed were moved from their proposed location for the same reason (Figure 17).

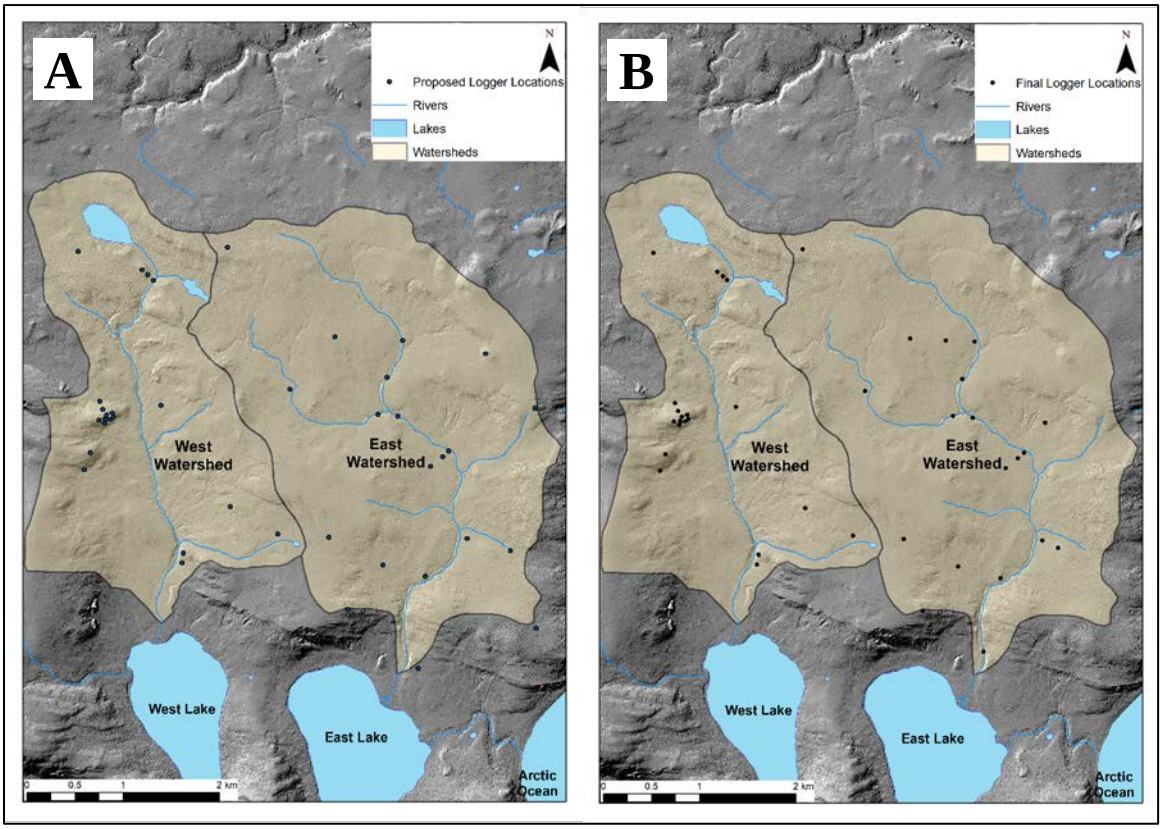

Figure 17. A) Map of proposed logger locations B) Map of the actual logger placement. Loggers along the eastern side of the East watershed were moved inward due to concern with bear encounters.

3.3 Data Processing Methods

3.3.1 Current Temperature Variability Models

Once the air and ground temperature were collected at points sites the data were converted from hourly measurements into daily, monthly, and annual (Aug-Aug) averages. Freezing and thawing degree-days (FDD_g and TDD_g) at each site were calculated through the absolute value of summation of all the daily average temperatures in the freezing season (below 0 °C) and the thawing season (above 0 °C) for August 2016- July 2017. For sites with air and ground temperature measurements n-factors were calculated directly. At sites with only ground temperature sensors the FDD_a and TDD_a from the nearest air temperature station were used to determine the n-factors. r_k values for sites were determined using the dominant vegetation type and known r_k values (Hinzman et al., 1998; Bonnaventure et al., 2016; Juszak et al., 2016). The values used were 0.63, 0.68, 0.70, and 0.73 respectively for channel beds, wet sedge, mesic tundra, and bare ground / polar desert. Next, point TTOP values for each ground temperature site were calculated using the TTOP model. For sites without 365 days of data (35 loggers ranging from 1-11 missing days) the average temperature for the month was used to gap-fill the record for the missing data.

3.3.1.1 Air Temperature Model

The relation found between air temperature and elevation was used to create the air temperature model (Lewkowicz & Bonnaventure, 2011). Since more air temperature stations were operational during the 2013-2014 season, regression analysis was used to calculate the surface lapse rate (SLR) using the annual average temperatures from stations during this year. This SLR was then applied with the 2016-2017 air temperature data and

the DEM to create the air temperature surface across both watersheds. The FDD_a and TDD_a surfaces were created using the same method as the AMAT surfaces, with a linear regression analysis between observed FDD_a and TDD_a and elevation used to determine the change with elevation. The value of change was then applied to the DEM to create the surfaces over both watersheds.

3.3.1.2 Ground Surface Temperature Model

To create the ground temperature model, multivariable linear regression was used to test for significance between the measured annual mean ground surface temperature (AMGST) and the topographic variables including: TPI, PISR, and elevation. As TPI was the only variable which produced a significant p-value, polynomial and linear regressions were run using the TPI values and the AMGST for selected, observed ground temperatures. A ground temperature surface for each regression was produced and compared against the measured AMGST at 5 sites which had been excluded in the model creation. After this it was determined that the polynomial surface produced the smallest error compared to the point data. Subsequently, regression was run for sites only in the West watershed and sites only in the East watershed. Both linear and polynomial trend lines were fit to the data and surfaces for each study area were created. The models were then tested in the other watershed for validation and the polynomial surfaces were chosen to be used in the subsequent modelling process. The AMGST values were capped at the highest observed AMGST of -3.8 °C as this was assumed to be the maximum possible temperature for the study area.

3.3.1.3 TTOP Model

The TTOP surface was generated through the creation of surfaces for each variable in the TTOP model equation. To create the n_f surface multivariable linear regression was utilized to determine the effect of different topographic variables. TPI was the only variable to have a significant p-value, and a linear and polynomial regression was run for TPI and the calculated n_f values for each site. Linear and polynomial regression n_f surfaces were generated and validated using 5 n_f values excluded from the model generation. Models for the East and West watersheds were then produced using the same method, only using East watershed and West watershed values respectively. These models were then validated against points in the opposite watershed. Modelled n_f values were capped at the minimum observed value (0.27) as it was assumed that n_f values at Cape Bounty would not surpass this value based on previous studies and theoretical estimations of the n_f values under the air temperature regime (Smith & Riseborough, 2002; Bonnaventure et al., 2016). Multivariable linear regression was then run for n_t with only n_f yielding a significant p-value. The n_t surface was then produced using the relation between n_t and n_f. Both linear and polynomial surfaces were generated for the combined watershed, the West watershed individually, and the East watershed individually and these were then validated as previously described. Generation of the r_k surface was completed using a land cover classification surface for Cape Bounty and known r_k values for each class (Figure 18).

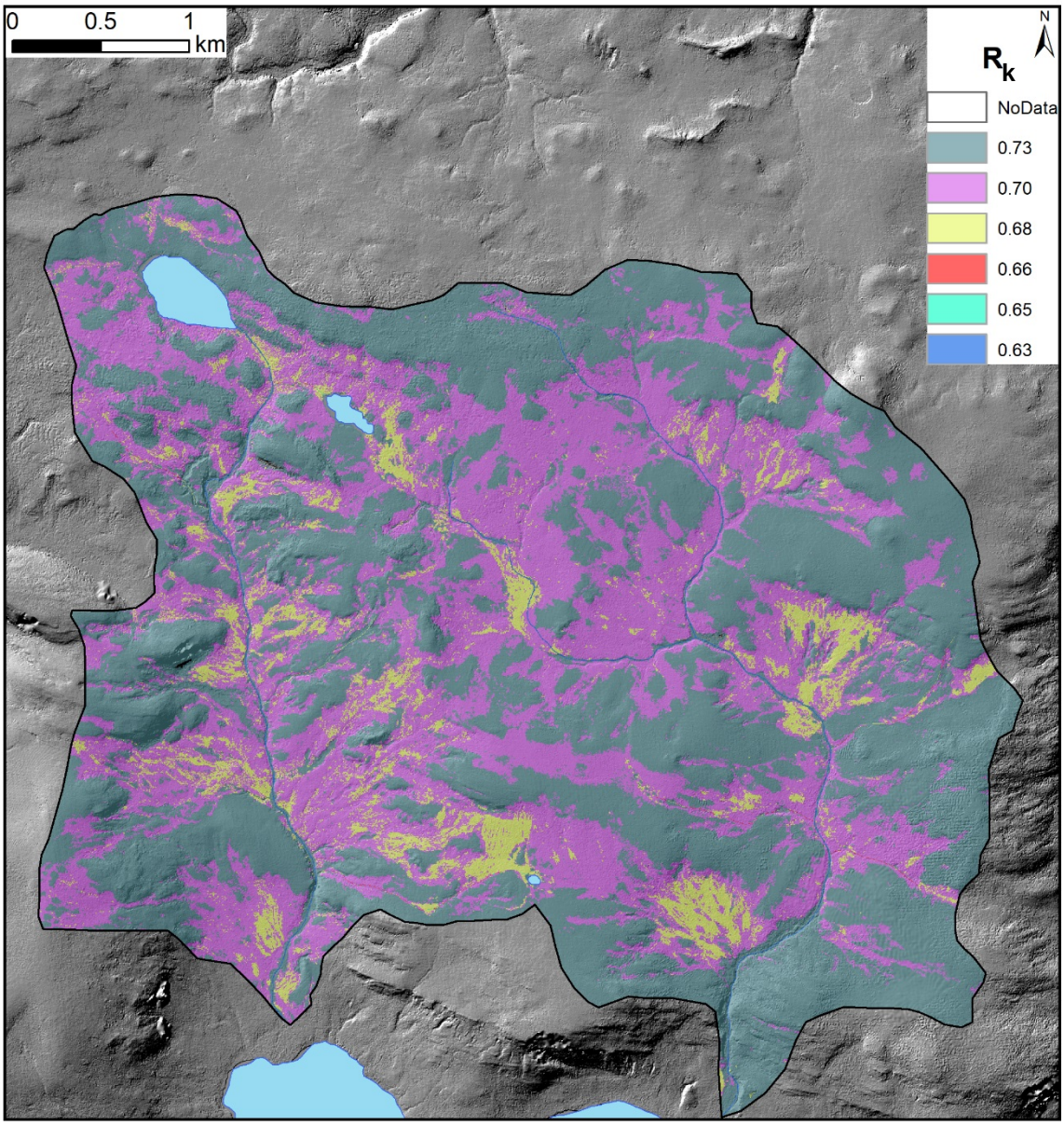

Figure 18. r_k surface created using a land-cover classification.

To input the channel bed r_k value, a feature file for the rivers at Cape Bounty was used with a 2 m buffer applied to tributary streams and a 5 m buffer applied to the East and West River. Pixels in the land cover classification raster overlapping with the main channels were given an r_k value of 0.63, while the r_k value for tributary streams was determined by the average of the standard channel bed value (0.63) and the r_k value of the underlying land cover classification. These surfaces were then combined using the TTOP

model to generate three TTOP surfaces, one using the Dual Watershed model, one using the West Watershed model, and one using the East Watershed model.

3.3.2 Future Temperature Variability Models

3.3.2.1 Air Temperature Model

To assess the impact of climate change on air temperature at Cape Bounty, the magnitude of predicted air temperature warming was derived using ClimateNa's (AdaptWest Project, 2015; Wang et al., 2016) 1981-2010 climate normal as the base year. The climate change scenarios were derived using the predicted new MAATs for RCP4.5 and RCP 8.5 for the 2050 and 2080 climate normals. The 2050 climate normal encompasses 2041-2070 and the 2080 climate normal is the average from 2071-2100. The ClimateNa predicted MAAT was determined using the ensemble projects, which are averages across 15 CMIP5 models (AdaptWest Project, 2015; Wang et al., 2016). These scenarios were chosen since they encompass the range of possible temperature variation in both the best and worst-case scenarios for each new climate normal. The magnitude of change for each climate change scenario was calculated by determining the difference between the MAAT over Cape Bounty for the 1981-2010 climate normal and each MAAT predicted over Cape Bounty for each climate change scenario. Once this was complete, each was added to the AMAT for Cape Bounty for 2016-17, to determine the new MAAT under each warming scenario. The change in FDD_a was calculated using the same method. ClimateNa only provides projected growing degree-days (degree days with temperatures greater than 5 °C), therefore, to calculate the change in TDD_a, linear regression analysis was utilized to derive a relation between the two variables. Using the

equation, TDD_a for each scenario and the climate normal were calculated. The magnitude of change was then derived and applied to the observed data.

3.3.2.2 TTOP Model

In order to create the new TTOP surfaces, the changes in the TTOP model variables first needed to be quantified. The derivation of the FDD_a and TDD_a changes were described in the previous section. Due to limited data on predicted soil moisture and vegetation changes and the limited impact of r_k on TTOP at Cape Bounty, the r_k values were held constant. The change in n_f under each scenario was determined using theoretical curves based on air temperature and snow depth (Figure 4). To derive n_f curves for MAAT between those expressed on the graph, averages were taken at each snow depth for the curves of MAAT above and below the chosen MAAT (Figure 19).

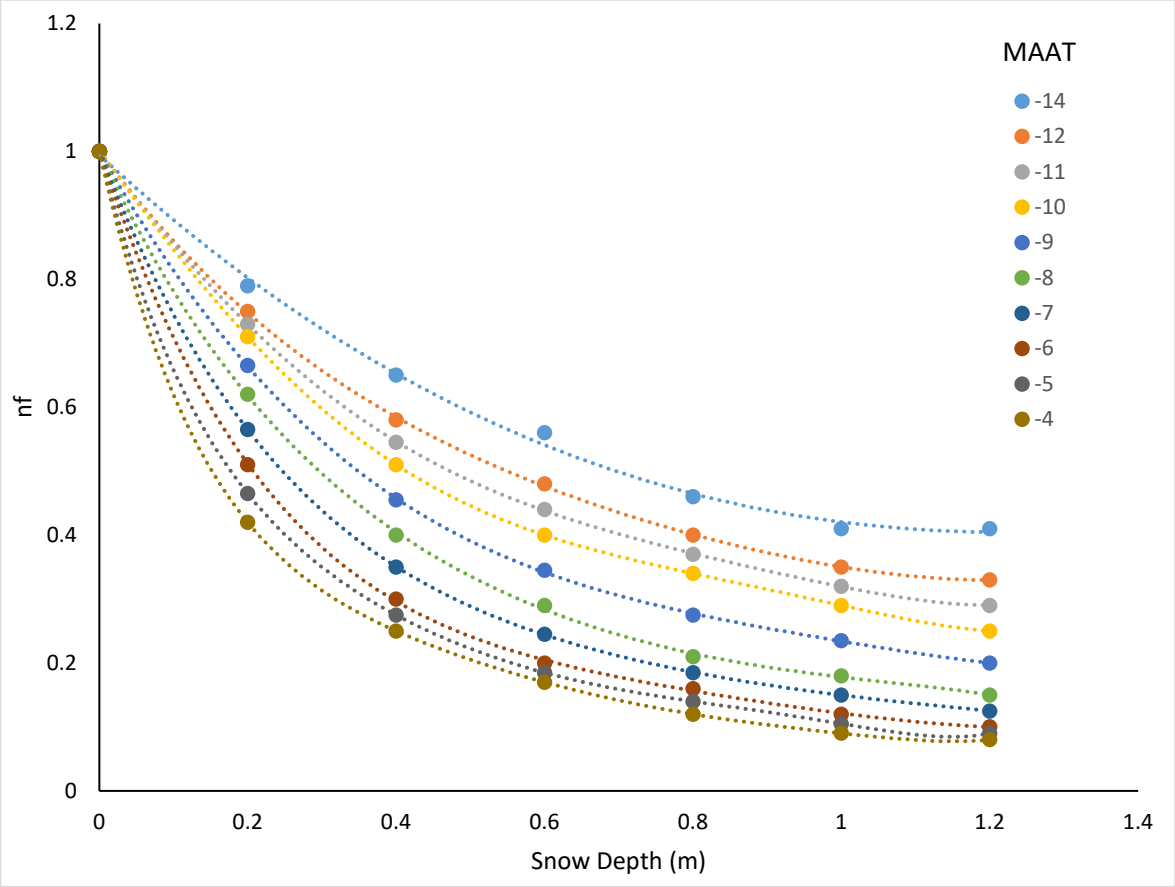

Figure 19. Theoretical n_f curves reproduced from Smith & Riseborough (2002).

Since the AMAT for Cape Bounty during the year of observed n_f data was -14.7 °C, a curve was created by applying the magnitude of difference in n_f values between the -12 °C and -10 °C curves to the -12 °C curve in the opposite direction. The new n_f curve was chosen based on the predicted new MAAT. Polynomial regression was used to find the new n_f values, by plotting n_f values along the -14 °C curve against those for the new predicted temperature curve at the same snow depth and fitted with a polynomial trendline. The equation for this line and the original n_f surface were then utilized to create new n_f surfaces for each scenario. n_t for each scenario was held constant as it was assumed that the ratio between TDD_g and TDD_a would remain constant. The new perturbed surfaces were then combined using the TTOP model to generate the new TTOP surfaces.

Chapter 4

Results

4.1 Measured or Modelled Point Data

4.1.1 Air Temperature

Measured AMAT over the watershed varied by only 0.2 °C while observed annual FDD_a and TDD_a ranged by 36 (0.6%) and 24 (10%) degree-days respectively (Table 1).

Table 1. Measured air temperature metrics for 2016-17

Station	AMAT (°C)	FDD_a	TDD_a
Mainmet	-14.8	5584	227
Westmet	-14.7	5581	240
Upper Goose	-14.9	5608	220
Lower Ptarmigan	-14.7	5571	245
Upper Ptarmigan	-14.8	5596	233

4.1.2 Ground Surface Temperature and TTOP

Of the 39 ground temperature sensors deployed, a complete data set was only recovered for 36. The logger at site W1 failed in December 2016, the logger at site W5 was still buried in snow and was irretrievable, and the logger at site W18 was ejected from the ground at some time during the year.

Observed ground surface temperatures and point modelled TTOP varied substantially more than air temperatures over both watersheds (Table 2).

Table 2. Measured ground surface temperature metrics and point modelled TTOP for 2016-17

Site	AMGST (°C)	FDD_g	n_f	TDD_g	n_t	TTOP (°C)
W2	-9.67	3845	0.69	327	1.48	-9.9
W3	-12.3	4502	0.80	140	0.64	-12.1
W4	-13.0	5071	0.90	411	1.86	-13.1
W6	-13.2	5211	0.94	460	1.88	-13.4
W7	-4.8	1858	0.33	144	0.60	-4.8
W8	-10.8	4248	0.76	374	1.53	-10.9
W9	-13.1	5064	0.91	382	1.56	-13.1
W10	-12.8	5041	0.91	428	1.75	-13.0
W11	-7.4	2900	0.52	240	0.98	-7.5
W12	-12.2	4816	0.86	422	1.72	-12.4
W13	-13.0	5202	0.93	541	2.21	-13.2
W14	-12.8	4959	0.89	384	1.57	-12.8
W15	-7.0	2617	0.47	147	0.60	-6.90
W16	-12.8	4978	0.89	361	1.47	-12.9
W17	-11.7	4417	0.79	250	0.92	-11.6
W18	*-13.4*	*5380*	*0.96*	*618*	*2.28*	*-13.5*
W19	-8.8	3400	0.61	263	0.97	-8.8
W20	-7.0	2739	0.49	156	0.58	-7.2
E1	-12.7	4898	0.88	347	1.53	-12.7
E2	-10.3	3900	0.70	233	1.03	-10.2
E3	-5.7	2218	0.40	193	0.85	-5.7
E4	-9.0	3333	0.60	97	0.43	-8.9
E5	-10.1	3838	0.69	224	0.99	-10.1
E6	-13.8	5299	0.95	364	1.65	-13.8
E7	-13.8	5267	0.94	378	1.72	-13.7
E8	-12.0	4576	0.81	297	1.35	-12.0
E9	-11.9	4414	0.79	253	1.15	-11.6
E11	-3.8	1501	0.27	151	0.67	-3.9
E12	-11.9	4613	0.83	373	1.64	-11.9
E13	-11.8	4524	0.81	294	1.30	-11.8
E14	-7.1	2753	0.49	216	0.95	-7.2
E15	-12.2	4726	0.85	384	1.69	-12.2
E16	-11.0	4252	0.76	318	1.40	-11.0
E17	-13.0	5023	0.90	372	1.37	-13.0
E18	-6.1	2253	0.40	76	0.01	-6.2
E19	-13.4	5189	0.93	383	1.69	-13.5
E20	-11.7	4445	0.80	275	1.21	-11.7
Range	**10**	**3798**	**0.73**	**465**	**1.19**	**9.9**

W18 is italicized as it was recovered unburied which may impact the timing and value of the temperatures especially during the thawing season

Sites with the warmest ground surface temperatures for each watershed were E11 and W7, while sites with the coldest ground surface temperatures were sites W6 and E6. Sites with warmer AMGSTs generally had lower n_f values than sites with colder AMGSTs. Similarly, sites with high FDD_g correspondingly had high n_f and low AMGSTs. However, sites with high TDD_g and n_t did not have the warmest AMGSTs. Generally, sites with these metrics had lower AMGST than sites with lower n_t values. Additionally, sites with high n_f values generally had high n_t values.

Sites with the warmest AMGST also had the warmest TTOP, E11 and W7. Similarly, sites with the coldest AMGST also had the coldest TTOP, W6 and E6. Overall TTOP and AMGST showed a similar distribution across both watersheds. Colder TTOP also generally corresponded with higher n_f and n_t values along with higher FDD_g and lower TDD_g. Ground temperature metrics and TTOP had a consistent distribution of sampled values, with similar maximum, minimum and average values for both watersheds (Table 3).

Table 3. Comparison of statistics for each watershed's temperature metrics

	West Watershed			**East Watershed**		
	Max	Min	Average	Max	Min	Average
AMGST (°C)	-4.8	-13.2	-10.7	-3.8	-13.8	-10.6
FDD_g	5211	1858	4169	5299	1501	4054
TDD_g	541	140	320	384	76	275
n_f	0.94	0.33	0.75	0.95	0.27	0.72
n_t	2.21	0.58	1.31	1.72	0.01	1.19
TTOP (°C)	-4.8	-13.4	-10.8	-3.9	-13.8	-10.6

The thermal variability at Cape Bounty is demonstrated not only through the measured ground surface temperatures but also in the lag between the air and ground

surface temperature which varies from 0 (W18 and E7) to 193 (E11) days, for -10 °C (Table 4).

Table 4. Ground surface temperature thresholds and important temperature timing for all sites.

	2016					2017	
Site and Class	Timing of Temp < 0 °C (dd/mm)	No. of Days Following Air Temp < 0 °C	Timing of Temp < -10 °C (dd/mm)	No. of Days Following Air Temp < -10 °C	Timing of Lowest Temp °C (dd/mm)	Timing of Temp > 0 °C (mm/dd)	No. of Days Following Air Temp > 0 °C
W2(w)	09/29	+ 40	12/06	+67	-31 (03/07)	06/18	+3
W3(w)	09/02	+13	10/30	+30	-32 (03/07)	06/21	+6
W4(p)	08/22 * 09/04 **	+2	10/11* 10/26 **	+10	-42 (03/07)	05/23 * 06/08 **	-23
W6(b)	08/20 * 09/04 **	0	10/11 * 10/24	+10	-43 (03/05)	05/19 * 06/05 **	-27
W7(b)	10/01	+42	03/15	+166	-11 (04/16)	07/14	+29
W8(b)	08/20 * 09/11 **	0	10/30	+30	-33 (03/07)	06/11 * 06/13 **	-4
W9(b)	08/20 * 09/02 **	0	10/11 * 10/27 **	+11	-42 (03/05)	05/22 * 06/05 **	-24
W10(b)	09/06	+17	10/11 * 10/26 **	+11	-42 (03/06)	05/19 * 06/05 **	-27
W11(p)	08/20 * 09/09	0	12/17	+78	-19 (03/09)	06/20 * 06/22 **	+5
W12(p)	08/22 * 09/04	+2	10/11 * 10/26 **	+11	-39 (03/06)	05/22 * 06/05 **	-24
W13(b)	08/22 * 09/06	+2	10/11 * 10/24 **	+11	-44 (03/05)	05/19	-27
W14(p)	08/20 * 09/04 **	0	10/12 * 11/04 **	+12	-41 (03/05)	5/23 * 06/05 **	-23
W15(m)	09/14 * 09/27 **	+25	01/08	+100	-14 (03/13)	07/10	+25
W16(p)	08/22 * 09/06 **	+2	10/11 * 11/11 **	+11	-40 (03/05)	06/19	+4
W17(m)	08/22 * 09/06 **	+2	11/11	+42	-32 (03/07)	06/25	+10
W18(p)	*08/20 * 09/04* **	*0*	*10/1 * 10/24* **	*0*	*-44 (03/06)*	*05/19 * 06/01* **	*-27*
W19(p)	09/30	+41	12/08 * 12/12 **	+69	-22 (03/08)	06/23	+8
W20(m)	09/11 * 09/26 **	+22	12/24	+85	-14 (03/27)	07/14	+29
E1(p)	08/21 * 09/04 **	+1	10/29	+29	-37 (03/07)	06/17	+2

Table 4 Continued.

	2016					2017	
Site and Class	Timing of Temp < 0 °C (dd/mm)	No. of Days Following Air Temp < 0 °C	Timing of Temp < -10 °C (dd/mm)	No. of Days Following Air Temp < -10 °C	Timing of Lowest Temp °C (dd/mm)	Timing of Temp > 0 °C (mm/dd)	No. of Days Following Air Temp > 0 °C
E2(m)	09/04 * 09/11 **	+15	11/13 * 11/23 **	+44	-24 (03/08)	06/30	+15
E3(m)	09/06 * 09/09 **	+17	02/12	+135	-13 (03/28)	07/05	+20
E4(m)	09/14	+25	11/12 * 11/21 **	+43	-15 (03/29)	07/29	+44
E5(w)	09/29	+40	11/27 * 12/03 **	+58	-27 (03/07)	06/28	+13
E6(p)	08/21 * 09/01 **	+1	10/10 * 10/26 **	+10	-43 (03/05)	05/28 * 06/13 **	-18
E7(b)	08/21 * 09/02 **	+1	10/01 * 10/26 **	0	-44 (03/05)	05/19 * 06/10 **	-27
E8(w)	09/13 * 09/25 **	+24	11/05	+36	-36 (03/07)	06/16	+1
E9(m)	09/04 * 09/06 **	+15	11/02 * 11/05 **	+33	-29 (03/07)	06/27	+12
E11(b)	08/22 * 09/27 **	+2	04/11	+193	-10 (4/30)	07/19	+34
E12(p)	09/02 * 09/04 **	+13	11/11	+42	-37 (03/06)	06/21	+6
E13(w)	09/04 * 09/06 **	+15	11/02 * 11/08 **	+33	-33 (03/07)	06/21	+6
E14(b)	09/06	+17	01/07	+99	-17 (03/08)	07/05	+20
E15(p)	08/22 * 09/06 **	+2	11/02 * 11/04 **	+33	-37 (03/07)	06/14	-1
E16(p)	08/20 * 09/02 **	0	11/24	+55	-31 (03/07)	06/23	+8
E17(b)	08/20 * 09/01 **	0	10/15 * 10/26 **	+15	-41 (03/07)	05/28 * 06/13 **	-18
E18(b)	09/06	+17	03/05	+156	-11 (4/19)	08/02	+48
E19(p)	08/22* 09/04 **	+2	10/11 * 10/26 **	+11	-42 (03/07)	05/23 * 06/12 **	+23
E20(p)	08/22 * 09/04 **	+2	11/08	+39	-28 (03/07)	06/27	+12

* First recorded temperature

** Sustained recorded temperature

b= bare ground p= polar desert m= mesic tundra w= wet sedge

W18 is italicized as it was recovered unburied which may impact the timing and value of the temperatures especially during the thawing season.

Temp stands for temperature

A large number of ground surface temperature sites also reach temperatures above 0 °C before the air did, especially at sites with the coldest winter temperatures (W4, W6, W9, W10, W12, W13, W14, E6, and E7). This is indicated by a negative number for days. Most of the sites reached their lowest daily ground surface temperature during the beginning of March with a few exceptions (E3, E4, E18, E11, W7, and W20). These exceptions are also the sites with the warmest minimum daily ground surface temperature, ranging from -10 to -15 °C.

4.2 Modelled Surfaces

4.2.1 Air Temperature

Using the observed AMAT values, the 2013-2014 SLR of -6.7 °C km^{-1}, and the Cape Bounty DEM, an air temperature surface over both watersheds was generated (Figure 20).

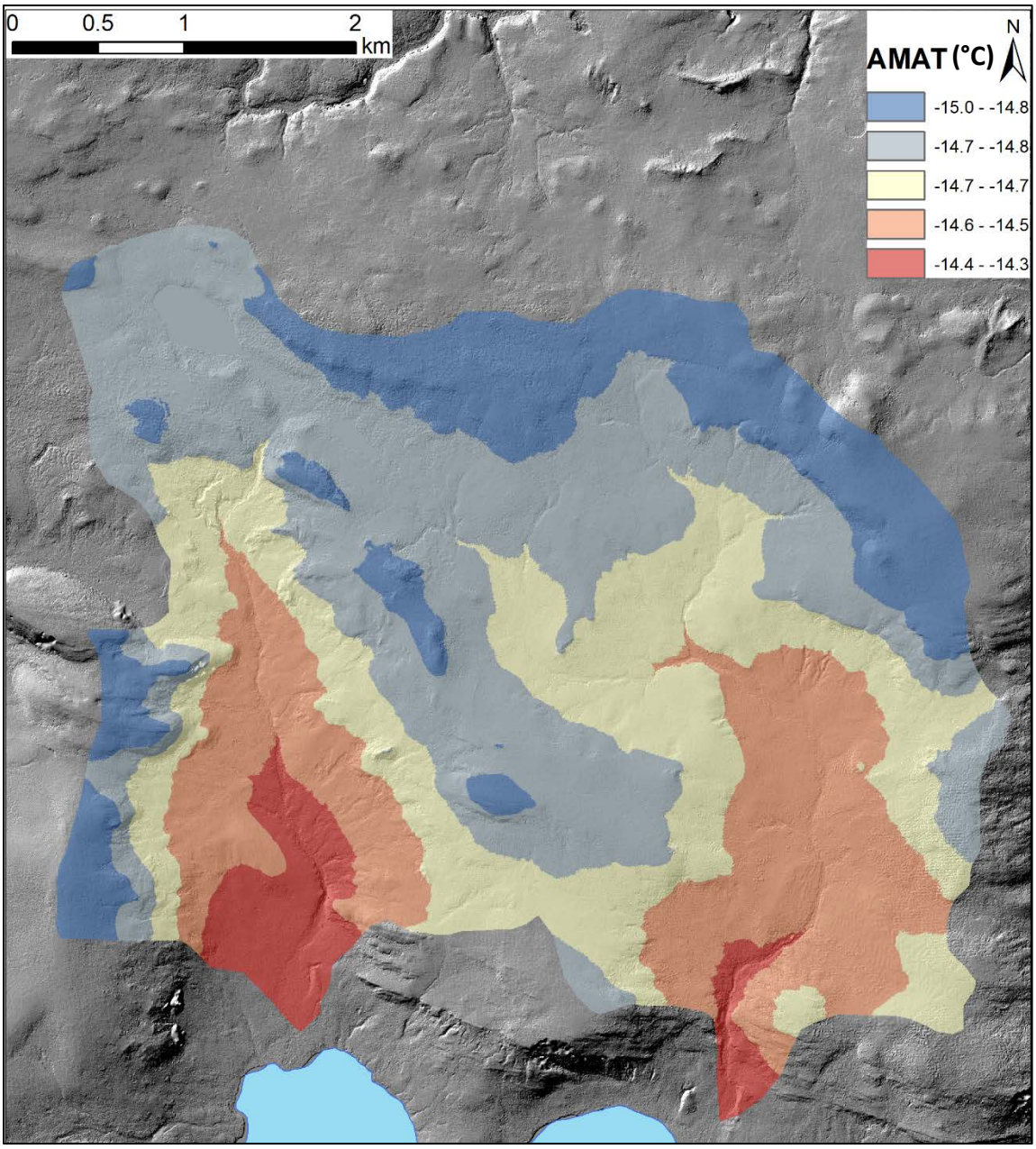

Figure 20. Modelled AMAT over both watersheds.

The modelled air temperatures show a 0.7 °C difference between the warmest temperatures in the river channels and the coldest temperatures on the hilltops.

An elevational relation of-827.5 DD km^{-1} was calculated and utilized to generate the TDD_a surface over the watersheds (Figure 21).

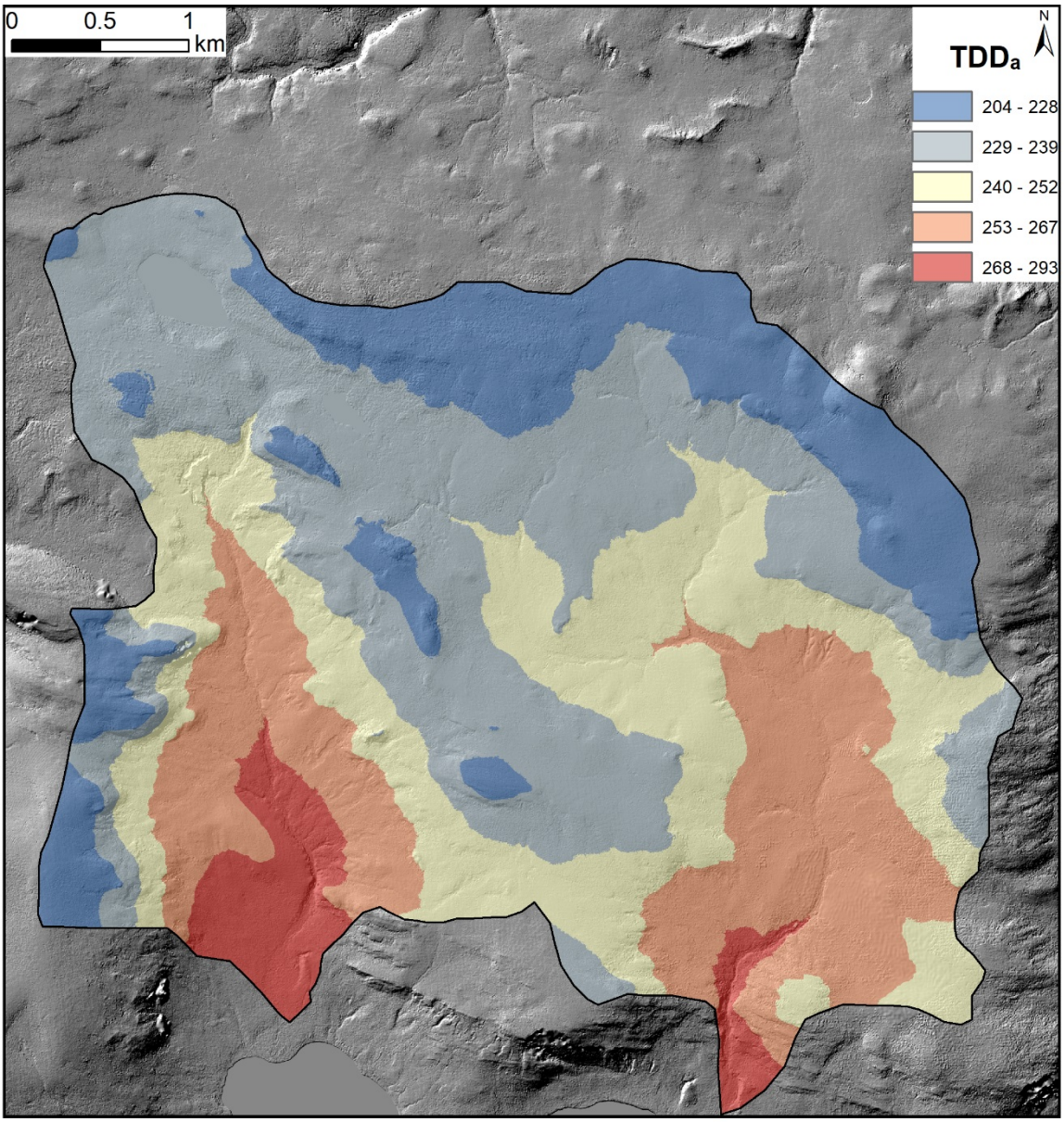

Figure 21. Modelled TDD_a over both watersheds.

Over the study area, modelled TDD_a had a range of about 89 degree-days with the lowest areas in the landscape having the most TDD_a and the highest having the least.

For the FDD_a an elevational relation of 1992 DD km^{-1} was calculated and used to generate the surface (Figure 22).

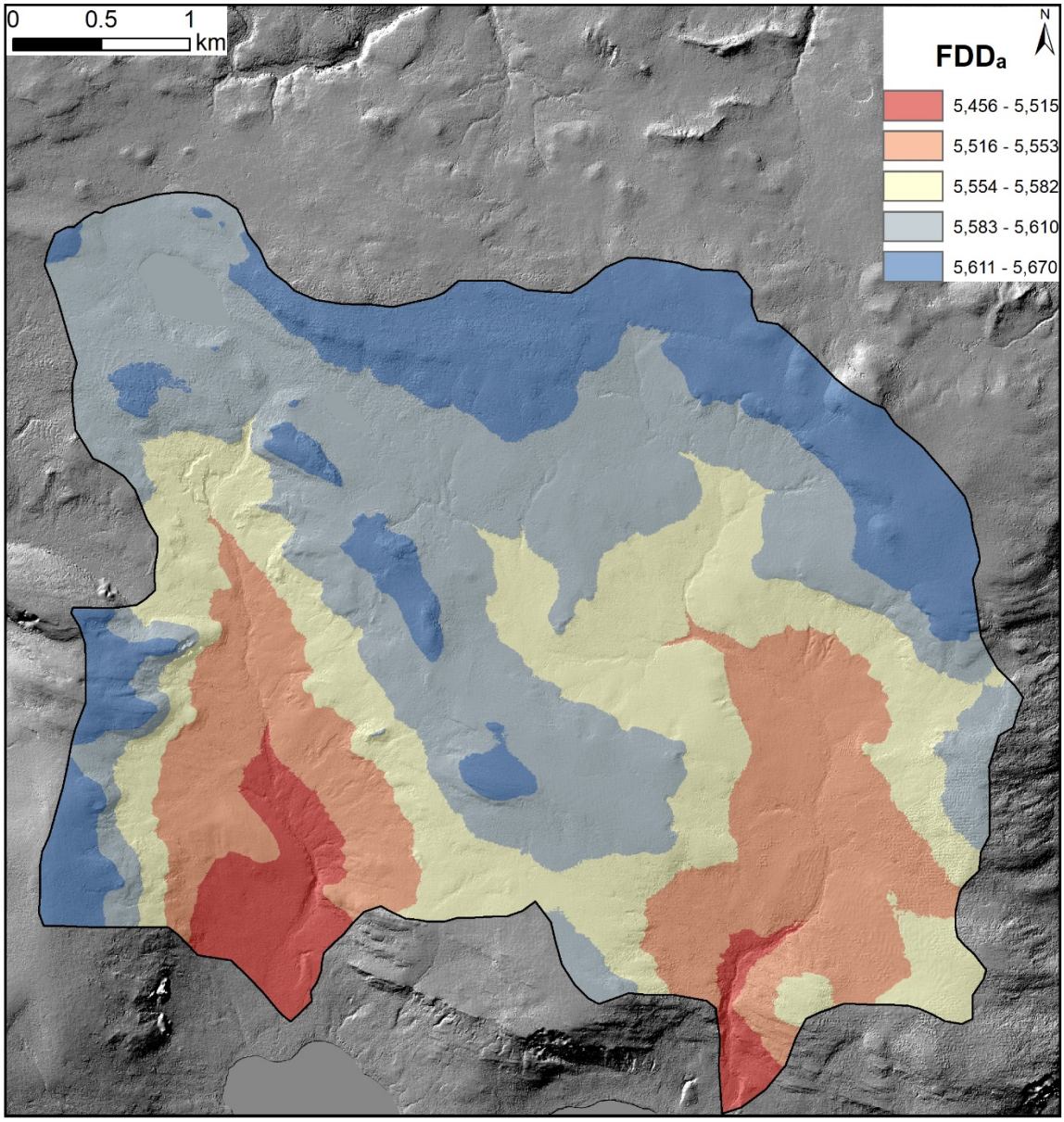

Figure 22. Modelled FDD_a over both watersheds.

The modelled FDD_a had a range of about 214 degree-days, with the highest parts of the watersheds having the most FDD_a and the lowest parts having the least. Overall, the air temperature trends showed warmer conditions at the lowest elevations and relatively colder conditions at the highest.

4.2.2 Ground Surface Temperature

Modelled AMGST ranged from -13.8 °C in the Dual Watershed model to -3.8 °C in all three models. Coldest AMGST were modelled at high TPI locations, along hill tops and the higher elevation plateaus, while the warmest AMGST in the model were found in the low TPI locations, river channels and at slope bottoms (Figure 23).

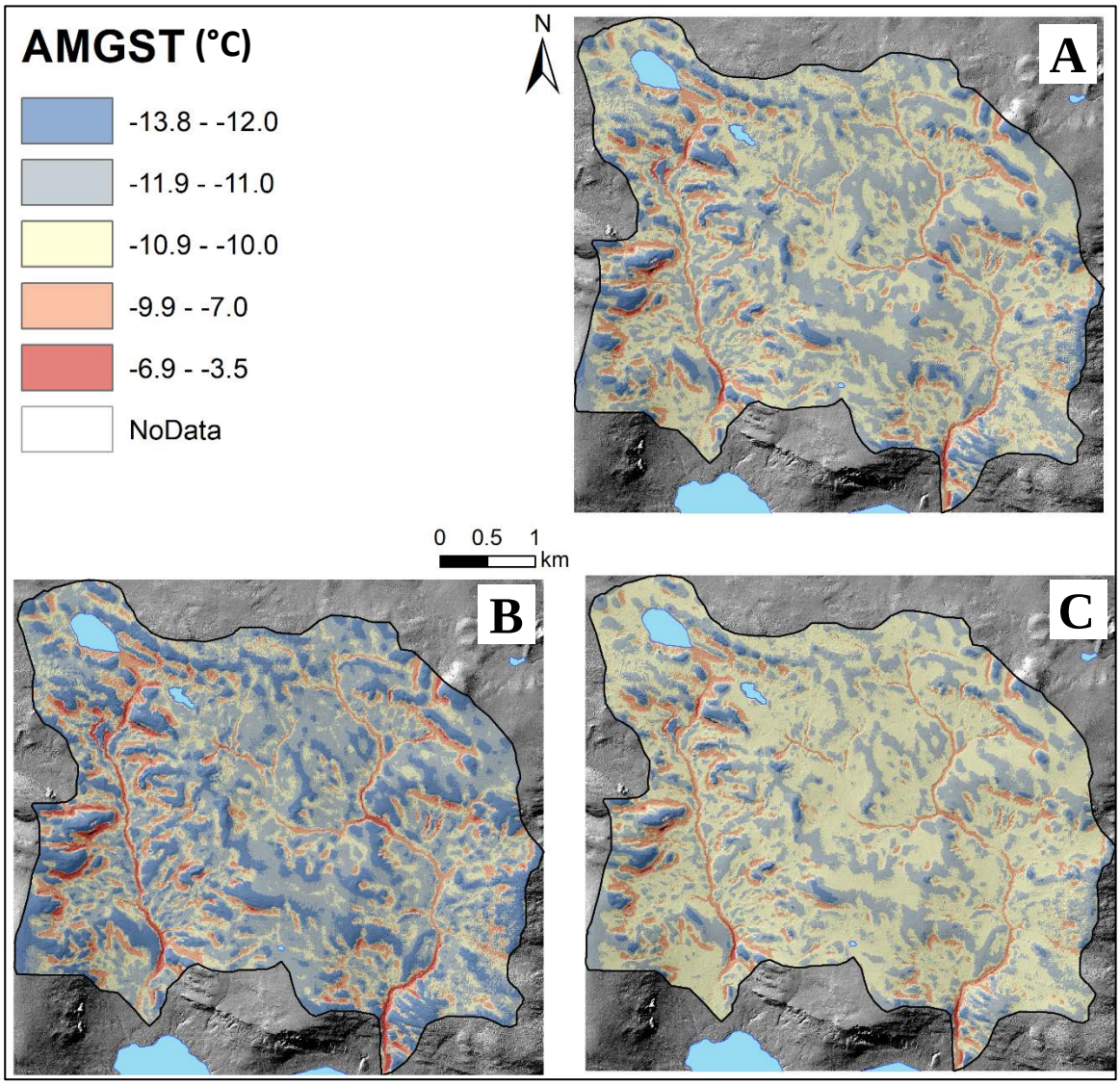

Figure 23. A) Modelled AMGST over both watersheds using the Dual Watershed Model B) Modelled AMGST over both watersheds using the East Watershed Model C) Modelled AMGST over both watersheds using the West Watershed Model.

n_f values modelled across the watersheds varied from 0.27 across all models and 0.95 in the East Watershed model. The highest n_f values were modelled at high TPI locations such as hill tops, while lower n_f values were modelled in the low TPI areas such as river channels and at the bottom of slopes (Figure 24).

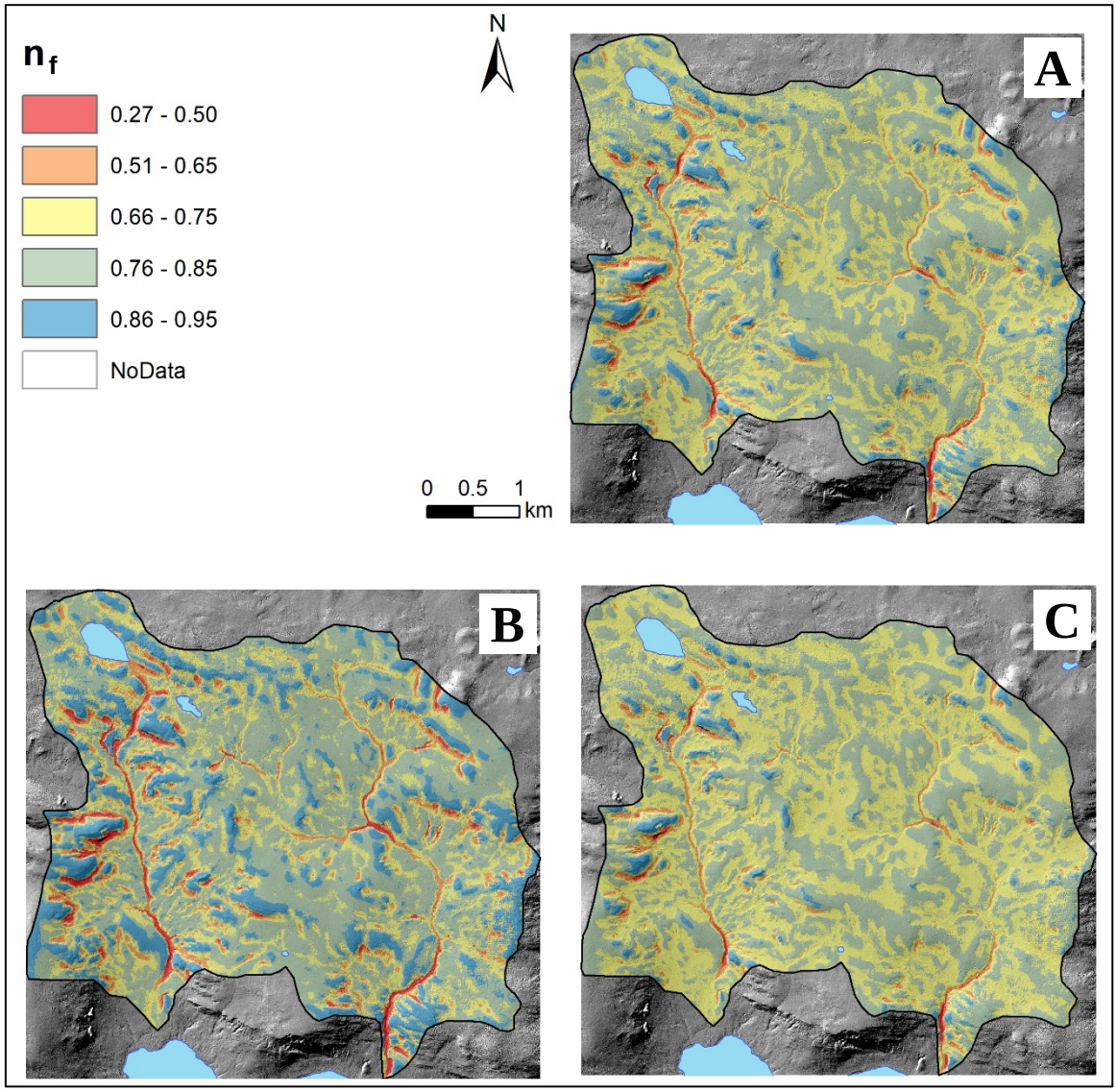

Figure 24. A) Modelled n_f over both watersheds using the Dual Watershed Model B) Modelled n_f over both watersheds using the East Watershed Model C) Modelled n_f over both watersheds using the West Watershed Model.

Over all three models n_t ranged from 0.64 in the West Watershed model to 1.77 in the Dual Watershed model. Highest modelled n_t values were found at high TPI locations such as hilltops, while the lowest values were modelled at low TPI locations such as in river channels and slope bottoms (Figure 25).

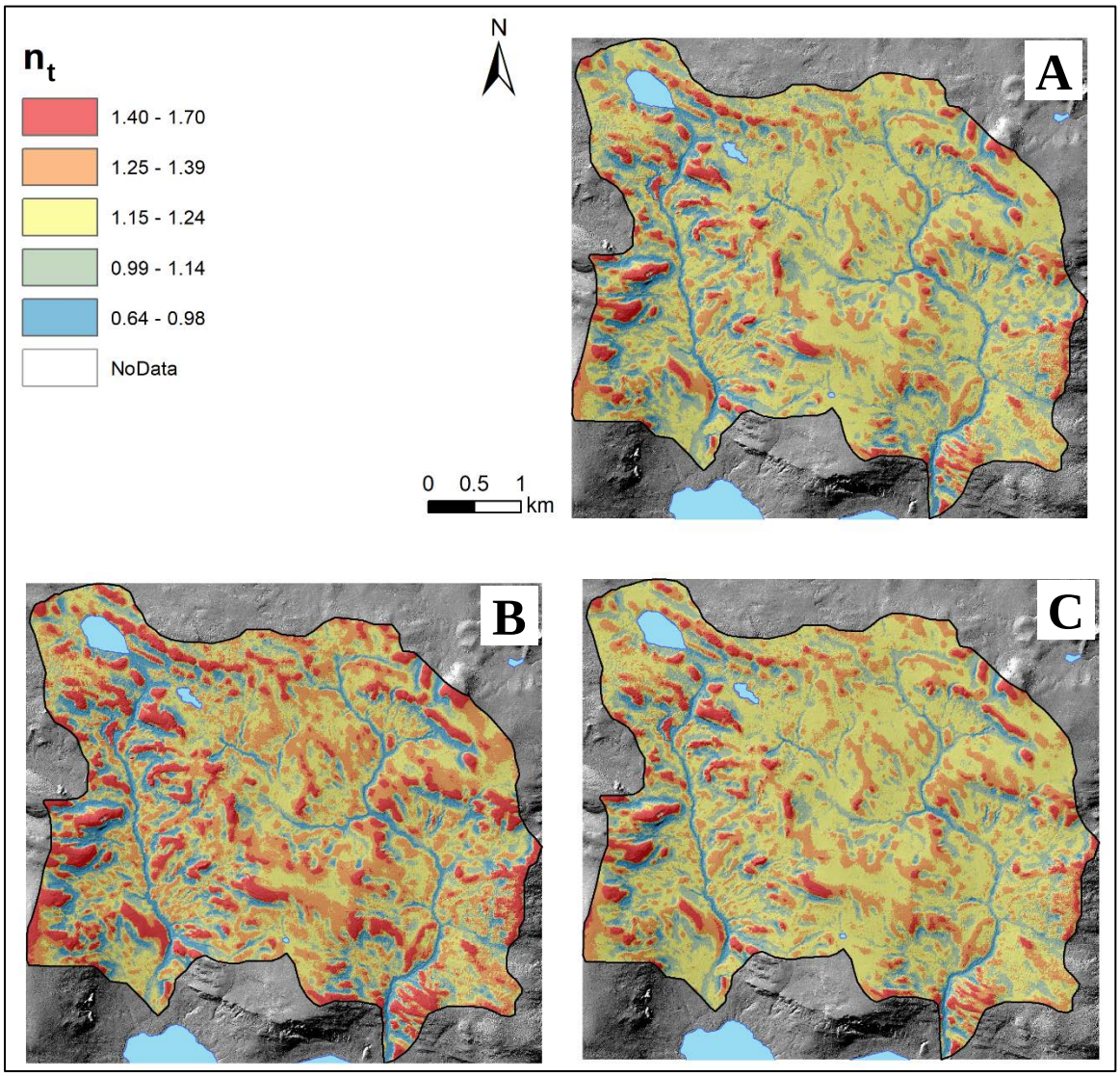

Figure 25. A) Modelled n_t for both watersheds using the Dual Watershed Model B) Modelled n_t for both watersheds using the East Watershed Model C) Modelled n_t for both watersheds using the West Watershed Model.

FDD_g and TDD_g were not modelled over the watersheds as they are not required for the TTOP model to compute permafrost temperature.

4.2.3 TTOP

Modelled TTOP varied from -3.6 °C to -14.0 °C in the East Watershed model. Following the observed trends, modelled TTOP is warmest in the river channels and slope bottoms and coldest on hilltops (Figure 26).

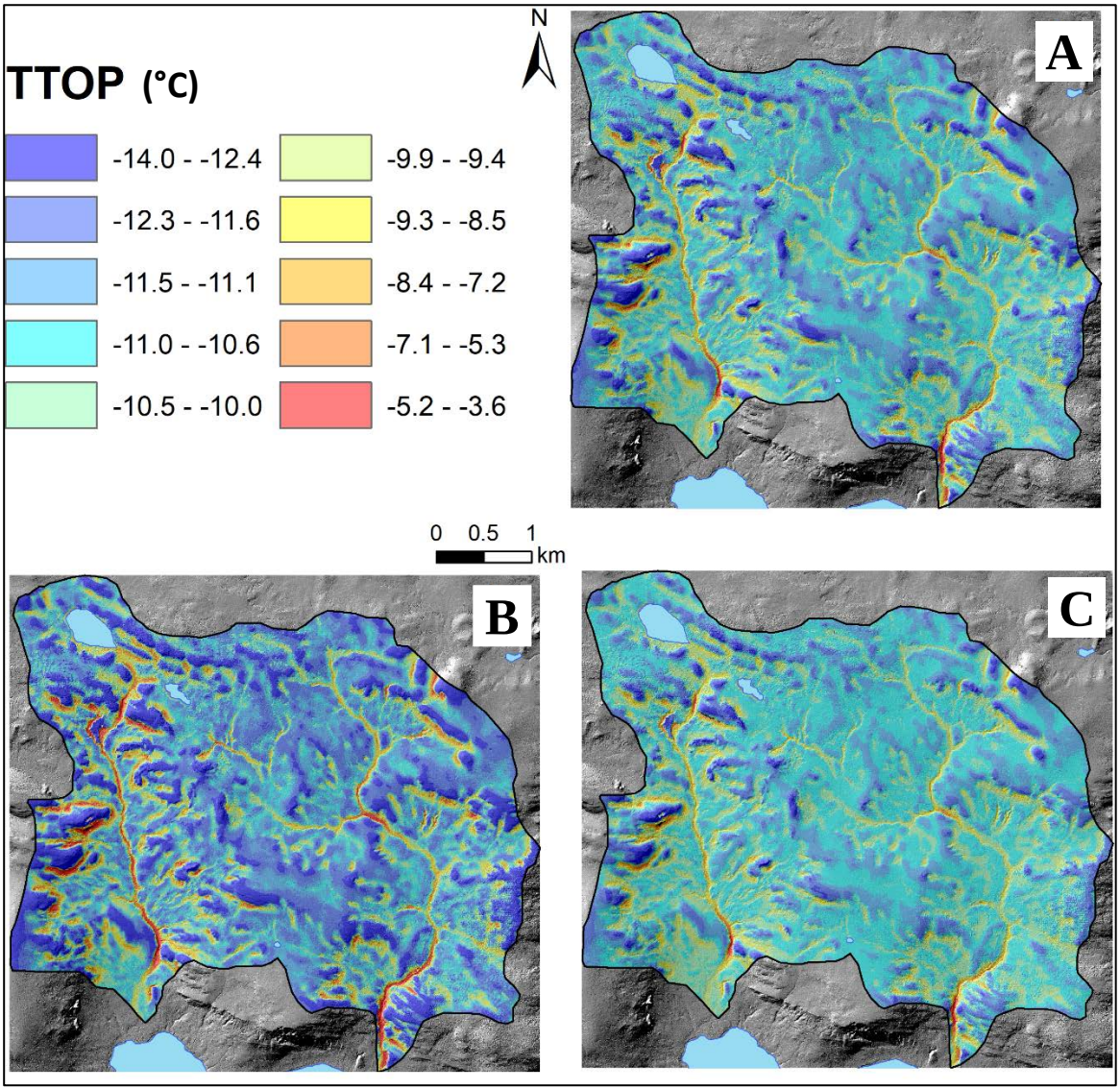

Figure 26. A) Modelled TTOP for both watersheds using the Dual Watershed Model B) Modelled TTOP for both watersheds using the East Watershed Model C) Modelled TTOP for both watersheds using the West Watershed Model.

4.2.4 Model Comparison

All three models predicted similar results and trends for all metrics (Table 5).

Table 5. Comparison of statistics for ground surface temperature metrics and TTOP for each model.

	Dual Watershed Model			**East Watershed Model**			**West Watershed Model**		
	Min	Max	Mean	Min	Max	Mean	Min	Max	Mean
AMGST (°C)	-13.4	-3.8	-10.9	-13.8	-3.8	-11.2	-12.9	-3.8	-10.8
N_f	0.27	0.93	0.79	0.27	0.95	0.77	0.27	0.90	0.74
N_t	0.68	1.77	1.19	0.71	1.76	1.25	0.64	1.70	1.20
TTOP (°C)	-13.8	-3.6	-10.9	-14.0	-3.6	-11.1	-13.2	-3.65	-10.8

The models had the same minimum AMGST and n_f values due to the cap used to eliminate erroneous results. Generally, the East Watershed model had a larger range of predicted values than the other two models, while the West Watershed model had the smallest predicted range of values.

4.3 Simulated Climate Change Surfaces

4.3.1 Air Temperature

At Cape Bounty, under each climate change scenario MAAT and TDD_a were expected to increase while the number of FDD_a was expected to decrease. The magnitude of the change was dependent on the severity of the climate change scenario, with the RCP4.5 2050 scenario predicting the most moderate and the RCP8.5 2080 scenario predicting the largest changes (Table 6).

Table 6. Air temperature metrics for each climate change scenario and the expected magnitude of change from current conditions including the percentage of change

Predicted Values of Air Temperature Metrics					
	Current	*RCP 4.5*		*RCP8.5*	
	1981-2010	2050	2080	2050	2080
MAAT (°C)	-16.9	-12.7	-11.5	-11.0	-6.9
FDD_a	6362	4952	4589	4444	3174
TDD_a	230	249	257	266	322

Magnitude of Predicted Change (from Modeled Current)				
	RCP4.5		*RCP8.5*	
	2050	2080	2050	2080
MAAT (°C)	+ 4.1 (24%)	+ 5.3 (31%)	+ 5.8 (34%)	+ 10.0 (59%)
FDD_a	- 1413 (22%)	- 1773 (28%)	- 1917 (30%)	- 3187 (50%)
TDD_a	+ 19 (8%)	+ 27 (12%)	+ 36 (16%)	+ 92 (40%)

The change in FDD_a was more substantial than the change in TDD_a across all scenarios. The air temperature surfaces created for each scenario indicated substantial warming over the watersheds with limited variability within each modelled surface (Figure 27).

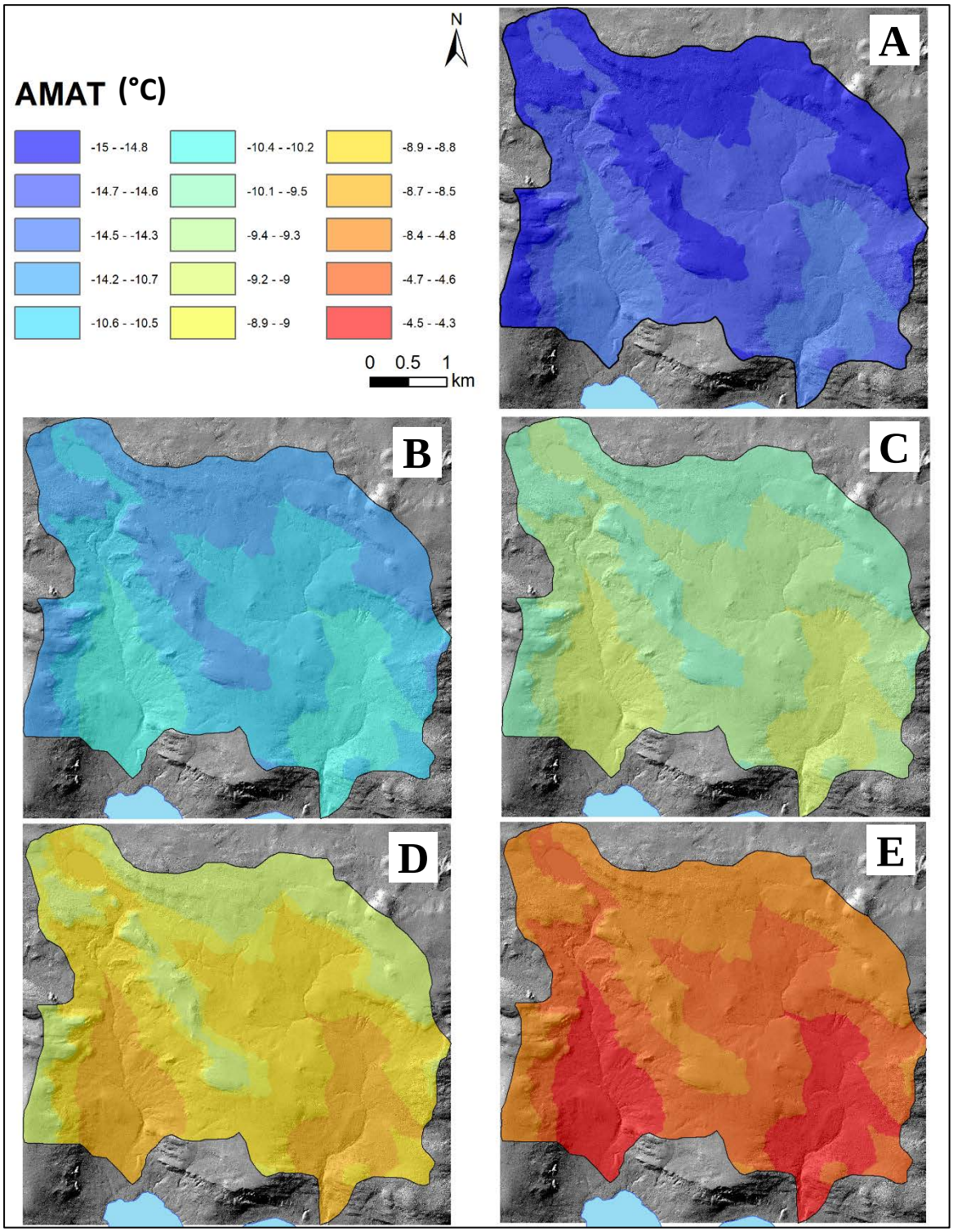

Figure 27. A) Modelled current (2016-17) AMAT over Cape Bounty B) Modelled predicted air temperature for the RCP4.5 2050 climate normal C) Modelled predicted air temperature for the RCP4.5 2080 climate normal D) Modelled predicted air temperature for the RCP8.5 2050 climate normal E) Modelled predicted air temperature for the RCP8.5 2080 climate normal.

The total range was approximately 10.7 °C from the current modelled air temperature to the RCP8.5 2080 climate normal. Individually, the variability within each scenario is small, only about 1 °C while the variability between subsequent scenarios ranges from 0.5 °C between the two RCP4.5 climate normals and 3.5 °C between the two RCP8.5 climate normals.

Modelled FDD_a ranged from 5670 degree-days currently at Cape Bounty to 2269 under the RCP8.5 2080 climate normal (Figure 28).

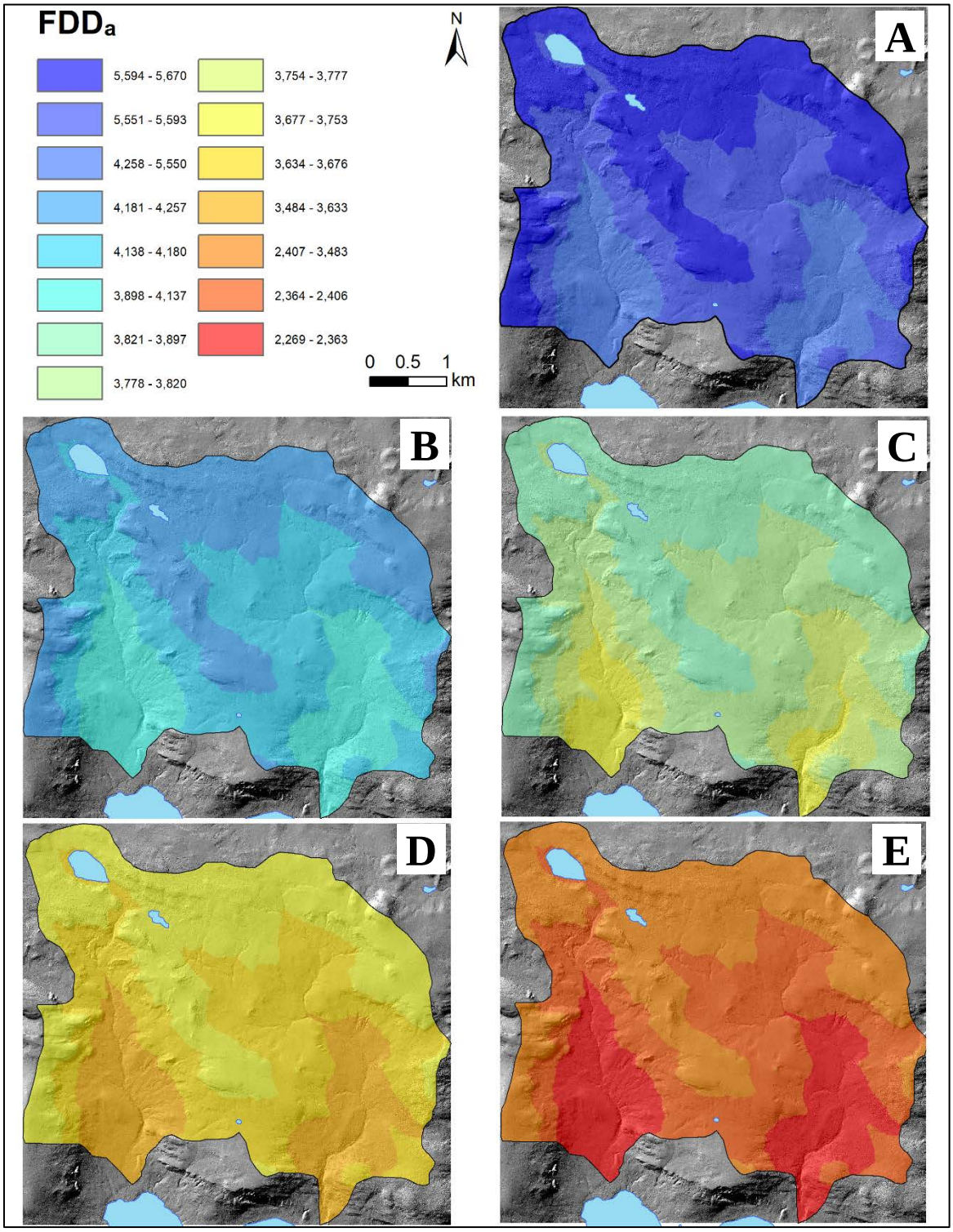

Figure 28. A) Modelled current (2016-17) FDD_a over Cape Bounty B) Modelled predicted FDD_a for the RCP4.5 2050 climate normal C) Modelled predicted FDD_a for the RCP4.5 2080 climate normal D) Modelled predicted FDD_a for the RCP8.5 2050 climate normal E) Modelled predicted FDD_a for the RCP8.5 2080 climate normal.

Within each scenario FDD_a ranged by 214 degree-days. Between the scenarios, FDD_a ranged by an average of 1452 degree-days between the current values and both 2050 climate normals. In contrast to the air temperature, the range between the two RCP4.5 climate normals was larger than the range between the two RCP8.5 climate normals, 146 and 56 degree-days respectively.

Modelled TDD_a had less variability within and between climate change scenarios than FDD_a (Figure 29).

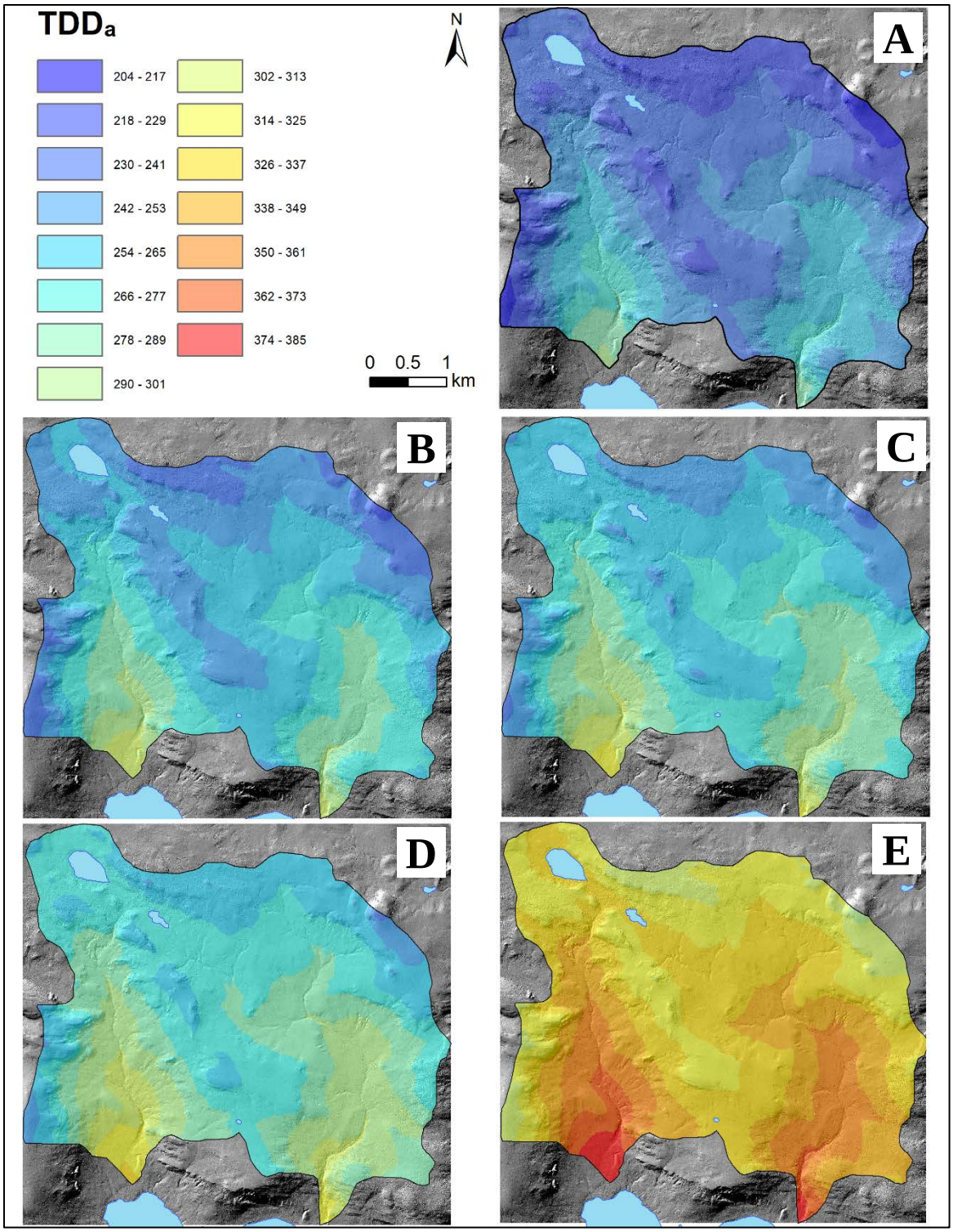

Figure 29. A) Modelled current (2016-17) TDD_a over Cape Bounty B) Modelled predicted TDD_a for the RCP4.5 2050 climate normal C) Modelled predicted TDD_a for the RCP4.5 2080 climate normal D) Modelled predicted TDD_a for the RCP8.5 2050 climate normal E) Modelled predicted TDD_a for the RCP8.5 2080 climate normal.

TDD_a within each scenario ranged by 58 degree-days. Unlike the other metrics there was overlap in TDD_a values between scenarios. Therefore, the range between scenarios was negligible.

4.3.2 TTOP

In order to model TTOP under the perturbed scenarios, a new modelled surface for n_f was created to account for changes resulting from variation in the MAAT (Figure 30). The resulting surfaces do not account for changes in n_f resulting from variation in snow cover.

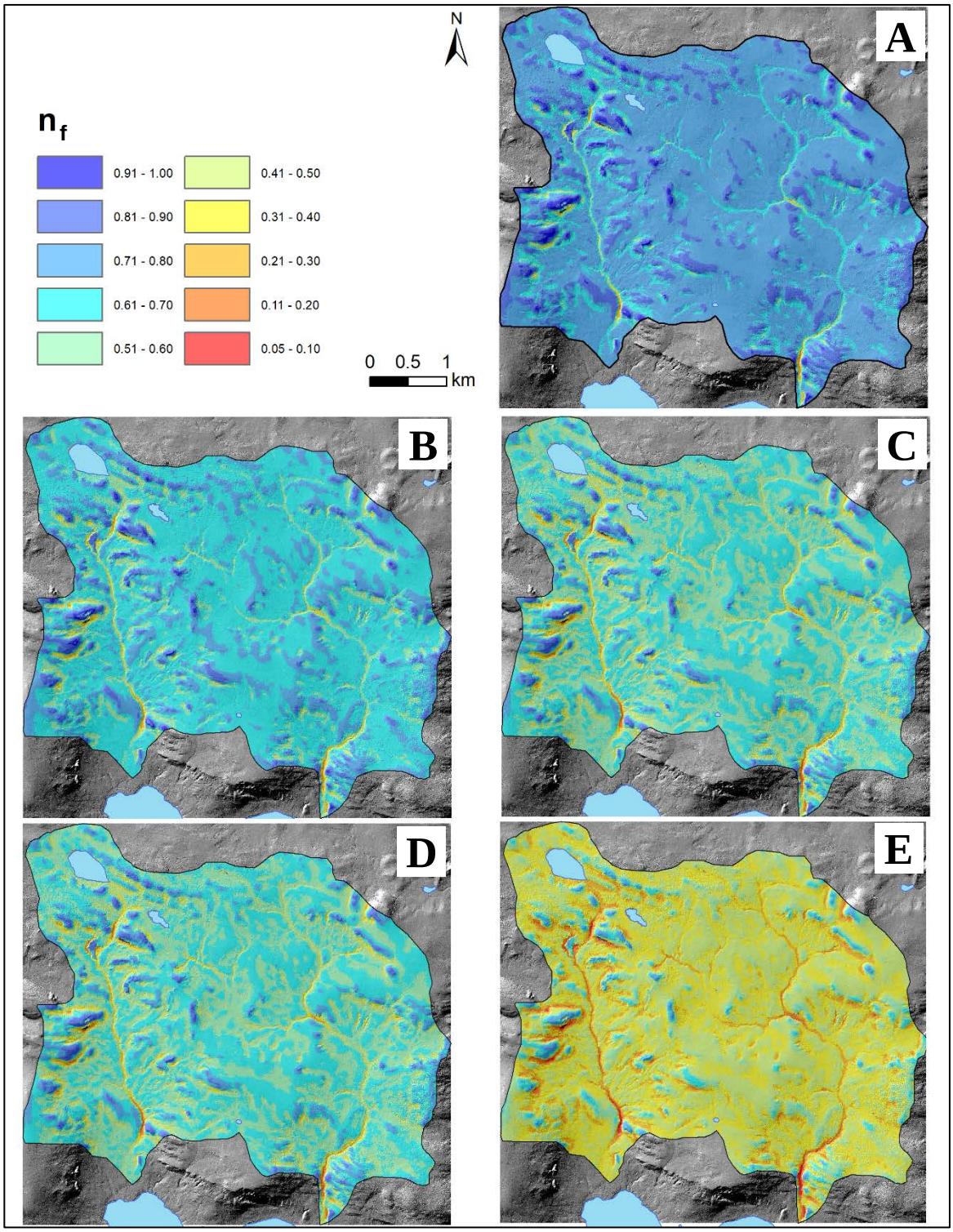

Figure 30. A) Modelled current (2016-17) n_f over Cape Bounty B) Modelled n_f for an -11 °C MAAT during the RCP4.5 2050 climate normal (rounded from -10.63 °C) C) Modelled n_f for a 9 °C MAAT during the RCP4.5 2080 climate normal (rounded from -9.43 °C) D) Modelled n_f for a -9 °C MAAT during the RCP8.5 2050 climate normal (rounded from -8.93 °C) E) Modelled n_f for a -5 °C MAAT during the RCP8.5 2080 climate normal.

n_f, across both watersheds did not respond uniformly to MAAT warming with extreme values having limited variability and middle values demonstrating the most variation. Hilltops showed the least amount of change with the n_f values remaining close to 1 for each scenario. Low n_f values in the river channels and slope bottoms also show limited variability, staying close to 0.10. Average n_f values ranged from 0.75 for current conditions to 0.40 for the RCP8.5 2080 climate normal. Although the difference between the two RCP4.5 and RCP8.5 climate normals was only 1 °C, the difference in n_f for the RCP4.5 climate normals was 0.07, while the difference between the two RCP 8.5 scenarios was 0.2.

The n_t and r_k values for 2016-17 were used to calculate TTOP for each scenario as they were expected to remain relatively constant and an attempt to quantify their change would dramatically increase the computation complexity of the model.

TTOP varied substantially between and within each scenario, with the RCP8.5 2080 climate normal showing the most dramatic increase (Figure 31).

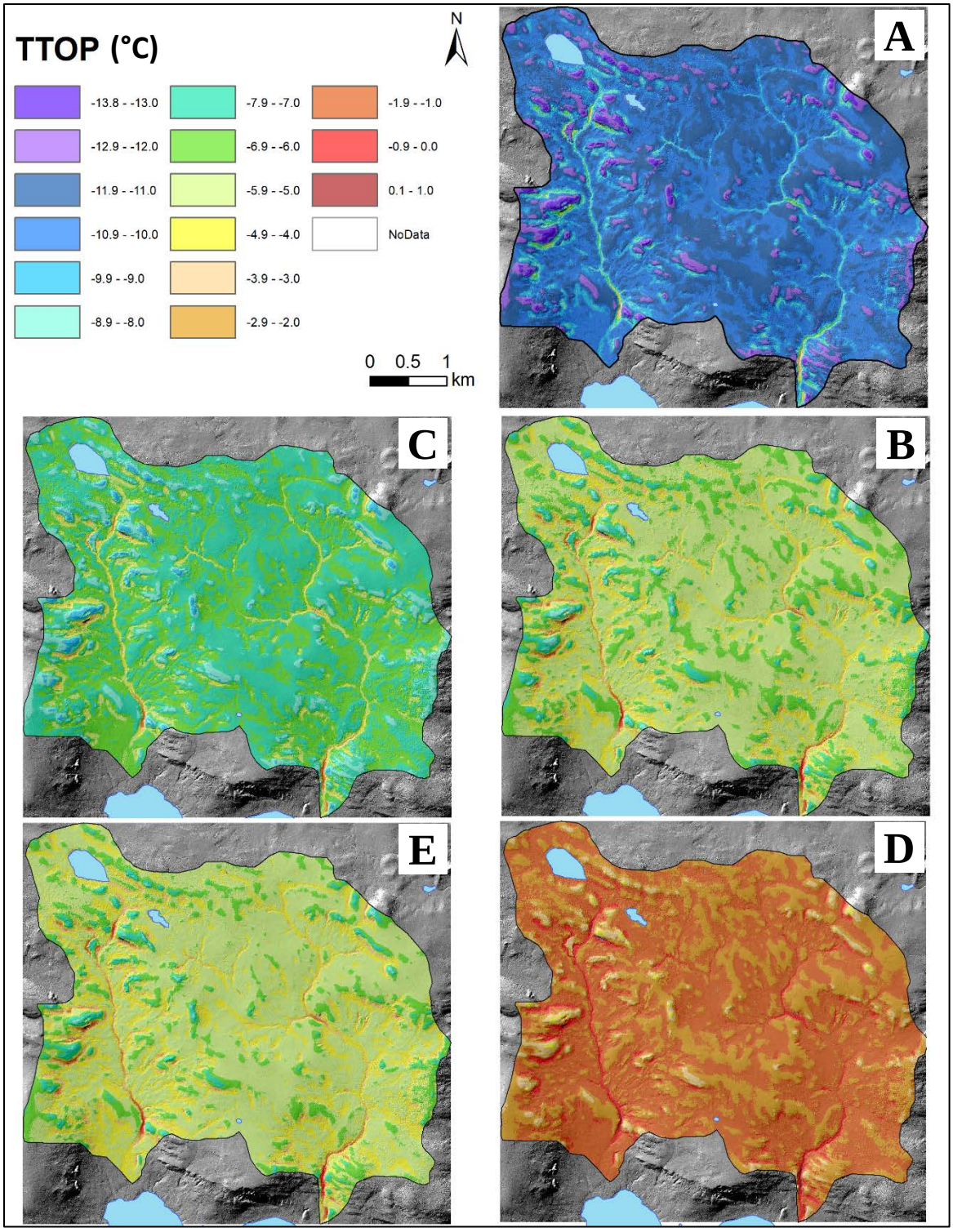

Figure 31. A) Modelled TTOP for current (2016-17) period over Cape Bounty B) Modelled predicted TTOP for the RCP4.5 2050 climate normal C) Modelled predicted TTOP for the RCP4.5 2080 climate normal D) Modelled predicted TTOP for the RCP8.5 2050 climate normal E) Modelled predicted TTOP for the RCP8.5 2080 climate normal.

Average TTOP ranged from -10.9 °C under current conditions to -1.9 °C under the RCP8.5 2080 climate normal. Under current conditions the coldest modelled permafrost temperature at Cape Bounty was -13.76 °C while the warmest modelled permafrost was -3.62 °C. Under the RCP4.5 climate change scenario these temperatures were predicted to increase to -9.76 and -1.94 °C for the 2050 climate normal and -8.60 and -0.83 for the 2080 climate normal. These temperatures were predicted to further increase under the RCP8.5 climate change scenario to -8.22 and -0.77 °C for the 2050 climate normal and -4.33 and 0.26 °C for the 2080 climate normal. The positive TTOP in the RCP8.5 2080 climate normal indicated the loss of permafrost in locations as the annual average permafrost temperature was above freezing. Although the warmest temperatures were found in the river channel and slope bottoms, the largest magnitude of change was observed in the coldest permafrost locations, such as hilltops. As a result, the RCP8.5 2080 climate normal showed much less variability in TTOP than under current conditions, a predicted range of 4.59 °C compared to a range of 10.14 °C currently.

Chapter 5

Discussion

5.1 Gaps and Uncertainties

5.1.1 TTOP

The TTOP model is an equilibrium model, and as such can only model the TSP at equilibrium conditions (Henry & Smith, 2001; Riseborough, 2007; Riseborough et al., 2008). Therefore, the results of the TTOP model assume steady state conditions and that the permafrost has reached equilibrium with the climate (Etzelmüller, 2013; Gisnås et al., 2013; Bonnaventure et al., 2016). Consequently, one of the major limitations of the TTOP model is its inability to model the TSP through time or under transient conditions (Gisnås et al., 2013). Therefore, TTOP used in reference to a current or future year refers to the TSP after the permafrost has reached equilibrium with the air temperature regime (permafrost temperatures are slightly warmer or colder than the MAAT) (Halsey et al., 1995). Since permafrost in the High Arctic is largely influenced by climate, it will likely reach the new equilibrium in a few years after disturbance (Shur & Jorgenson, 2007).

5.1.2 Error Quantification

Measured point values were compared to the results of the modelled surfaces using the root mean squared error (RMSE) method to quantify the uncertainty in the models (Table 7).

Table 7. Root mean square error for each of the models. "'Excluded" are points not used in the creation of the model, "Used" are points that were utilized in the model creation, and "Combined" is the RMSE for both used and excluded.

Air Temperature Model			
	AMAT	FDD_a	TDD_a
Used	0.06	0.12%	0.51%

Dual Watershed Model				
	AMGST	n_f	n_t	TTOP
Excluded	0.85	0.05	0.14	0.71
Used	1.84	0.28	0.31	1.74
Combined	1.75	0.26	0.30	1.65

East Watershed Model				
	AMGST	n_f	n_t	TTOP
Excluded	2.27	0.15	0.39	1.89
Used	1.58	0.11	0.19	1.59
Combined	1.94	0.13	0.30	1.74

West Watershed Model				
	AMGST	n_f	n_t	TTOP
Excluded	2.07	0.14	0.23	2.07
Used	1.69	0.12	0.38	1.56
Combined	1.90	0.13	0.31	1.84

The Dual Watershed model produced the smallest error against the validation points for all metrics, which was expected as this model was created using 36 ground temperature loggers. The East Watershed model had the largest error for points at high and low TPIs as there were limited measured ground surface temperatures at these

extremes. Additionally, some of the errors may have been larger for the uncorrected values for the East and West Watershed models, however, as a cap was applied to each, the errors were minimized.

A majority of the modelled TTOP values were similar to those measured at the Headwater and West Lake boreholes, -11.1 °C (at 2.0 m) and -7.8 °C (at 1.3 m) respectively. In the models, TTOP over the Headwater borehole was estimated to be -10.6. -10.7 and -10.6 °C in the Dual, East, and West Watershed models respectively. The TTOP at the West Lake borehole was estimated to be -12.6 °C, -13.3 °C, and -12.2 °C for the Dual, East, and West Watersheds, respectively. The large discrepancy between the West Lake borehole temperatures and the modelled TTOP temperatures may stem from residual climatic conditions from previous years (Table 8).

Table 8. Annual average borehole temperature data from Headwater and Westlake borehole and measured TTOP.

	Annual Average Temperatures (°C)			
	2016-17	**2015-16**	**2014-15**	**2013-14**
Headwater (2.0 m)	-11.1	-12.3	-13.0	-12.8
West Lake (1.3 m)	-7.8	-10.8	-11.4	-10.7
CB3	-13.9			-13.5
CB2	-14.4			-13.7
Ptarmigan Upper	-11.2			
Goose Lower	-11.2			
Goose Upper	-12.1			

The temperatures of the boreholes may be influenced by the proximity of Headwater Lake and West Lake which are not accounted for in the model. The RMSE between the measured and surface modelled TTOP was 0.63, 0.38, and 0.72 °C for the Dual, East, and West Watershed models, respectively.

5.1.3 Models for Current Conditions

One of the major assumptions in the creation of the model was the r_k values as they were generalized and only indirectly accounted for soil moisture through the land cover classification. However, since there is limited to no organic material, the differential thermal conductivity between the thawing and freezing season, represented by r_k, is relatively small and has little impact on the modelled TTOP (Figure 32).

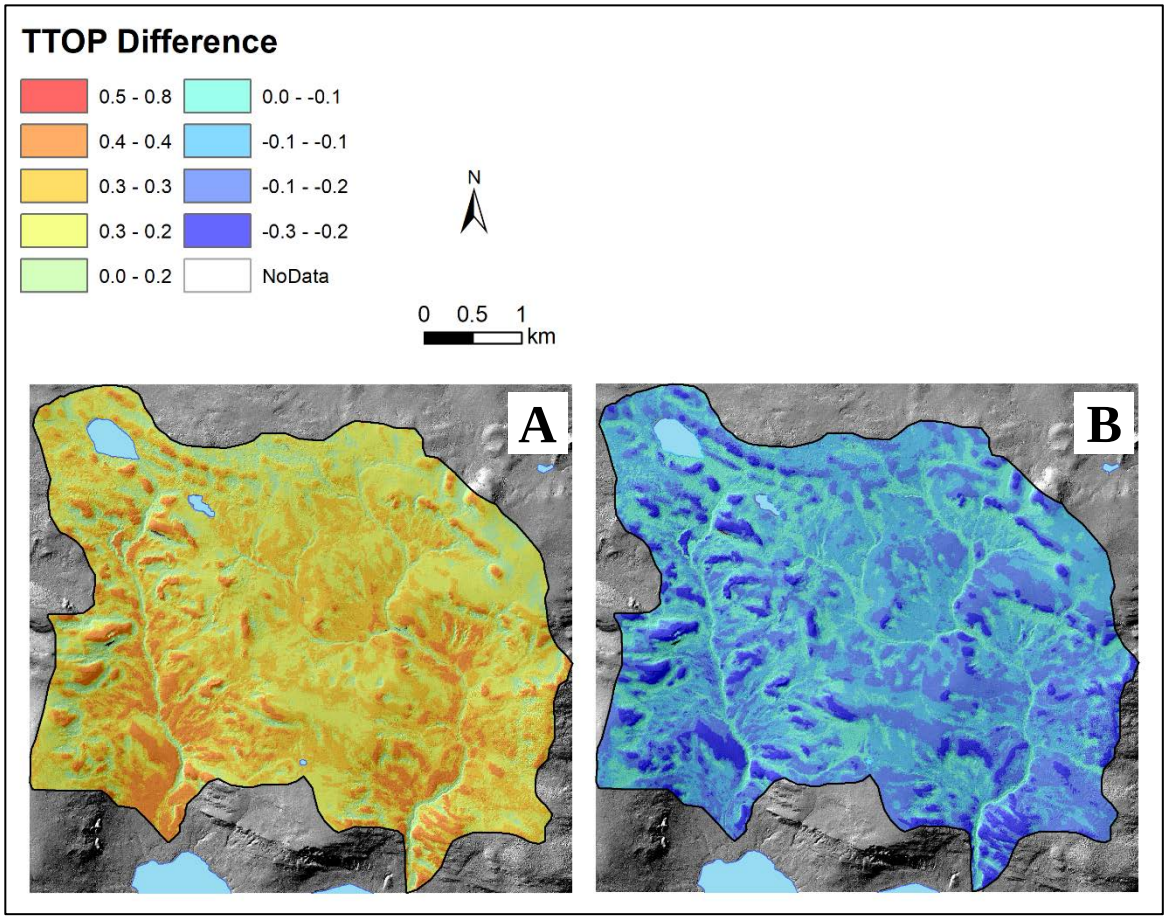

Figure 32. Difference between modelled TTOP with variable rk values and TTOP with one uniform rk value. A) uniform rk of 1 B) uniform rk of 0.5.

In both cases modelled TTOP only differed by a maximum of 0.6 °C and a minimum of -0.31 °C, with the majority of the difference limited to between -0.2 and -0.1 °C for a standard r_k of 0.5 and between 0.20 and 0.3 °C for a standard r_k of 1. A standard r_k value of 0.5 resulted in an average difference of -0.2 °C, while using a standard r_k value of 1 resulted in an average difference of 0.2 °C. The slight variance in the average

difference likely resulted from the slight difference in the variation between the standard r_k values, 0.5 and 1, and the average r_k value in the original surface, 0.71. The 0.5 standard r_k resulted in colder permafrost temperatures as it underestimated the influence of TDD_a and n_t on the permafrost, while the standard 1 r_k value resulted in warmer permafrost temperatures by overestimating the influence of TDD_a and n_t. Both, however, showed limited difference from the TTOP modelled using the original r_k surface, demonstrating its limited impact on TTOP and the dominance of the winter season, FDD_a and n_f, in determining the permafrost temperature.

5.1.4 Models for Future Scenarios

Several assumptions were made in the creation of the climate change models. The biggest uncertainty in the creation of the models was the assumption that snow depth remains constant. Changes in snow depth may have a large impact on the values of n_f, however, there is uncertainty as to how climate change will impact snowfall as it is highly spatially variable, there is limited observation networks, and the lack of sunlight during winter presents a challenge for satellite monitoring (Callaghan et al., 2011). Currently snow cover duration is decreasing, a trend that is predicted to continue, with a later onset of snow in autumn and an earlier spring melt (Bokhorst et al., 2016; AMS, 2016; Callaghan et al., 2011). Snow depth and accumulation over the High Arctic is predicted to increase, resulting from increases in the amount winter precipitation, however, snow depth during the shoulder seasons is expected to decline (SWIPA, 2017; IPCC, 2013). However, the general circulation models used to generate these predictions only represent large-scale changes in precipitation and other snow cover variables and may not adequately capture variation at specific locations (Callaghan et al., 2011). It is therefore

difficult to predict the magnitude and timing of change for each climate change scenario. This issue is compounded by the limited amount of base snow depth data for current conditions. However, areas which currently accumulate snow will still accumulate snow, while areas from which snow is scoured will still have snow removed. Therefore, although the magnitude of snow depth may not be the same, snow accumulation and scouring sites will still have higher or lower snow relative to each other (Huning & Margulis, 2017).

The next assumption made in the creation of these models was the idea that n_t remains constant. The value of n_t is strongly influenced by vegetation which keeps the ground cooler than the air in summer (Klene et al., 2001; Karunaratne & Burn, 2004; Bonnaventure & Lamoureux, 2013). Arctic greening, the increase of biomass and productivity, is observed and expected to increase as air temperature and the growing season increases (Tucker et al., 2001; Moffat et al., 2016). At Cape Bounty average NDVI increased from 1985 to 2015, with the largest increase in the mesic tundra and polar desert classifications (Edwards & Treitz, 2017). While the increase in vegetation may decrease the values of n_t, especially over areas of bare ground and polar deserts, the earlier loss of snow cover may increase n_t as the ground will be exposed to warmer air temperatures sooner (Bonnaventure et al., 2016). Additionally, surface color, soil moisture, and thermal diffusivity may all impact n_t at varying strengths, and are difficult to predict (Klene et al., 2001; Karunaratne & Burn, 2004). However, since in cold environments FDD is typically greater than TDD, TTOP is more sensitive to changes in n_f than n_t (Gisnås et al., 2013). Since the complexities associated with predicting n_t make

it difficult to model for future scenarios and it has less of an impact than changes in n_f, it was held constant.

r_k values were also held constant despite possible changes in soil moisture and vegetation, since it is also difficult to quantify, and as shown has a limited impact on TTOP.

Lastly, AMGST was not calculated for any climate change scenarios as the variables derived for the scenarios did not allow for the calculation of an annual average since they were broken into the freezing and thawing seasons.

5.2 Environmental Influences

5.2.1 Snow depth (TPI)

The largest influence on AMGST and TTOP at Cape Bounty is snow depth, most importantly the redistribution of snow by wind. The relative snow depth at sites can be determined through the comparison of AMGST. Snow increases the variability of AMGST as areas with high snow cover remain warm, through insulation, while areas with little to no snow cover remain close to the winter air temperature (Figure 33).

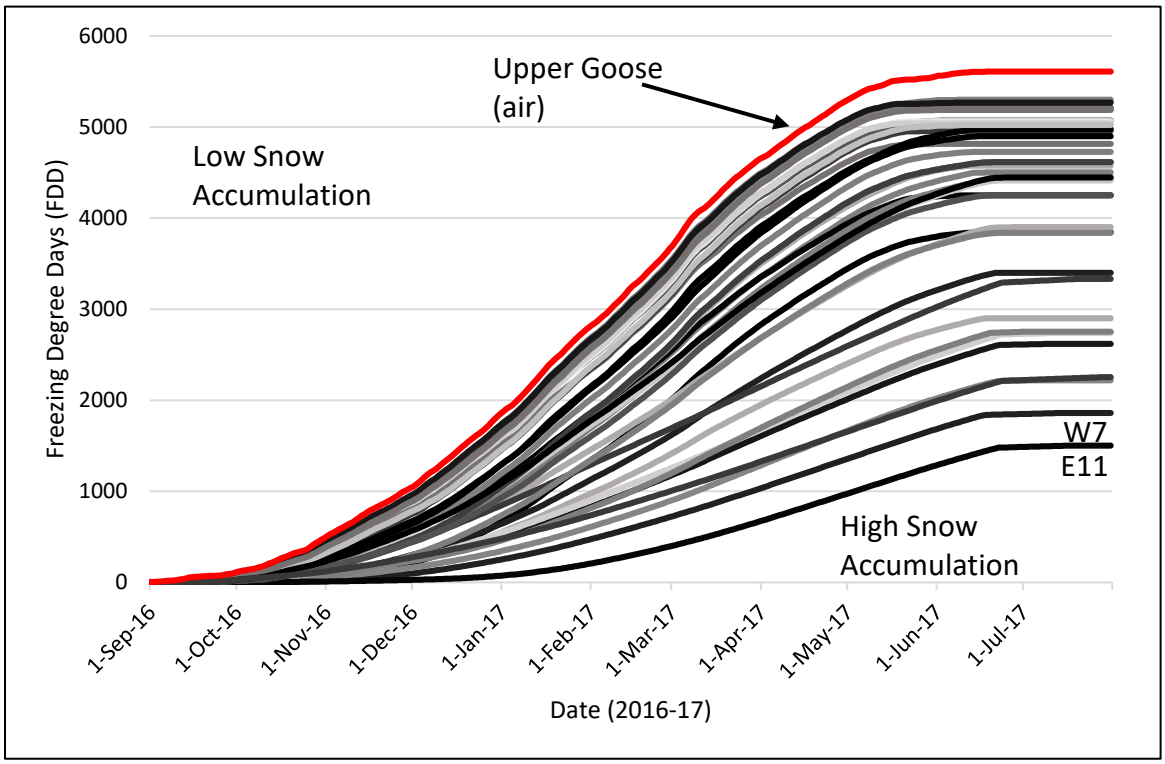

Figure 33. Cumulative freezing degree days for all ground temperatures and one air temperature (Upper Goose). Higher FDD_g values indicate sites with low snow cover, while lower FDD_g values indicate sites with high snow accumulation.

Since there is little vegetation at Cape Bounty and the vegetation that is present is limited in height, it has a negligible impact on snow redistribution and as result the only influence on snow redistribution is topography (Woo & Young, 1997; Yang & Woo, 1999; Essery & Pomeroy, 2004). Snow, therefore, accumulates in topographic hollows, while snow is scoured from areas with prominent topography. The relation of snow cover, and subsequently AMGST to topography is evident through the distribution of measured AMGST. The warmest AMGST for each watershed were sites E11 and W7 located in a channel bed and at a slope bottom respectively, while the coldest AMGST for each watershed were found at sites E6 and W6, an open flat area and a hilltop, respectively (Figure 34).

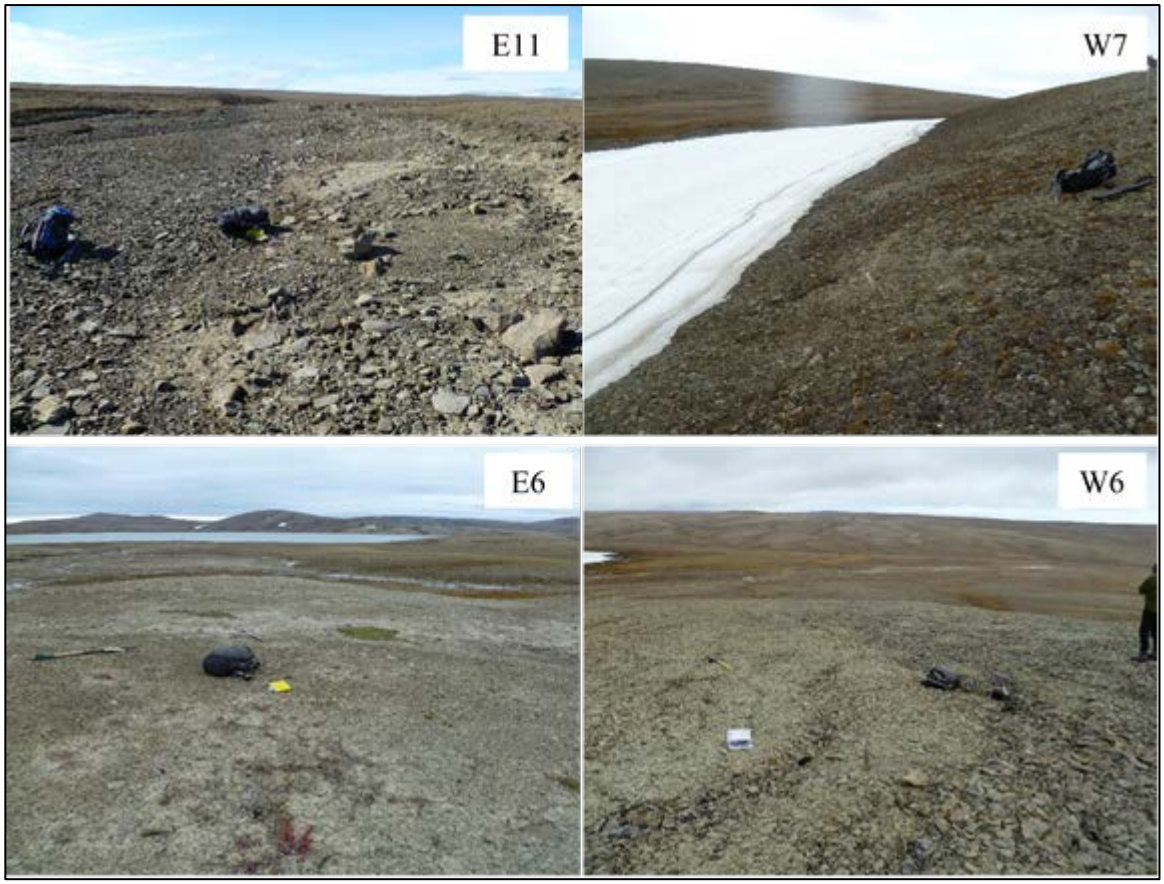

Figure 34. Photos of the locations of the warmest and coldest AMGST for each watershed.

Snow cover also influences n_f as it disrupts the connection between the air and the ground, keeping the ground surface warm relative to the air temperature, through insulation (Riseborough & Smith, 1998; Karunaratne & Burn, 2004). The larger the n_f the greater the connection between the ground surface and the atmosphere, which results from little to no snow cover. The smaller the n_f the greater the disconnect between the ground surface and the atmosphere, indicating greater snow cover. TTOP is also impacted by snow cover variability since lower n_f keeps the ground surface warm in winter, and subsequently keeps the permafrost warm.

In this study the magnitude and variability of AMGST was similar to that of Bonnaventure et al. (2016), with the coldest daily ground temperature reaching -43.5 °C

(W13) and the warmest -10.21 °C (E11). However, relative to the AMAT, the AMGST was warmer for 2016-17 than for the previous study. Measured n_f ranging from 0.27 to 0.95, was similar to the measured range from 2012-13, which was 0.48 to 0.99. However, both the maximum and minimum values for 2016-17 were smaller than those from 2012-13. The warmer AMGST, relative to the air temperature, and the smaller n_f values indicated greater snow cover. The n_f at E11 and W7 both exceed the theoretical n_f value for snow depth of 1.2 meters (Smith & Riseborough, 2002). Additionally, the distribution of the ground surface temperatures and n_f were also similar, with the relatively warm AMGST and small n_f located in the channel bed and the relatively cold AMGST and large n_f located outside of the channel bed, generally found in polar desert or bare ground conditions following the pattern of predicted snow accumulation and removal. Across the transects in both the East and West watershed (E12-14 and W19-20), AMGST increased moving towards the channel bed while n_f decreased.

Snow cover also influenced the value of n_t depending on how long the snow persisted into the thawing season or how soon it melted. At sites with late snow melt the ground was protected from the warmer air temperatures, keeping the ground surface colder, longer into the spring. Site E18 was still buried in snow upon collection, resulting in the substantially smaller n_t and TDD_g than the other sites, 0.01 and 76, respectively. At sites with early snow removal the n_t may be larger as the ground surface has contact with warmer air temperatures sooner. Sites with the coldest daily ground surface temperatures and AMGST also had the largest n_t (W6, W13, E7, and E19). The large n_t values at these sites may also be a product of the limited vegetation cover at these sites.

As snow depth is the most important variable in determining AMGST and TTOP it is important that accurate snow depth predictions are used to model AMGST and TTOP in future thermal regime scenarios. Due to a lack of baseline snow depth data to downscale global predictions, snow depth for each climate change scenario was held constant. In order to remedy this in future calculations, snow depth measurements were taken at each logger location during May 2018. Remote sensing is another possible method of estimating present day snow depth across the watersheds (Pulliainen, 2006; Deems et al., 2017), however, this is limited by logistical complications and cost. For the purposes of this thesis, holding snow depth constant is supported by the notion that, since topography will not change, locations which accumulate snow will still accumulate more snow than locations from which snow is scoured (Huning & Margulis, 2017). Attempting to estimate future snow depth with the limited data will likely result in large errors and the assumptions may not have adequate support.

5.2.2 Vegetation

Aside from altering snow redistribution, vegetation keeps the ground surface cool during summer through shading and evapotranspiration. At the majority of sites, the n_t exceeds 1 indicating that the ground temperature remains warmer than the air temperature during the thawing season. This is likely partially a product of the limited vegetation cover as a majority of sites with n_t exceeding 1 are found in the polar desert and bare ground land-cover classifications (Figure 35).

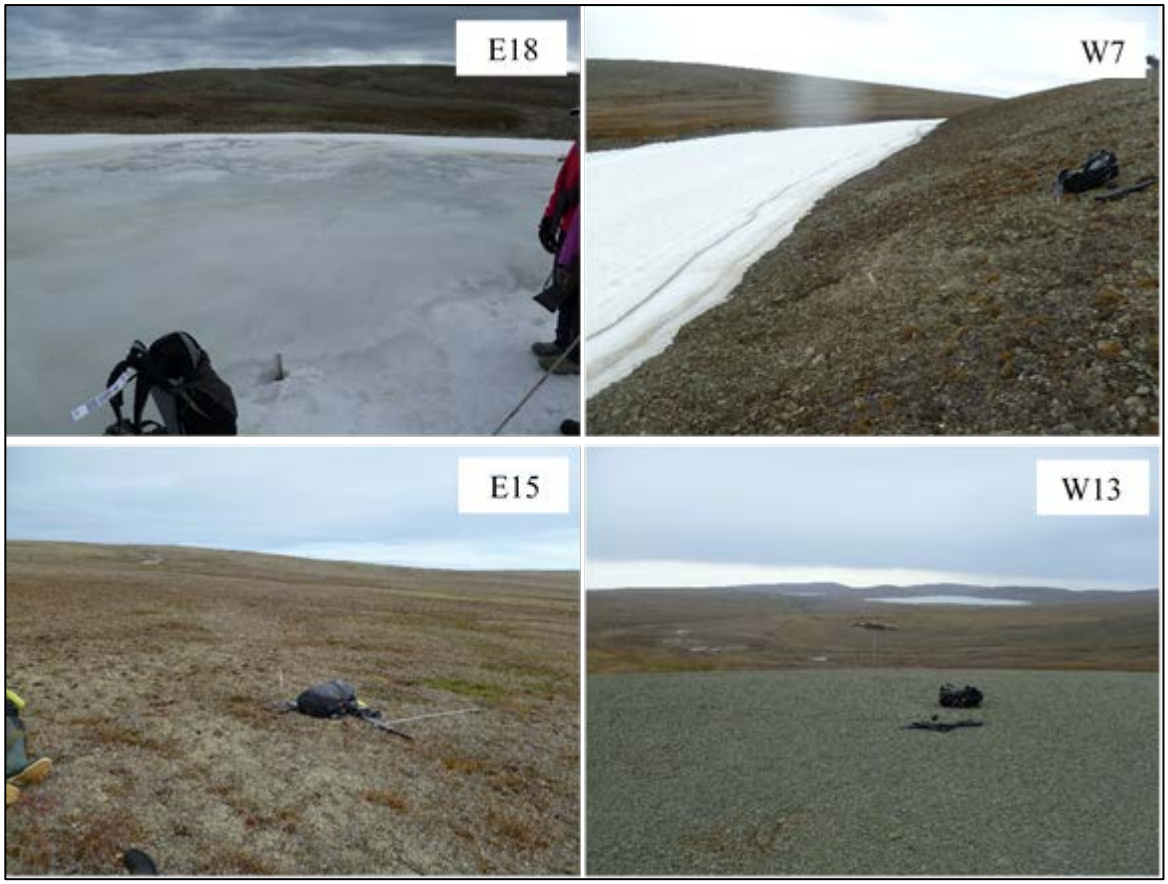

Figure 35. Sites with the smallest nt for each watershed, E18 and W7, and sites with the largest nt for each watershed, E15 and W13.

In an earlier study, n_t values exceeding 1 have been documented at Cape Bounty, although none were close to the magnitude of the largest n_t recorded during this study, possibly since the sites were limited to locations in and around channel beds (Bonnaventure et al., 2016).

Slight relation with ground temperature metrics exists for some of the land cover classifications, however, there is still a large degree of variability within each (Table 9).

Table 9. Average value and standard deviation for AMGST, n_f, n_t, and TTOP for each land-cover classification. Bare ground includes channel beds

	Bare Ground	Polar Desert	Mesic Tundra	Wet Sedge
AMGST (°C)	-10.1 ± 3.5	-12.3 ± 1.4	-9.3 ± 2.3	-11.8 ± 1.1
N_f	0.71 ± 0.3	0.85 ± 0.1	0.63 ± 0.2	0.76 ± 0.1
N_t	1.30 ± 0.6	1.53 ± 0.2	0.84 ± 0.3	1.13 ± 0.3
TTOP (°C)	-10.2 ± 3.5	-12.3 ± 1.4	-9.2 ± 2.3	-11.2 ± 1.0

The variability within land-cover classifications indicates that vegetation type or lack of vegetation has a limited impact on ground and permafrost temperature. Instead, snow cover is likely the dominant influence. The observed trends may not reflect the influence of the land-cover type but instead may be a product of the topography. The topography determines snow redistribution, which impacts soil moisture, which in turn impacts land-cover. Additionally, while channel bed and hill and ridge tops have the same land-cover classification, they have vastly different thermal regimes, indicated by the large range and standard deviation for all metrics, as a result of differential snow cover. At bare ground channel bed sites (W20, E11, and E14) the n_t values were 0.58, 0.67, and 0.95 respectively, while at bare ground hilltop sites (W6, W13, and E7) the n_t values were 1.88, 2.21, 1.67 and 1.69 respectively. Therefore, at Cape Bounty it appears that topography and snow cover have a larger impact on the ground and permafrost temperatures than vegetation.

5.2.3 Water flow

Surface and subsurface water acts to protect the ground surface from cold winter temperatures, keeping the ground surface warm and, in the case of large lakes, preventing the formation of permafrost (Williams & Smith, 1989; Levy et al., 2011). At Cape Bounty, channel beds, especially the permanent river channels, also have the influence of streamflow and consistent snow melt runoff.

The observed trends in AMGST, n_f and n_t match those from the previous study with the warmest AMGST and largest surface offset in the channel beds. The same trend was also observed along the two transects as n_t increased with increasing distance from the channel bed, although, despite being farther apart, E13 is more similar to E12 than E14 (the site in the channel bed). However, this may not result from the water but from the increased snow that collects in the incised channels and persists longer into the thawing season. As an example, although the site with the warmest AMGST, smallest n_f, and small n_t, was located in a channel bed (E11) another site in a high snow location outside of a channel bed (W7) had similar values for each metric, indicating that snow cover had a more important influence than the snow melt runoff.

5.3 Comparison of TTOP Model to Previous Studies

In Henry and Smith (2001), permafrost at Cape Bounty was classified as less than -15 °C (Figure 6). However, under equilibrium conditions of -14.73 °C, none of the permafrost reached these low temperatures. The majority of permafrost was in compliance with the Henry and Smith (2001) classification with a majority between -14.0 and -10.0 °C (Figure 36)

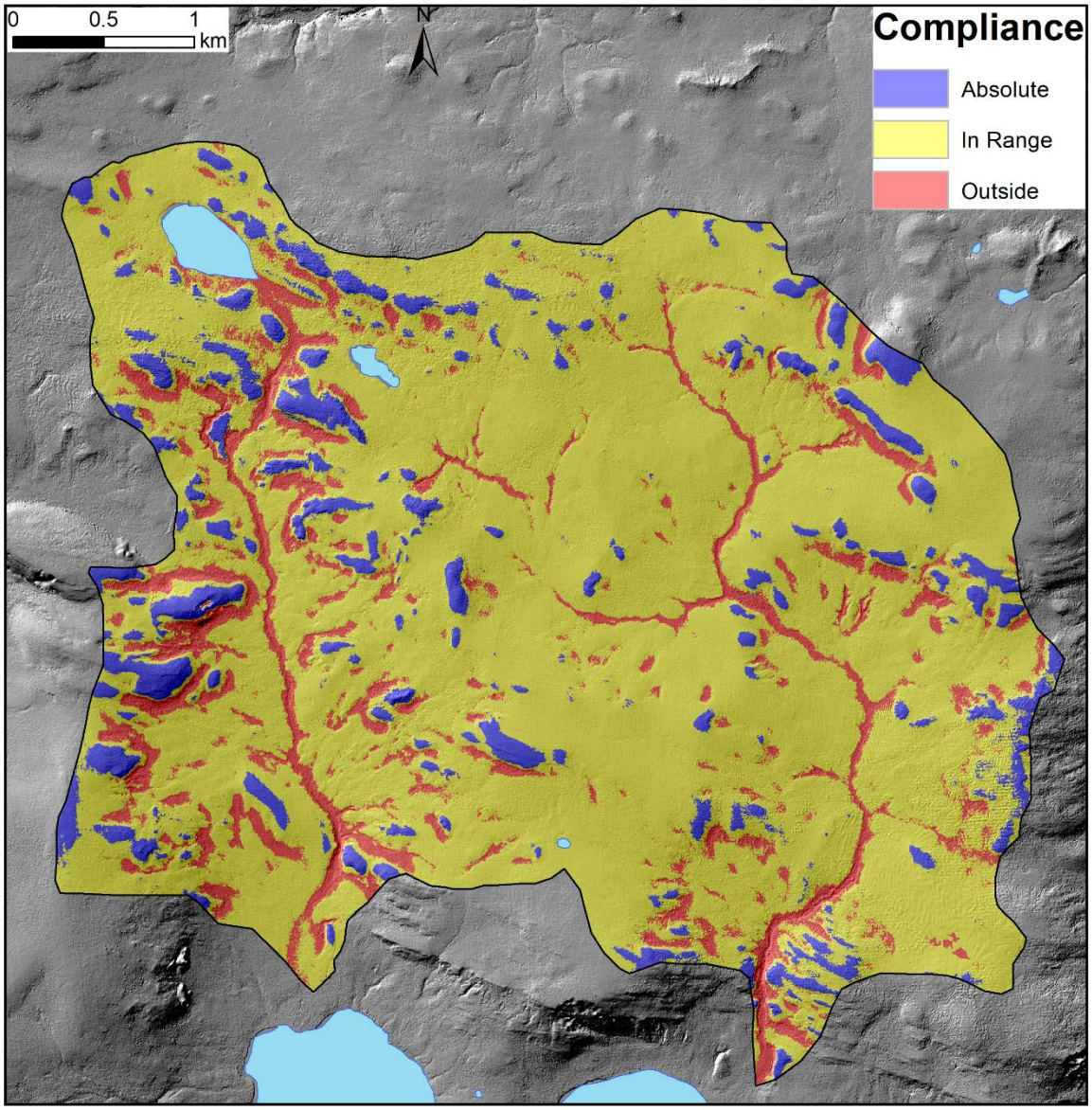

Figure 36. Compliance between 2016-17 TTOP model and the Henry and Smith (2001) TTOP model. “Absolute” compliance is TTOP between -14 and -12 °C, “In range” is TTOP between -12 and -10 °C, “Outside” is TTOP between -10 and -3.6 °C.

Only 8.9% of the permafrost at Cape Bounty was classified as having absolute compliance with the Henry and Smith (2001) model, however, 79.0% was classified as within a range of compliance. Interestingly, 12.1% was classified as outside compliance, meaning the Henry and Smith (2001) model incorrectly estimated TTOP more than it correctly identified TTOP at Cape Bounty. The largest differences between the Henry and

Smith (2001) classification and the 2016-17 TTOP model were found in areas of predicted high-snow cover, channel bed and slope bottoms. The low resolution of the model leads to a fairly accurate representation of permafrost temperatures over the majority of Cape Bounty, however, its resolution does not account for small variations in topography which change the accumulation of snow cover, leading to misrepresentation of TTOP in these areas. Although the area of permafrost outside the range of compliance was small relative to the area in compliance, these areas likely have physical susceptibility to disturbance, increased hydrological connectivity early in the spring and later in the fall as a result of warmer temperature and may provide biological refugia (Rivkina et al., 2000; Quinton et al., 2004; Nicole et al., 2009; Bakermans & Skidmore, 2011; Rudy et al., 2016).

5.4 Permafrost Susceptibility

Permafrost susceptibility is often classified based on the thermal and physical response to warming, with the thermal response representing the magnitude of the permafrost temperature change, and the physical response based on the probability of subsidence or detachment slides (Smith & Burgess, 1999). Areas of permafrost which have a greater thermal response to atmospheric warming lack the necessary buffering characteristics, including snow cover, vegetation, organic material, and substrate (Smith & Burgess, 1999). A physical response to warming, most commonly manifested as ground instability, is a result of substrate and ground ice content (Smith & Burgess, 1999). Susceptibility is derived through an evaluation of both the thermal and physical response, with the physical response often having more weight than the thermal response,

as the physical consequences of thaw are thought to be more impactful (Figure 37) (Smith & Riseborough, 1996).

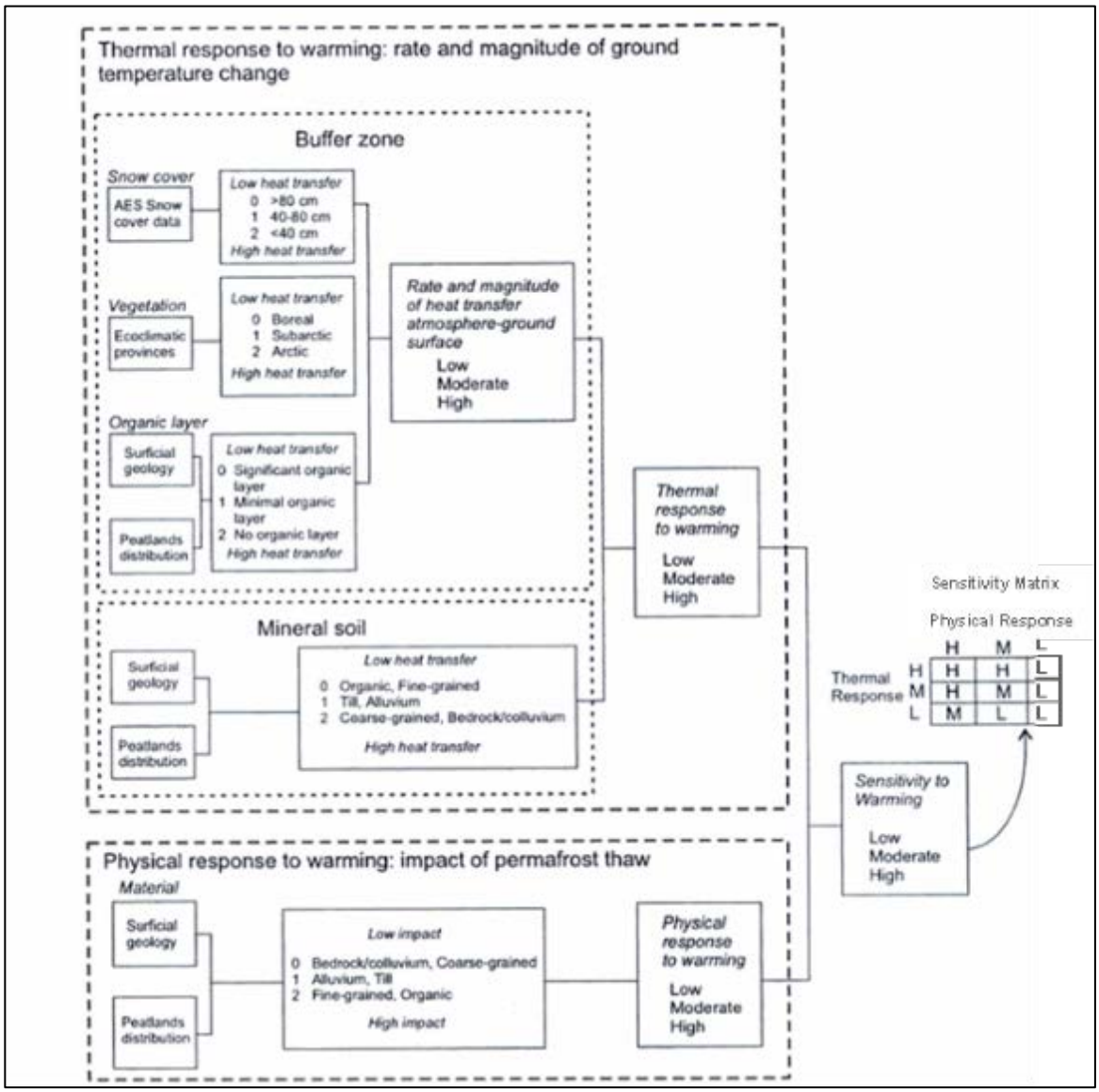

Figure 37. Classification of physical and thermal response and susceptibility of permafrost to thaw Smith and Burgess (1999).

Therefore, permafrost with a high thermal response but low physical response is deemed to have low sensitivity, while permafrost with the low thermal response but a high physical response is considered to have moderate sensitivity.

5.4.1 Thermal Response

With climate change, all of the permafrost underlying Cape Bounty is expected to warm. However, the magnitude of warming is not uniform across the watersheds. Areas of expected low snow accumulation are predicted to warm by about 9 °C while areas of high snow accumulation are predicted to warm anywhere from 4-6 °C, under equilibrium conditions for the RCP8.5 2080 climate change projection (Figure 38a).

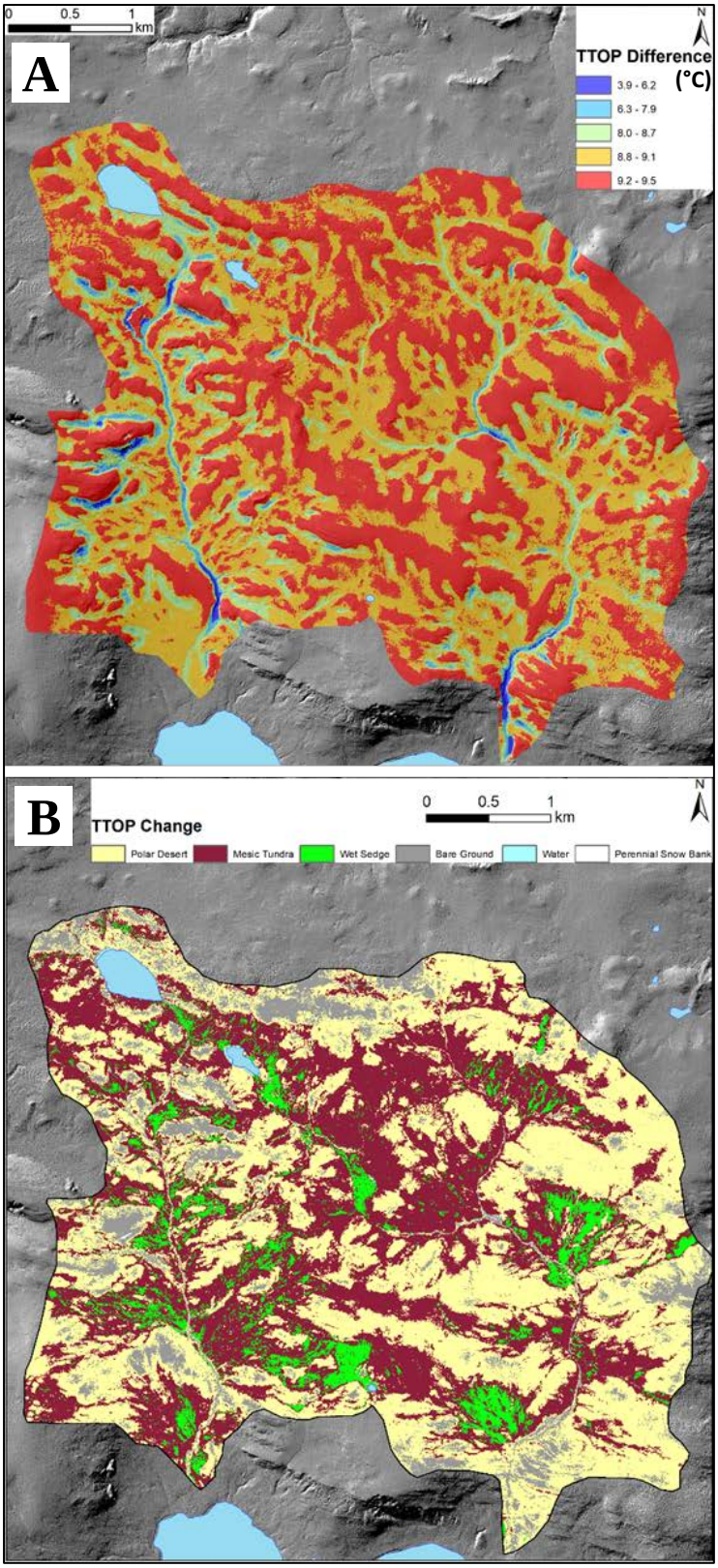

Figure 38. A) Magnitude of TTOP change from current conditions to equilibrium conditions for RCP8.5 2080 B) Land-cover classification.

This variability leads to a decrease of 5.56 °C in the total range of permafrost temperatures and moves the system toward a more homogeneous permafrost temperature regime. This is likely a product of the warmer winter air temperatures and the value of n_f. In areas of high snow accumulation (low n_f), TTOP is partially independent of winter air temperatures as the ground is shielded by snow, while TTOP for low snow accumulation areas (high n_f) is largely dependent on the winter air temperatures (Smith & Burgess, 1999; Bonnaventure et al., 2016). Therefore, a warmer winter will have a greater impact on the coldest permafrost locations as observed in the model results making these areas thermally susceptible to climate change.

The model, however, does not account for ground ice, which buffers the impact of a warmer AMAT on TTOP (Shur et al., 2005). Therefore, areas with high ground ice will show a smaller magnitude of warming than predicted in the model. Areas with limited soil moisture do not have this thermal buffering and will warm at a more rapid rate. In Cape Bounty, mesic tundra and wet sedge generally have more volumetric water content than polar desert and bare ground (excluding channel bed) land cover classifications (Atkinson & Treitz, 2012). The relative ground ice content based on soil moisture can generally be inferred using these classifications. Comparing the vegetation classification to the TTOP difference surface, the areas of largest change are generally found in the polar desert and bare ground (excluding the river channel) land-cover classifications, indicating that these areas likely have limited moisture inputs for ground ice formation (Figure 38). Additionally, the areas of coldest permafrost tend to be upland areas where water will drain away from, supporting the assumption of limited ground ice in these locations.

5.4.2 Physical Response

There is a negligible physical response in thawing permafrost with little to no ground ice, while thawing of ice rich permafrost often results in surface disturbance as the melted ice lost mass and shape (Smith & Burgess, 1999; Jorgenson & Osterkamp, 2005; Shur et al., 2005; Kokelj & Jorgenson, 2013). This physical response to warming is often manifested as ground instability, resulting in thaw settlement, thermokarst, and active layer detachment failures (ALDs) (Smith & Burgess, 1999; Jorgenson & Osterkamp, 2005; Kokelj & Jorgenson, 2013). At Cape Bounty, disturbances are generally found on slopes between 4° and 15° and areas of low PISR (Rudy et al., 2016). The relation between PISR and disturbance is attributed to varying ALT, location of ground ice within the soil profile, and snow accumulation and persistence (Young et al., 1997; Carey & Woo, 1999; Shur et al., 2005; Rudy et al., 2016). In comparison to the Dual Watershed TTOP model, areas with the highest probability of disturbance are located around and within areas of warmer permafrost (Figure 39).

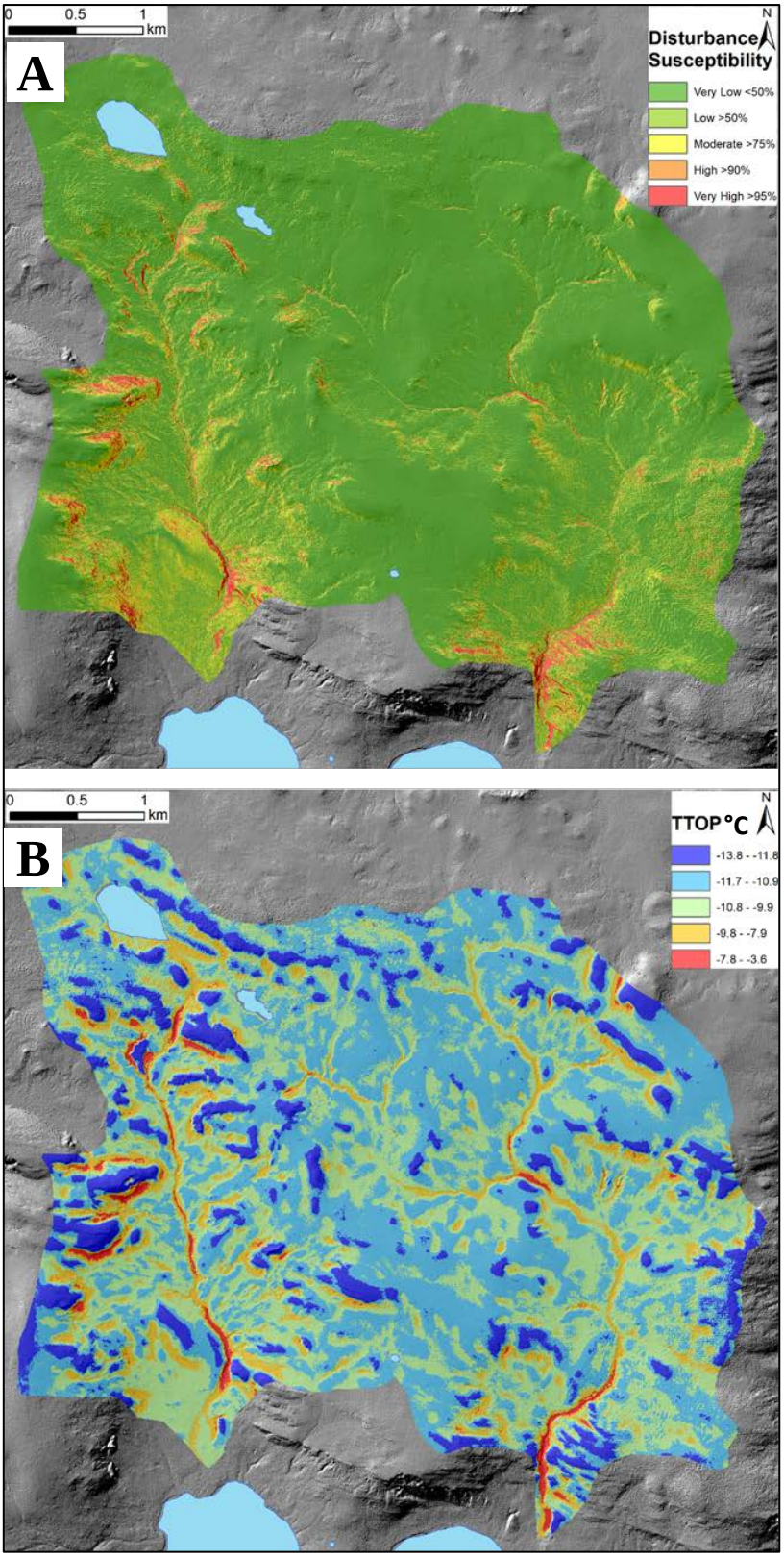

Figure 39. A) Probability of disturbance for Cape Bounty based on terrain variables B) Average annual TTOP

Locations with warm permafrost are expected to have high snow accumulation (Riseborough & Smith, 1998). The overlap between locations of warm permafrost and high disturbance susceptibility supports notion of snow accumulation and persistence as a cause of instability, represented in the model as low PISR.

As ground surface and permafrost temperature over Cape Bounty warm, areas with warm permafrost may be susceptible to disturbance based on ground ice content and substrate (Kokelj & Burn, 2005; Lewkowicz, 2007). Although locations of cold permafrost are expected to warm more, these locations are upland areas with more course grained materials and limited ice content and are not likely to show a large physical response to warming (Atkinson & Treitz, 2012). Additionally, these locations are beyond the local marine limit (as determined by elevation), implying the lack of frost susceptible marine clays and a reduced chance of failure (Kokelj & Burn, 2005; Rudy et al., 2016).

5.5 Hydrological and Microbial activity

5.5.1 Hydrological Connectivity

Warmer ground surface and permafrost temperatures than those of the surrounding areas may result in hotspots for hydrological movement (Woo, 1986). On slopes, uneven soil thawing has been shown to impact the mode of water flow (Quinton et al., 2004; Nicole et al., 2009). In the areas of discontinuous permafrost, permafrost under peat plateaus creates barriers to lateral water movement (Nicole et al., 2009). At the watershed scale, areas of warmer AMGST, which delay freezing and early thaw, are likely to provide pathways for lateral water flow, which otherwise would be blocked by the frozen active layer (Woo, 1986). Although the lateral flow of water is primarily determined by substrate and existing soil moisture, the locations of warmer AMGST and

TTOP are important areas for future studies of hydrological connectivity as they may provide linkages later into the freezing season and earlier in the spring for water and solute transportation (McNamara et al., 2005; Levy et al., 2011).

5.5.2 Solute movement

The historic marine limit at Cape Bounty has been determined to range from 70-90 m above sea level, indicating the presence of marine solutes within the sediment (Hodgson et al., 1984). Over permafrost terrain, solutes accumulate in the ice rich zone (transient layer) above the permafrost as they are flushed from the surface of the active layer downward, and become entrapped in the frozen sediment (Kokelj & Burn, 2003, 2005; Lafrenière & Lamoureux, 2013). Once the ground thaws, either through thermal or physical disturbance, these solutes become liberated and travel into lakes and rivers (Lafrenière & Lamoureux, 2013; Lamhonwah et al., 2016; Lafrenière et al., 2017; Lamhonwah et al., 2017; Roberts et al., 2017).

At Cape Bounty, ion concentrations are found to be highest 80-100 cm below the maximum active layer depth (Roberts et al., 2017). Under climate change, the warmer ground temperatures are expected to result in increased solute flushing as active layers deepen, allowing for more export through enhanced surface and subsurface flow (Lafrenière & Lamoureux, 2013; Lamhonwah et al., 2017; Roberts et al., 2017). As discussed previously, the equilibrium permafrost temperature model produced suggests that the largest magnitude of warming will be in low snow accumulation areas, likely corresponding to deeper thaw during the summer. However, despite the deeper thaw, these locations may not contribute as readily to the solute transport as the high snow accumulation areas due to the limited soil moisture, since solute flushing is maximized at

locations with deep thaw and high soil moisture (Lamhonwah et al., 2017). The locations with the largest magnitude of warming are found on well drained uplands in the polar desert and bare ground (excluding channel bed) land-cover classifications, which are considered to be dry (Gregory, 2011; Atkinson & Treitz, 2012). Instead these areas will develop increased storage potential (Lamhonwah et al., 2017). Increased solute export is likely to come from areas with moderate to high temperature changes and high soil moisture to result in flushing of solutes from the newly thawed permafrost (Lamhonwah et al., 2017). These locations are likely to be found in the mesic tundra and wet sedge classifications, which are considered to have an intermediate to high moisture regime (Gregory, 2011; Atkinson & Treitz, 2012). Aside from general warming, increased solute transport also results from ALDs and retrogressive thaw slumps, through the increased thaw depth following disturbance (Lafrenière & Lamoureux, 2013; Lamhonwah et al., 2016). However, as the impact of ALDs and thaw slumps are limited by discharge and hydrological connectivity of the disturbed area, thermal perturbations have a greater impact on solute discharge seasonally (Lafrenière & Lamoureux, 2013).

5.5.3 Microbial activity

Microbiological activity has been observed at temperatures well below 0 °C and at temperatures as low as -10 °C (Rivkina et al., 2000; Price & Sowers, 2004; Bakermans & Skidmore, 2011). In permafrost the doubling time of bacteria was shown to be delayed from 20 days at -10 °C to 160 days at -20 °C (Rivkina et al., 2000). Under the current thermal regime, locations with the warmest AMGST and TTOP remain above this threshold, potentially allowing for microbiological activity year-round, given the availability of sufficient nutrients. Therefore, in a thermal sense, it is possible that these

areas act as biological refugia, which potentially allow for mercury and carbon release from the soil over winter. Outside of these hotspots, winter ground and permafrost temperatures likely become too cold to support this kind of activity or the same magnitude of activity. This study merely identifies possible locations for biological hotspots for further study and does not aim to quantify or validate the presence of increased or prolonged microbial activity in these locations. With increased ground and permafrost temperatures under conditions of climate change, it is likely that microbiological activity will increase across the study area. Although areas of cold permafrost will have the largest magnitude of warming, these locations lack buffering in winter, resulting in larger annual temperature variability and colder winter temperatures, possibly limiting microbial activity (Rivkina et al., 2000).

Microbial activity and thawing permafrost also have implications for the liberation of mercury previously locked in the frozen permafrost (Obrist et al., 2017; Schuster et al., 2018). On Melville Island, modelled predictions of mercury concentrations in the sediment and permafrost show a majority of the mercury is contained within permafrost (Figure 40) (Schuster et al., 2018).

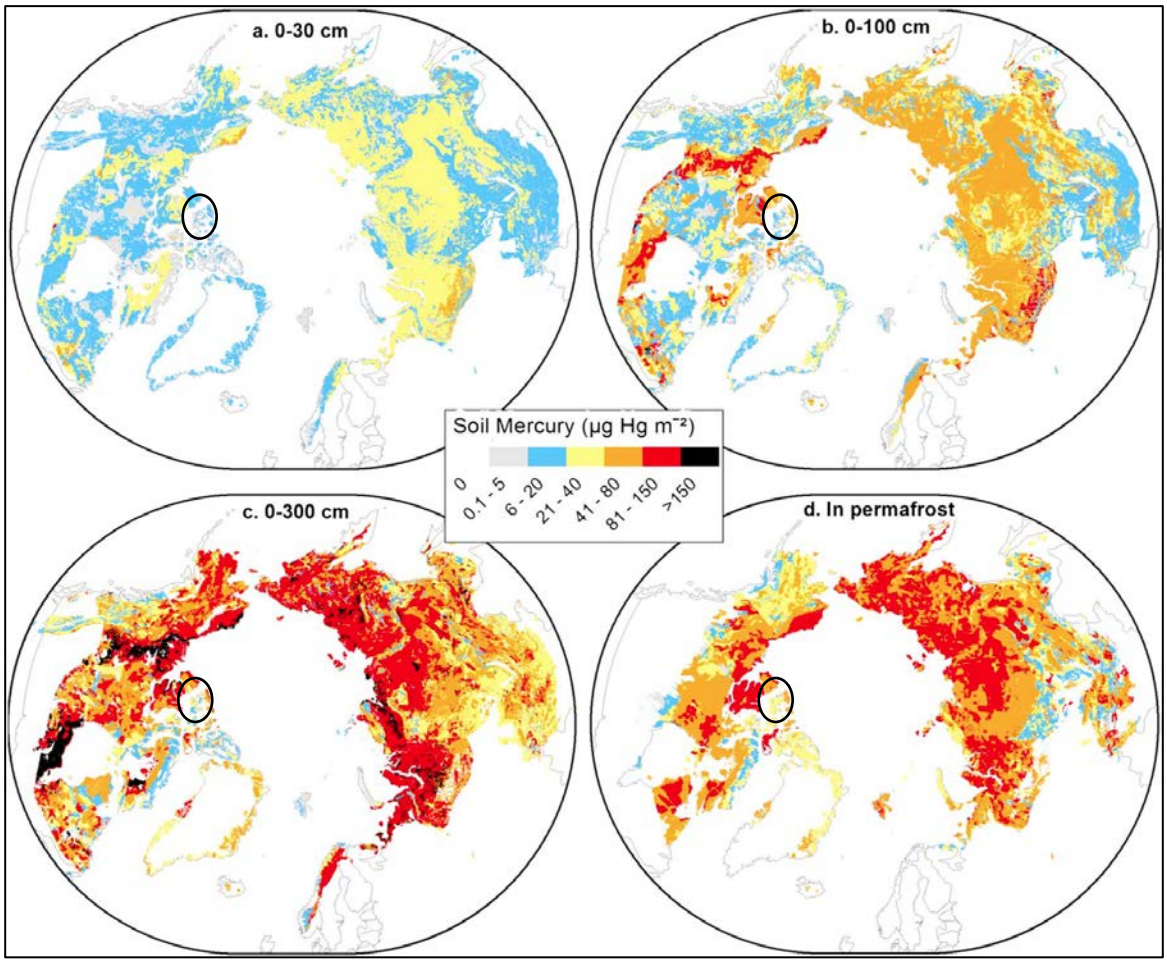

Figure 40. Maps of predicted mercury concentration in permafrost areas of the Northern Hemisphere, Melville Island is circled. Schuster et al. (2018).

As the permafrost at Cape Bounty begins to thaw this mercury will be liberated through microbial activity and subsequently transported to either lakes or the Arctic Ocean through fluvial transport. Given the uneven thermal regime currently in both AMGST and TTOP, it is possible that microbial activity, releasing mercury, is active in the locations which remain relatively warm throughout the year. Additionally, the location of the warmer ground and permafrost near the river channels will allow for fast export of the released mercury to East and West Lake. The release of mercury into High Arctic lakes will have consequences for aquatic life and negatively impacting the health of communities which depend on these resources (El-Hayek, 2007). Additional studies

are needed to confirm the idea of biological refugia in locations of warmer permafrost, which, in combination with studies of mercury content, will be vital in determining mercury release and the health of the lake ecosystems at Cape Bounty.

Chapter 6

Conclusion

6.1 Summary of Findings

Based on the results of this thesis, it can be concluded that, while air temperature remains spatially constant, ground surface and permafrost temperatures at Cape Bounty, Melville Island, Nunavut, show considerable variability. This variability results from the topographic redistribution of snow by wind, allowing some locations within the landscape to be insulated from the air during winter and others to be directly influenced for a majority of the year. As a result areas of snow accumulation remain relatively warm throughout the winter in comparison to the air temperature, while areas of snow removal closely mirror winter air temperatures. The models from this research predict warmer AMGST and TTOP locations to be in topographic hollows, such as river channels and at the base of slopes, as these features tend to accumulate snow. The coldest AMGST and TTOP locations are predicted to be in areas of topographic prominence, hill tops and plateaus, from which snow is removed.

The results of the model show that a substantial portion of the permafrost at Cape Bounty exceeds the predictions of a national permafrost temperature model of Canada (Henry & Smith, 2001). This demonstrates the need to consider microclimatic temperature variability, as these locations may have hydrological connections and may act as biological refugia, which are not recognized in the small scale model. The presence of these hotspots may have implications for solute movement and mercury release, previously overlooked.

The variability in AMGST and TTOP also influences the response of the thermal regimes at Cape Bounty with climate change. Areas with the coldest permafrost are predicted to have the largest magnitude of warming, while areas of relatively warm permafrost are expected to move closer to thaw, with the predicted loss of permafrost in a small portion of the watersheds. The distribution of the thermal change may have implications not only for TSP but also the physical stability of the landscape.

6.2 Future Work

To make the results more robust, snow depth measurements were taken at each of the logger sites in May 2018. Additionally, the loggers were replaced and restarted to collect data for another year. This in combination with the snow depth probes, will allow for the establishment of a direct relation between snow depth and the ground thermal regime. The snow depth can also be directly related to TPI to possibly remove some error associated with relating the ground thermal regime to snow depth indirectly through TPI.

Although the presence of warmer AMGST and TTOP can be used to infer about hydrological connections and microbial productivity, it cannot be used to definitively confirm their existence. Therefore, these areas should be the focus of such studies to confirm or refute their importance. Similarly, areas of warmer AMGST and TTOP should be investigated in correspondence to physical disturbance probability. Specifically, whether the warm temperatures result from the same conditions which increase the probability of disturbance or whether the temperatures may actually increase the chance of disturbance. Finally, it may be valuable to investigate the implications for the predicted thermal regimes for each climate change scenarios on ground stability, microbial activity, and the hydrology of Cape Bounty.

References

AdaptWest Project. (2015). Gridded current and projected climate data for North America at 1km resolution, interpolated using the ClimateNA v5.10 software (T. Wang et al., 2015). Available at adaptwest.databasin.org.

Aplin, P. (2004). Remote sensing: land cover. *Progress in Physical Geography: Earth and Environment, 28*(2), 283-293. doi:10.1191/0309133304pp413pr

Atkinson, D., & Treitz, P. (2012). Arctic Ecological Classifications Derived from Vegetation Community and Satellite Spectral Data. *Remote Sensing, 4*(12), 3948.

Bakermans, C., & Skidmore, M. (2011). Microbial respiration in ice at subzero temperatures (−4°C to −33°C). *Environmental Microbiology Reports, 3*(6), 774-782. doi:10.1111/j.1758-2229.2011.00298.x

Berteaux, D., Gauthier, G., Domine, F., Ims, R. A., Lamoureux, S. F., Lévesque, E., & Yoccoz, N. (2016). Effects of changing permafrost and snow conditions on tundra wildlife: critical places and times. *Arctic Science, 3*(2), 65-90. doi:10.1139/as-2016-0023

Bonnaventure, P. P., & Lamoureux, S. F. (2013). The active layer: A conceptual review of monitoring, modelling techniques and changes in a warming climate. *Progress in Physical Geography, 37*(3), 352-376. doi:10.1177/0309133313478314

Bonnaventure, P. P., Lamoureux, S. F., & Favaro, E. A. (2016). Over-Winter Channel Bed Temperature Regimes Generated by Contrasting Snow Accumulation in a High Arctic River. *Permafrost and Periglacial Processes*. doi:10.1002/ppp.1902

Bonnaventure, P. P., & Lewkowicz, A. G. (2008). Mountain permafrost probability mapping using the BTS method in two climatically dissimilar locations, northwest Canada. *Canadian Journal of Earth Sciences, 45*(4), 443-455. doi:10.1139/E08-013

Bonnaventure, P. P., & Lewkowicz, A. G. (2013). Impacts of mean annual air temperature change on a regional permafrost probability model for the southern Yukon and northern British Columbia, Canada. *The Cryosphere, 7*(3), 935-946. doi:10.5194/tc-7-935-2013

Brown, R. (1966). *Influence of vegetation on permafrost.* Paper presented at the Permafrost international conference: proceedings 11-15 November 1963 Lafayette, Indiana.

Brown, R. J. E. (1972). *Permafrost in the Canadian Arctic archipelago*: National Research Council of Canada, Division of Building Research.

Brown, R., Schuler D. V., Bulygina, O., Derksen, C., Loujus, K., Mudryk, L., Wang, L., Yang, D. (2017). Arctic terrestrial snow cover. In: Snow, Water, Ice and Permafrost in the Arctic (SWIPA) 2017. pp. 26-55. Arctic Monitoring and Assessment Programme (AMAP), Oslo, Norway

Burn, C. R., & Smith, C. A. S. (1988). Observations of the "Thermal Offset" in Near-Surface Mean Annual Ground Temperatures at Several Sites near Mayo, Yukon Territory, Canada. *Arctic, 41*(2), 99-104.

Callaghan, T. V., Johansson, M., Brown, R. D., Groisman, P. Y., Labba, N., Radionov, V., . . . Yang, D. (2011). The Changing Face of Arctic Snow Cover: A Synthesis of Observed and Projected Changes. *Ambio, 40*(Suppl 1), 17-31. doi:10.1007/s13280-011-0212-y

Carey, S. K., & Woo, M. K. (1999). Hydrology of two slopes in subarctic Yukon, Canada. *Hydrological Processes, 13*(16), 2549-2562. doi:doi:10.1002/(SICI)1099-1085(199911)13:16<2549::AID-HYP938>3.0.CO;2-H

Collins, M., Knutti, R., Arblaster, J., Dufresne, J. L., Fichefet, T., Friedlingstein, P., Gao, X., Gutowski, W.J., Johns, T., Krinner, G., Shongwe, M., Tebaldi, C., Weaver, A.J., & Wehner, M. (2013). Long-term Climate Change: Projections, Commitments and Irreversibility. In: Climate Change 2013: The Physical Science Basis. Contribution of Working Group I to the Fifth Assessment Report of the Intergovernmental Panel on Climate Change [Stocker, T.F., D. Qin, G.-K. Plattner, M. Tignor, S.K. Allen, J. Boschung, A. Nauels, Y. Xia, V. Bex and P.M. Midgley (eds.)]. Cambridge University Press, Cambridge, United Kingdom and New York, NY, USA.

Deems, J. S., Painter, T. H., & Finnegan, D. C. (2017). Lidar measurement of snow depth: a review. *Journal of Glaciology*, *59*(215), 467-479. doi:10.3189/2013JoG12J154

Derksen.C., Brown, R., Mudryk, L., & Luojus, K., 2016: Terrestrial snow cover [in “State of the Climate in 2015”]. Bull. Amer. Meteor. Soc., 97 (8), S145–S147.

Edwards, R., & Treitz, P. (2017). Vegetation Greening Trends at Two Sites in the Canadian Arctic: 1984–2015. *Arctic, Antarctic, and Alpine Research, 49*(4), 601-619. doi:10.1657/AAAR0016-075

El-Hayek, Y. H. (2007). Mercury contamination in Arctic Canada: possible implications for Aboriginal health. *J. Dev. Disabil*, *13*, 67-89

Essery, R., & Pomeroy, J. (2004). Vegetation and topographic control of wind-blown snow distributions in distributed and aggregated simulations for an Arctic tundra basin. *Journal of hydrometeorology*, *5*(5), 735-744.

Etzelmüller, B. (2013). Recent Advances in Mountain Permafrost Research. *Permafrost and Periglacial Processes, 24*(2), 99-107. doi:10.1002/ppp.1772

Etzelmüller, B., Berthling, I., & Sollid, J. L. (1998). *The distribution of permafrost in Southern Norway; a GIS approach.* Paper presented at the Seventh International Conference on Permafrost, Proceedings. Collection Nordicana. Centre d'Etudes Nordiques, Universite Laval, Quebec, PQ, Canada.

Etzelmüller, B., Heggem, E. S. F., Sharkhuu, N., Frauenfelder, R., Kääb, A., & Goulden, C. (2006). Mountain permafrost distribution modelling using a multi-criteria approach in the Hövsgöl area, northern Mongolia. *Permafrost and Periglacial Processes*, *17*(2), 91-104. doi:10.1002/ppp.554

French, H. M. (2007). *The Periglacial Environment* (third ed.). Chichester, England: John Wiley & Sons.

Gisnås, K., Etzelmüller, B., Farbrot, H., Schuler, T. V., & Westermann, S. (2013). CryoGRID 1.0: Permafrost Distribution in Norway estimated by a Spatial Numerical Model. *Permafrost and Periglacial Processes, 24*(1), 2-19. doi:10.1002/ppp.1765

Gold, L. W. (1963). *Influence of the snow cover on the average annual ground temperature at Ottawa, Canada*: Division of Building Research, National Research Council.

Goodrich, L. (1982). The influence of snow cover on the ground thermal regime. *Canadian geotechnical journal, 19*(4), 421-432.

Gregory, F. M. (2011). BIOPHYSICAL REMOTE SENSING AND TERRESTRIAL CO2 EXCHANGE AT CAPE BOUNTY, MELVILLE ISLAND. (Master of Science), Queen's University, Kingston, Ontario, Canada.

Hachem, S., Allard, M., & Duguay, C. (2009). Using the MODIS land surface temperature product for mapping permafrost: an application to northern Québec and Labrador, Canada. *Permafrost and Periglacial Processes, 20*(4), 407-416. doi:10.1002/ppp.672

Halsey, L. A., Vitt, D. H., & Zoltai, S. C. (1995). Disequilibrium response of permafrost in boreal continental western Canada to climate change. *Climatic Change, 30*(1), 57-73. doi:10.1007/bf01093225

Harris, C., Davies, M. C. R., & Etzelmüller, B. (2001). The assessment of potential geotechnical hazards associated with mountain permafrost in a warming global climate. *Permafrost and Periglacial Processes, 12*(1), 145-156. doi:10.1002/ppp.376

Heginbottom, J. (1995). *Canada, permafrost*: Canada Map Office.

Henry, K., & Smith, M. (2001). A model-based map of ground temperatures for the permafrost regions of Canada. *Permafrost and Periglacial Processes, 12*(4), 389-398. doi:10.1002/ppp.399

Hinzman, L. D., Goering, D. J., & Kane, D. L. (1998). A distributed thermal model for calculating soil temperature profiles and depth of thaw in permafrost regions. *Journal of Geophysical Research: Atmospheres, 103*(D22), 28975-28991. doi:doi:10.1029/98JD01731

Hodgson, D. A., Vincent, J.-S., & Fyles, J. G. (1984). Quaternary geology of central Melville Island, Northwest Territories. *Paper/Canada. Geol. survey*.

Hodgson, D. A., Vincent, J. S., & Fyles, J. G. (1984). *Quaternary Geology of Central Melville Island, Northwest Territories*: Canadian Government Pub. Centre.

Hoelzle, M., Mittaz, C., Etzelmüller, B., & Haeberli, W. (2001). Surface energy fluxes and distribution models of permafrost in European mountain areas: an overview of current developments. *Permafrost and Periglacial Processes, 12*(1), 53-68. doi:10.1002/ppp.385

Huning, L. S., & Margulis, S. A. (2017). Climatology of seasonal snowfall accumulation across the Sierra Nevada (USA): Accumulation rates, distributions, and variability. *Water Resources Research, 53*(7), 6033-6049. doi:doi:10.1002/2017WR020915

Inkpen, R. (2005). *Science, Philosophy and Physical Geography*: Routledge.

IPCC, 2014: Climate Change 2014: Synthesis Report. Contribution of Working Groups I, II and III to the Fifth Assessment Report of the Intergovernmental Panel on Climate Change [Core Writing Team, R.K. Pachauri and L.A. Meyer (eds.)]. IPCC, Geneva, Switzerland, 151 pp.

Jenson, J. R. (2007). *Remote Sensing of the Environment* (2 ed.): 2000 Pearson Education Inc.

Jorgenson, M. T., & Osterkamp, T. E. (2005). Response of boreal ecosystems to varying modes of permafrost degradation. *Canadian Journal of Forest Research, 35*(9), 2100-2111. doi:10.1139/x05-153

Juliussen, H., & Humlum, O. (2007). Towards a TTOP ground temperature model for mountainous terrain in central-eastern Norway. *Permafrost and Periglacial Processes, 18*(2), 161-184. doi:10.1002/ppp.586

Juszak, I., Eugster, W., Heijmans, M. M. P. D., & Schaepman-Strub, G. (2016). Contrasting radiation and soil heat fluxes in Arctic shrub and wet sedge tundra. *Biogeosciences, 13*(13), 4049-4064. doi:10.5194/bg-13-4049-2016

Kääb, A. (2008). Remote sensing of permafrost-related problems and hazards. *Permafrost and Periglacial Processes, 19*(2), 107-136. doi:10.1002/ppp.619

Karunaratne, K. C., & Burn, C. R. (2004). Relations between air and surface temperature in discontinuous permafrost terrain near Mayo, Yukon Territory. *Canadian Journal of Earth Sciences, 41*(12), 1437-1451. doi:10.1139/e04-082

Kirtman, B., Power, S.B., Adedoyin, J.A., Boer, G.J., Bojariu, R., Camilloni, I., Doblas-Reyes, F.J., Fiore, A.M., Kimoto, M., Meehl, G.A., Prather, M., Sarr, A.,Schär, C., Sutton, R., van Oldenborgh, G.J., Vecchi, G., & Wang, H.J. (2013). Near-term Climate Change: Projections and Predictability. In: Climate Change 2013: The Physical Science Basis. Contribution of Working Group I to the Fifth Assessment Report of the Intergovernmental Panel on Climate Change [Stocker, T.F., D. Qin, G.-K. Plattner, M. Tignor, S.K. Allen, J. Boschung, A. Nauels, Y. Xia, V. Bex and P.M. Midgley (eds.)]. Cambridge University Press, Cambridge, United Kingdom and New York, NY, USA.

Klene, A. E., Nelson, F. E., Shiklomanov, N. I., & Hinkel, K. M. (2001). The N-Factor in Natural Landscapes: Variability of Air and Soil-Surface Temperatures, Kuparuk River Basin, Alaska, U.S.A. *Arctic, Antarctic, and Alpine Research, 33*(2), 140-148. doi:10.2307/1552214

Kokelj, S. V., & Burn, C. R. (2003). Ground ice and soluble cations in near-surface permafrost, Inuvik, Northwest Territories, Canada. *Permafrost and Periglacial Processes, 14*(3), 275-289. doi:10.1002/ppp.458

Kokelj, S. V., & Burn, C. R. (2005). Geochemistry of the active layer and near-surface permafrost, Mackenzie delta region, Northwest Territories, Canada. *Canadian Journal of Earth Sciences, 42*(1), 37-48. doi:10.1139/e04-089

Kokelj, S. V., & Jorgenson, M. T. (2013). Advances in Thermokarst Research. *Permafrost and Periglacial Processes, 24*(2), 108-119. doi:10.1002/ppp.1779

Koven, C. D., Riley, W. J., & Stern, A. (2013). Analysis of Permafrost Thermal Dynamics and Response to Climate Change in the CMIP5 Earth System Models. *Journal of Climate, 26*(6), 1877-1900. doi:10.1175/jcli-d-12-00228.1

Kudryavtsev VA, Garagula LS Kondrat'yeva KA, et al. (1974) Osnovy merzlotnogo prognoza. CRREL draft translation 606 (1977): Fundamentals offrost forecasting in geological engineering investigations. Hanover, NH: Cold Regions Research and Engineering Lab, 489 pp.

Kurylyk, B. L., & Hayashi, M. (2016). Improved Stefan Equation Correction Factors to Accommodate Sensible Heat Storage during Soil Freezing or Thawing. *Permafrost and Periglacial Processes, 27*(2), 189-203. doi:10.1002/ppp.1865

Kurylyk, B. L., McKenzie, J. M., MacQuarrie, K. T. B., & Voss, C. I. (2014). Analytical solutions for benchmarking cold regions subsurface water flow and energy transport models: One-dimensional soil thaw with conduction and advection. *Advances in Water Resources, 70*, 172-184. doi:http://dx.doi.org/10.1016/j.advwatres.2014.05.005

Lachenbruch, A. H., Cladouhos, T. T., & Saltus, R. (1988). *Permafrost temperature and the changing climate.* Paper presented at the Proceedings of the Fifth International Conference on Permafrost.

Lafrenière, M. J., & Lamoureux, S. F. (2013). Thermal Perturbation and Rainfall Runoff have Greater Impact on Seasonal Solute Loads than Physical Disturbance of the Active Layer. *Permafrost and Periglacial Processes, 24*(3), 241-251. doi:10.1002/ppp.1784

Lafrenière, M. J., Louiseize, N. L., & Lamoureux, S. F. (2017). Active layer slope disturbances affect seasonality and composition of dissolved nitrogen export from High Arctic headwater catchments. *Arctic Science, 3*(2), 429-450. doi:10.1139/as-2015-0009

Lamhonwah, D., Lafrenière, M. J., Lamoureux, S. F., & Wolfe, B. B. (2016). Multi-year impacts of permafrost disturbance and thermal perturbation on High Arctic stream chemistry. *Arctic Science, 3*(2), 254-276. doi:10.1139/as-2016-0024

Lamhonwah, D., Lafrenière, M. J., Lamoureux, S. F., & Wolfe, B. B. (2017). Evaluating the hydrological and hydrochemical responses of a High Arctic catchment during an exceptionally warm summer. *Hydrological Processes, 31*(12), 2296-2313. doi:doi:10.1002/hyp.11191

Lantz, T. C., & Kokelj, S. V. (2008). Increasing rates of retrogressive thaw slump activity in the Mackenzie Delta region, N.W.T., Canada. *Geophysical Research Letters, 35*(6). doi:10.1029/2007GL032433

Levy, J. S., Fountain, A. G., Gooseff, M. N., Welch, K. A., & Lyons, W. B. (2011). Water tracks and permafrost in Taylor Valley, Antarctica: Extensive and shallow groundwater connectivity in a cold desert ecosystem. *GSA Bulletin, 123*(11-12), 2295-2311. doi:10.1130/B30436.1

Lewis, T., Lafrenière, M. J., & Lamoureux, S. F. (2012). Hydrochemical and sedimentary responses of paired High Arctic watersheds to unusual climate and permafrost disturbance, Cape Bounty, Melville Island, Canada. *Hydrological Processes, 26*(13), 2003-2018. doi:10.1002/hyp.8335

Lewkowicz, A. G. (2007). Dynamics of active-layer detachment failures, Fosheim Peninsula, Ellesmere Island, Nunavut, Canada. *Permafrost and Periglacial Processes, 18*(1), 89-103. doi:doi:10.1002/ppp.578

Lewkowicz, A. G., & Bonnaventure, P. P. (2011). Equivalent Elevation: A New Method to Incorporate Variable Surface Lapse Rates into Mountain Permafrost Modelling. *Permafrost and Periglacial Processes, 22*(2), 153-162. doi:10.1002/ppp.720

Lewkowicz, A. G., & Ednie, M. (2004). Probability mapping of mountain permafrost using the BTS method, Wolf Creek, Yukon Territory, Canada. *Permafrost and Periglacial Processes, 15*(1), 67-80. doi:10.1002/ppp.480

Lewkowicz, A. G., & Harris , C. (2005). Frequency and magnitude of active-layer detachment failures in discontinuous and continuous permafrost, northern Canada. *Permafrost and Periglacial Processes, 16*(1), 115-130. doi:doi:10.1002/ppp.522

Maxwell, J. B. (1981). Climatic Regions of the Canadian Arctic Islands. *Arctic, 34*(3), 225-240.

McNamara, J. P., Chandler, D., Seyfried , M., & Achet , S. (2005). Soil moisture states, lateral flow, and streamflow generation in a semi-arid, snowmelt-driven catchment. *Hydrological Processes, 19*(20), 4023-4038. doi:doi:10.1002/hyp.5869

Moffat, N. D., Lantz, T. C., Fraser, R. H., & Olthof, I. (2016). Recent Vegetation Change (1980–2013) in the Tundra Ecosystems of the Tuktoyaktuk Coastlands, NWT, Canada. *Arctic, Antarctic, and Alpine Research, 48*(3), 581-597. doi:10.1657/AAAR0015-063

Nguyen, T. N., Burn, C. R., King, D. J., & Smith, S. L. (2009). Estimating the extent of near-surface permafrost using remote sensing, Mackenzie Delta, Northwest Territories. *Permafrost and Periglacial Processes, 20*(2), 141-153. doi:10.1002/ppp.637

Nicole, W., Masaki, H., & L., Q. W. (2009). Spatial and temporal variations in active layer thawing and their implication on runoff generation in peat-covered permafrost terrain. *Water Resources Research, 45*(5). doi:doi:10.1029/2008WR006880

Obrist, D., Agnan, Y., Jiskra, M., Olson, C. L., Colegrove, D. P., Hueber, J., . . . Helmig, D. (2017). Tundra uptake of atmospheric elemental mercury drives Arctic mercury pollution. *Nature, 547*, 201. doi:10.1038/nature22997

https://www.nature.com/articles/nature22997#supplementary-information

Oelke, C., Zhang, T., Serreze, M. C., & Armstrong, R. L. (2003). Regional-scale modeling of soil freeze/thaw over the Arctic drainage basin. *Journal of Geophysical Research: Atmospheres (1984–2012), 108*(D10). doi:10.1029/2002JD002722

Ou, C., Zhang, Y., LaRocque, A., Leblon, B., Webster, K., McLaughlin, J., & Barnett, P. (2014, 13-18 July 2014). *Model calibration for mapping permafrost using Landsat-5 TM and RADARSAT-2 images.* Paper presented at the 2014 IEEE Geoscience and Remote Sensing Symposium.

Péwé, R., & Brown, T. (1973). *Distribution of permafrost in North America and its relationship to the environment: a review, 1963-1973.* Paper presented at the Permafrost: North American Contribution [to The] Second International Conference.

Price, P. B., & Sowers, T. (2004). Temperature dependence of metabolic rates for microbial growth, maintenance, and survival. *Proceedings of the National Academy of Sciences of the United States of America, 101*(13), 4631-4636.

Pulliainen, J. (2006). Mapping of snow water equivalent and snow depth in boreal and sub-arctic zones by assimilating space-borne microwave radiometer data and ground-based observations. *Remote sensing of Environment, 101*(2), 257-269. doi:https://doi.org/10.1016/j.rse.2006.01.002

Purkis, S., & Klemas, V. (2013). Remote sensing basics. In *Remote Sensing and Global Environmental Change*.

Quinton, W. L., Carey, S. K., & Goeller, N. T. (2004). Snowmelt runoff from northern alpine tundra hillslopes: major processes and methods of simulation. *Hydrol. Earth Syst. Sci., 8*(5), 877-890. doi:10.5194/hess-8-877-2004

Riseborough, D.W. (2004). Exploring the Parameters of a Simple Model of the Permafrost: Climate Relationship. Unpublished PhD dissertation, Carleton University, Ottawa, Canada, 328 pp

Riseborough, D. (2007). The effect of transient conditions on an equilibrium permafrost-climate model. *Permafrost and Periglacial Processes, 18*(1), 21-32. doi:10.1002/ppp.579

Riseborough, D. W. (2008). Estimating active layer and talik thickness from temperature data: Implications from modeling results. In *Proceedings of the Ninth International Conference on Permafrost, University of Alaska Fairbanks* (Vol. 29).

Riseborough, D., Shiklomanov, N., Etzelmüller, B., Gruber, S., & Marchenko, S. (2008). Recent advances in permafrost modelling. *Permafrost and Periglacial Processes, 19*(2), 137-156. doi:10.1002/ppp.615

Riseborough, D., & Smith, M. (1998). *Exploring the limits of permafrost.* Paper presented at the Proceedings Permafrost: 7th International Conference. Yellowknife, Canada. Edited by Lewkowicz, AG, and Allard, M. Nordicana, Quebec.

Riseborough, D. W. (2002). The mean annual temperature at the top of permafrost, the TTOP model, and the effect of unfrozen water. *Permafrost and Periglacial Processes, 13*(2), 137-143. doi:10.1002/ppp.418

Rivkina, E., Friedmann, E., McKay, C., & Gilichinsky, D. (2000). Metabolic activity of permafrost bacteria below the freezing point. *Applied and Environmental Microbiology, 66*(8), 3230-3233.

Roberts, K. E., Lamoureux, S. F., Kyser, T. K., Muir, D. C. G., Lafrenière, M. J., Iqaluk, D., . . . Normandeau, A. (2017). Climate and permafrost effects on the chemistry and ecosystems of High Arctic Lakes. *Scientific Reports, 7*(1), 13292. doi:10.1038/s41598-017-13658-9

Rudy, A. C. A., Lamoureux, S. F., Treitz, P., & van Ewijk, K. Y. (2016). Transferability of regional permafrost disturbance susceptibility modelling using generalized linear and generalized additive models. *Geomorphology, 264*, 95-108. doi:https://doi.org/10.1016/j.geomorph.2016.04.011

Santosh, K. M., & Sundaresan, J. (2014). Remote Sensing Basics. In J. Sundaresan, K. M. Santosh, A. Déri, R. Roggema, & R. Singh (Eds.), *Geospatial Technologies and Climate Change* (pp. 279-290). Cham: Springer International Publishing.

Sazonova, T. S., & Romanovsky, V. E. (2003). A model for regional-scale estimation of temporal and spatial variability of active layer thickness and mean annual ground temperatures. *Permafrost and Periglacial Processes, 14*(2), 125-139. doi:10.1002/ppp.449

Schuster, P. F., Schaefer, K. M., Aiken, G. R., Antweiler, R. C., Dewild, J. F., Gryziec, J. D., . . . Zhang, T. (2018). Permafrost Stores a Globally Significant Amount of Mercury. *Geophysical Research Letters, 45*(3), 1463-1471. doi:10.1002/2017GL075571

Schuur, E. A. G., Bockheim, J., Canadell, J. G., Euskirchen, E., Field, C. B., Goryachkin, S. V., . . . Zimov, S. A. (2008). Vulnerability of Permafrost Carbon to Climate Change: Implications for the Global Carbon Cycle. *BioScience, 58*(8), 701-714. doi:10.1641/B580807

Serreze, M. C., & Barry, R. G. (2011). Processes and impacts of Arctic amplification: A research synthesis. *Global and Planetary Change, 77*(1), 85-96. doi:https://doi.org/10.1016/j.gloplacha.2011.03.004

Shiklomanov, N. I., Anisimov, O. A., Zhang, T., Marchenko, S., Nelson, F. E., & Oelke, C. (2007). Comparison of model-produced active layer fields: Results for northern Alaska. *Journal of Geophysical Research: Earth Surface, 112*(F2), n/a-n/a. doi:10.1029/2006JF000571

Shur, Y., Hinkel, K. M., & Nelson, F. E. (2005). The transient layer: implications for geocryology and climate-change science. *Permafrost and Periglacial Processes, 16*(1), 5-17.

Shur, Y. L., & Jorgenson, M. T. (2007). Patterns of permafrost formation and degradation in relation to climate and ecosystems. *Permafrost and Periglacial Processes, 18*(1), 7-19. doi:10.1002/ppp.582

Smith, M. W., & Riseborough, D. W. (1996). Permafrost monitoring and detection of climate change. *Permafrost and Periglacial Processes, 7*(4), 301-309. doi:10.1002/(sici)1099-1530(199610)7:4<301::aid-ppp231>3.0.co;2-r

Smith, M. W., & Riseborough, D. W. (2002). Climate and the limits of permafrost: a zonal analysis. *Permafrost and Periglacial Processes, 13*(1), 1-15. doi:10.1002/ppp.410

Smith, S. L., & Burgess, M. M. (1999). Mapping the sensitivity of Canadian permafrost to climate warming. *IAHS PUBLICATION*, 71-80.

Smith, S. L., & Riseborough, D. W. (2010). Modelling the thermal response of permafrost terrain to right-of-way disturbance and climate warming. *Cold Regions Science and Technology, 60*(1), 92-103. doi:http://doi.org/10.1016/j.coldregions.2009.08.009

Storck, P., Lettenmaier, D. P., & Bolton, S. M. (2002). Measurement of snow interception and canopy effects on snow accumulation and melt in a mountainous maritime climate, Oregon, United States. *Water Resources Research, 38*(11), 5-1. doi:10.1029/2002WR001281

Sturm, M., Holmgren, J., McFadden, J. P., Liston, G. E., Chapin III, F. S., & Racine, C. H. (2001). Snow–shrub interactions in Arctic tundra: a hypothesis with climatic implications. *Journal of Climate, 14*(3), 336-344.

Tucker, C. J., Slayback, D. A., Pinzon, J. E., Los, S. O., Myneni, R. B., & Taylor, M. G. (2001). Higher northern latitude normalized difference vegetation index and growing season trends from 1982 to 1999. *International Journal of Biometeorology, 45*(4), 184-190. doi:10.1007/s00484-001-0109-8

Tyrtikov, A. P. (1976). Effects of vegetation on the freezing and thawing of soils.

Walker, D. A., Gould, W. A., Maier, H. A., & Raynolds, M. K. (2002). The Circumpolar Arctic Vegetation Map: AVHRR-derived base maps, environmental controls, and integrated mapping procedures. *International Journal of Remote Sensing, 23*(21), 4551-4570. doi:10.1080/01431160110113854

Wang, T., Hamann, A., Spittlehouse, D., & Carroll, C. (2016). Locally Downscaled and Spatially Customizable Climate Data for Historical and Future Periods for North America. *PLOS ONE, 11*(6), e0156720. doi:10.1371/journal.pone.0156720

Way, R. G., & Lewkowicz, A. G. (2016). Modelling the spatial distribution of permafrost in Labrador–Ungava using the temperature at the top of permafrost. *Canadian Journal of Earth Sciences, 53*(10), 1010-1028. doi:10.1139/cjes-2016-0034

Way, R. G., & Lewkowicz, A. G. (2018). Environmental controls on ground temperature and permafrost in Labrador, northeast Canada. *Permafrost and Periglacial Processes, 29*(2), 73-85. doi:doi:10.1002/ppp.1972

Westermann, S., Østby, T. I., Gisnås, K., Schuler, T. V., & Etzelmüller, B. (2015). A ground temperature map of the North Atlantic permafrost region based on remote sensing and reanalysis data. *The Cryosphere, 9*(3), 1303-1319. doi:10.5194/tc-9-1303-2015

Williams, P. J., & Smith, M. W. (1989). *The Frozen Earth: Fundamentals of Geocryology*: Cambridge University Press.

Woo, M. k. (1986). Permafrost hydrology in North America. *Atmosphere-Ocean, 24*(3), 201-234. doi:10.1080/07055900.1986.9649248

Woo, M. k., Heron, R., Marsh, P., & Steer, P. (1983). Comparison of weather station snowfall with winter snow accumulation in high arctic basins. *Atmosphere-Ocean, 21*(3), 312-325. doi:10.1080/07055900.1983.9649171

Woo, M. K., Kane, D. L., Carey, S. K., & Yang, D. (2008). Progress in permafrost hydrology in the new millennium. *Permafrost and Periglacial Processes, 19*(2), 237-254. doi:10.1002/ppp.613

Woo, M. k., & Young, K. L. (1997). Hydrology of a Small Drainage Basin with Polar Oasis Environment, Fosheim Peninsula, Ellesmere Island, Canada. *Permafrost and Periglacial Processes, 8*(3), 257-277. doi:10.1002/(SICI)1099-1530(199709)8:3<257::AID-PPP258>3.0.CO;2-T

Wright, J., Duchesne, C., & Côté, M. (2003). *Regional-scale permafrost mapping using the TTOP ground temperature model.* Paper presented at the Proceedings of the Eighth International Conference on Permafrost, Zurich, Switzerland, Phillips M, Springman SM, Arenson LU (eds). AA Balkema: Lisse.

Yang, D., & Woo, M. K. (1999). Representativeness of local snow data for large scale hydrologic investigations. *Hydrological Processes, 13*(12-13), 1977-1988. doi:10.1002/(SICI)1099-1085(199909)13:12/13<1977::AID-HYP894>3.0.CO;2-B

Yi, S., Woo, M.-k., & Arain, M. A. (2007). Impacts of peat and vegetation on permafrost degradation under climate warming. *Geophysical Research Letters, 34*(16), n/a-n/a. doi:10.1029/2007GL030550

Yin, G.-a., Niu, F.-j., Lin, Z.-j., Luo, J., & Liu, M.-h. (2016). Performance comparison of permafrost models in Wudaoliang Basin, Qinghai-Tibet Plateau, China. *Journal of Mountain Science, 13*(7), 1162-1173. doi:10.1007/s11629-015-3745-x

Young, K. L., Woo, M.-k., & Edlund, S. A. (1997). Influence of Local Topography, Soils, and Vegetation on Microclimate and Hydrology at a High Arctic Site, Ellesmere Island, Canada. *Arctic and Alpine Research, 29*(3), 270-284. doi:10.2307/1552141

Zhang, T. (2005). Influence of the seasonal snow cover on the ground thermal regime: An overview. *Reviews of Geophysics, 43*(4), n/a-n/a. doi:10.1029/2004RG000157

Zhang, T., Osterkamp, T. E., & Stamnes, K. (1996). Influence of the Depth Hoar Layer of the Seasonal Snow Cover on the Ground Thermal Regime. *Water Resources Research, 32*(7), 2075-2086. doi:10.1029/96WR00996

Zhang, T., Osterkamp, T. E., & Stamnes, K. (1997). Effects of Climate on the Active Layer and Permafrost on the North Slope of Alaska, U.S.A. *Permafrost and Periglacial Processes, 8*(1), 45-67. doi:10.1002/(SICI)1099-1530(199701)8:1<45::AID-PPP240>3.0.CO;2-K

Zhang, T., & Stamnes, K. (1998). Impact of climatic factors on the active layer and permafrost at Barrow, Alaska. *Permafrost and Periglacial Processes, 9*(3), 229-246. doi:10.1002/(SICI)1099-1530(199807/09)9:3<229::AID-PPP286>3.0.CO;2-T

Zhang, Y., Chen, W., & Cihlar, J. (2003). A process-based model for quantifying the impact of climate change on permafrost thermal regimes. *Journal of Geophysical Research: Atmospheres, 108*(D22), n/a-n/a. doi:10.1029/2002jd003354

Zhang, Y., Li, J., Wang, X., Chen, W., Sladen, W., Dyke, L., . . . Brook, Ryan K. (2012). Modelling and mapping permafrost at high spatial resolution in Wapusk National Park, Hudson Bay Lowlands1This article is one of a series of papers published in this CJES Special Issue on the theme of Fundamental and applied research on permafrost in Canada.2Earth Science Sector Contribution 20110058. *Canadian Journal of Earth Sciences, 49*(8), 925-937. doi:10.1139/e2012-031

Appendix

Table 10. Multivariable linear regression variables and p-values

Dependent Variable	Independent Variable	p-value
AMAT	Elevation	0.0049
FDD_a	Elevation	0.0095
TDD_a	Elevation	0.1210
AMGST	Elevation	0.7110
AMGST	TPI	0.0035
AMGST	Slope	0.9914
AMGST	PISR	0.4264
FDD_g	TPI	0.0015
FDD_g	Elevation	0.6656
FDD_g	PISR	0.4870
FDD_g	Slope	0.8683
nf	TPI	0.0014
nf	PISR	0.4929
nf	Elevation	0.6809
nf	Slope	0.8541
nt	TPI	0.0077
nt	Elevation	0.2238
nt	PISR	0.1204
nt	nf	1.7410E-06
nt	Slope	0.1465

Table 11. Regression Analysis variables and r^2 values

Dependent Variable	Independent Variable	Linear Regression r^2	Polynomial Regression r^2
AMAT	Elevation	0.9495	NA
FDD_a	Elevation	0.9216	NA
TDD_a	Elevation	0.5887	NA
AMGST (Dual watershed)	TPI	0.3475	0.5564
AMGST (West Watershed	TPI	0.4154	0.5965
AMGST (East watershed)	TPI	0.5823	0.6915
nf (Dual watershed)	TPI	0.3867	0.568
nf (West Watershed)	TPI	0.46	0.6108
nf (East watershed)	TPI	0.5918	0.6999
nt (Dual watershed	nf (Dual watershed)	0.6849	0.727
nt (West watershed)	nf (West watershed)	0.6655	0.6994
nt (East watershed)	nf (East watershed)	0.7158	0.7631

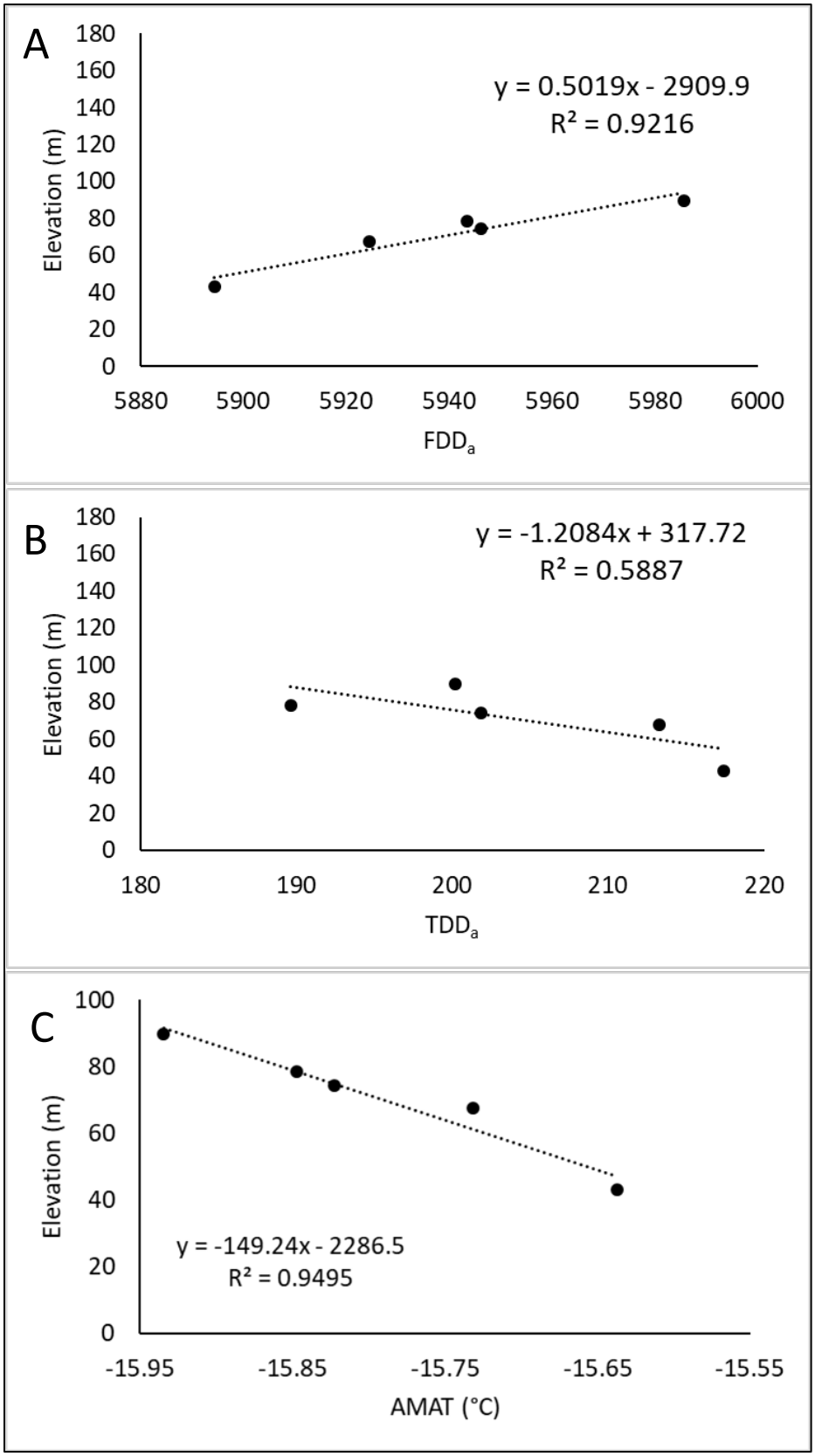

Figure 41. Linear regression plots for A) FDD_a B) TDD_a C) AMAT

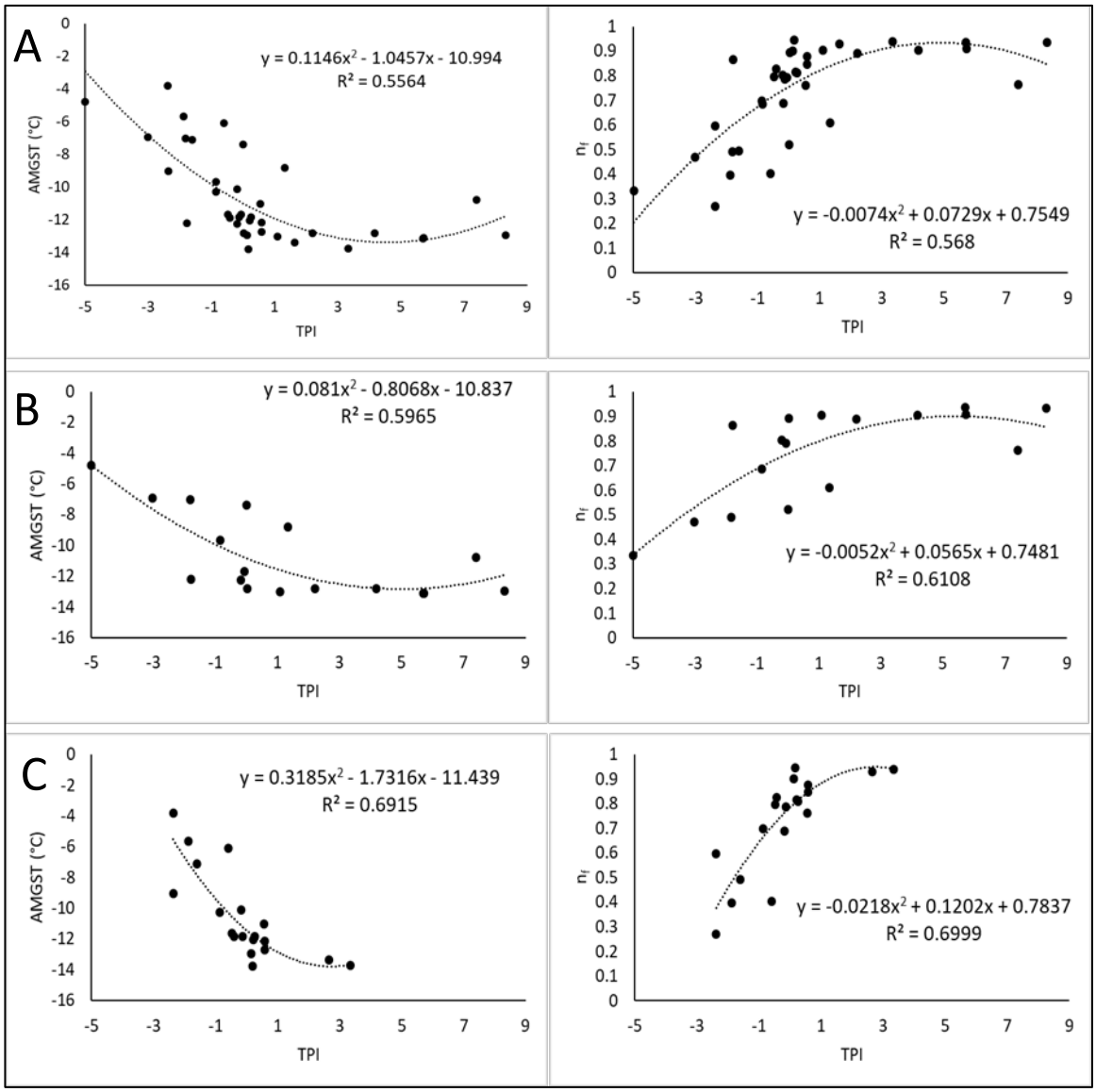

Figure 42. Polynomial regression plots for AMGST and n_f for A) Dual Watershed model B) West Watershed Model C) East Watershed model

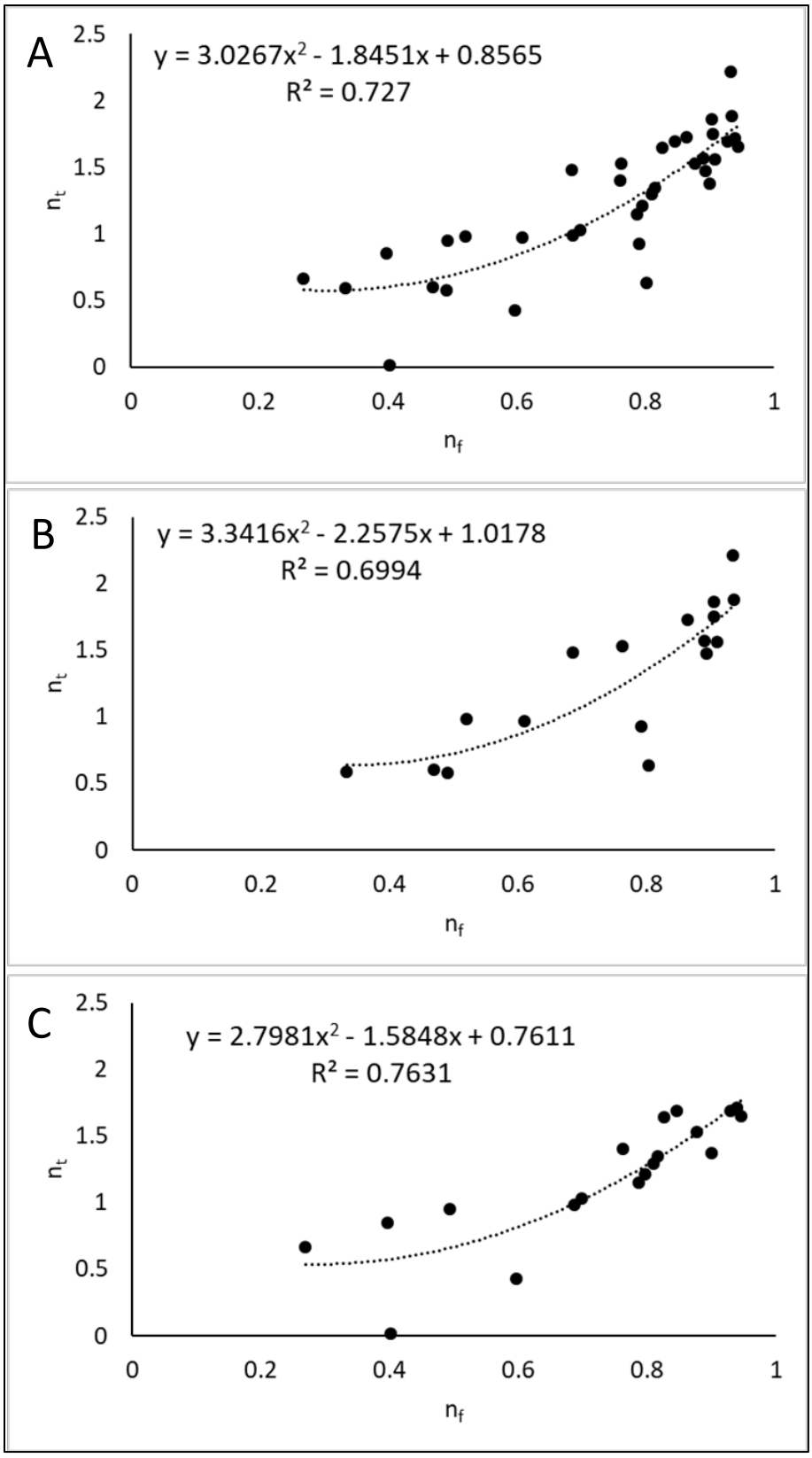

Figure 43. Polynomial regression plots for n_t for A) Dual Watershed Model B) West Watershed Model C) East Watershed Model

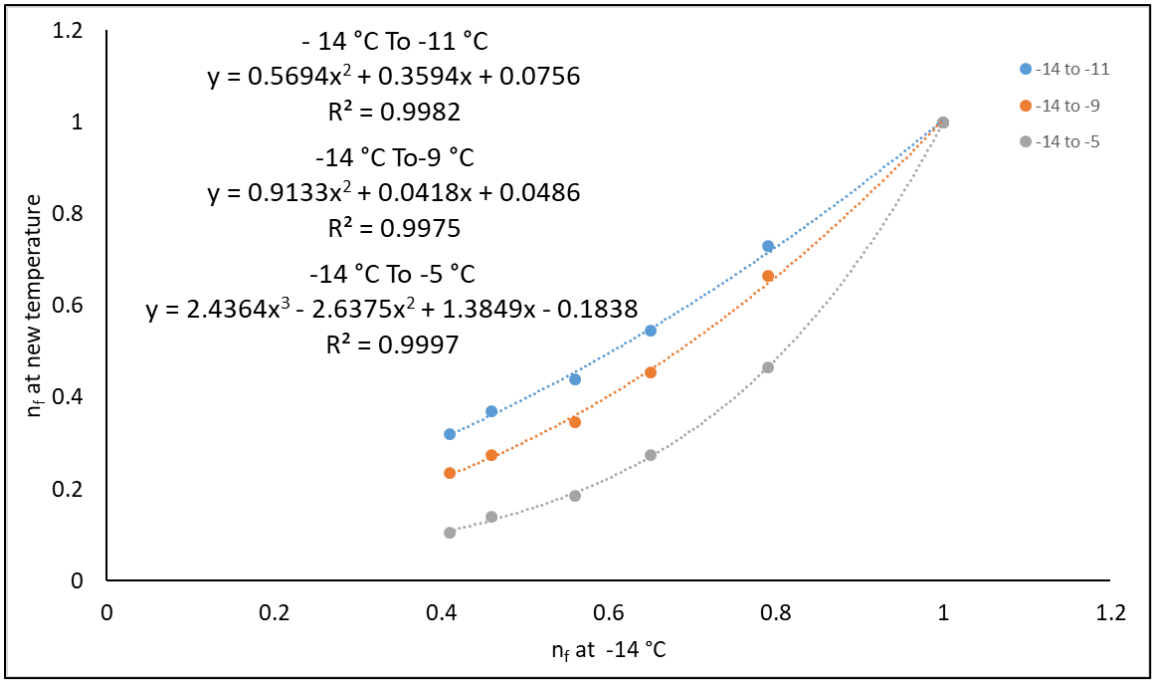

Figure 44. Graph for transformation of n_f from those at -14 °C to those under the new climate normal under each climate change scenario: RCP4.5 2050 -11 °C, RCP4.5 2080 and RCP8.5 2050 -9 °C, and RCP8.5 2080 -5 °C

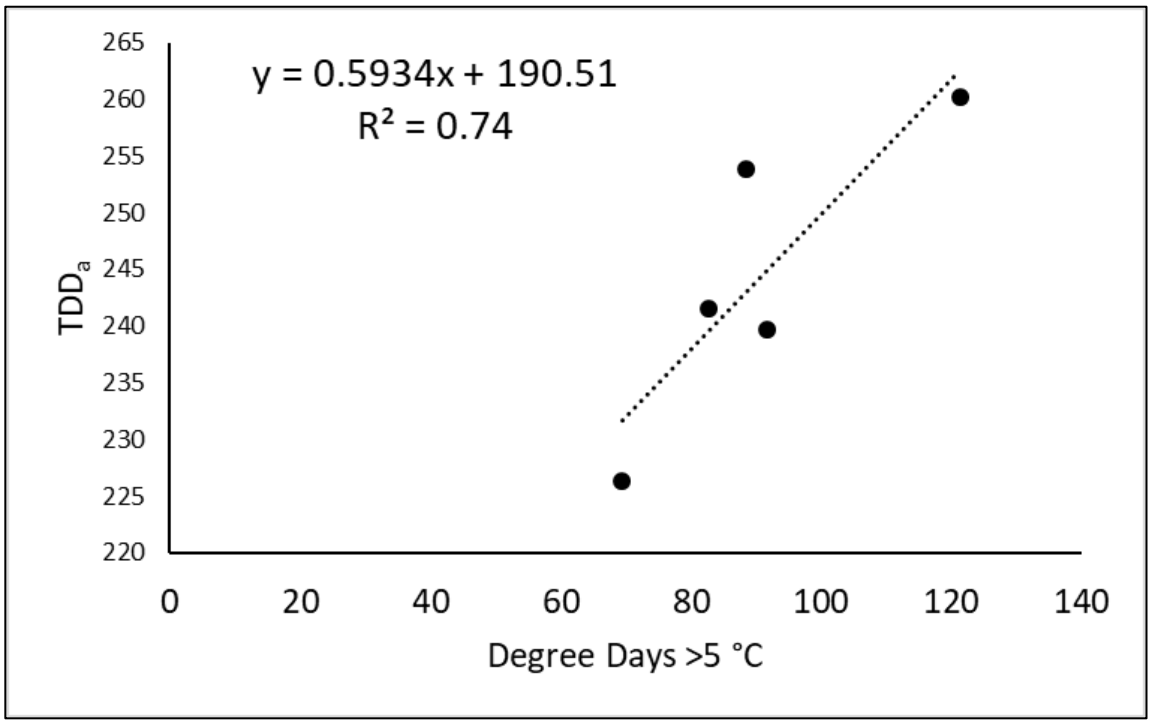

Figure 45. Linear regression used to transform the degree days >5 provided in the ClimateNA data to TDD_a